Distortions in bipeak interval timing by chronic methylmercury exposure are attenuated by the L-type Ca++ channel blocker isradipine: Effects of relative and absolute target duration and duration of exposure.

by

Derek Alan Pope

A dissertation submitted to the Graduate Faculty of
Auburn University
in partial fulfillment of the
requirements for the Degree of
Doctor of Philosophy

Auburn, Alabama
August 6th, 2016

Approved by

M. Christopher Newland, Chair, Alumni Professor of Psychology
Jeffrey Katz, Alumni Professor of Psychology
Jennifer Robinson, Assistant Professor of Psychology
John Rapp, Associate Professor of Psychology
Mark Carpenter, Associate Professor Mathematics & Statistics

Abstract

The fidelity of the perception of time in the seconds to minutes range – known as interval timing – is subject to distortion in both human and non-human animals. Alterations in interval timing induced by environmental/behavioral, pharmacological, lesion, or stimulation techniques or by particular disorders and diseases are postulated to be diagnostic of the underlying neuropsychological processes. Of particular interest here are the persistent distortions in interval timing linked to dopamine-related (DA) dysfunction in the basal ganglia, as epitomized in patients with Parkinson's disease (PD), an age-related neurodegenerative disorder characterized by the degeneration of DAergic neurons in the substantia nigra pars compacta (SNpc) that project to the striatum. The selective vulnerability of SNpc DAergic neurons in PD is likely related to intrinsic, autonomous pacemaking activities on these neurons, which depend on the engagement of the relatively rare CaV1.3 subtype of L-type, voltage-gated Ca^{2+}channels. Reducing Ca^{2+}flux via administration of L-type, voltage-gated Ca^{2+}channel blockers/antagonists that cross the blood-brain-barrier (BBB) and have a high affinity for the Cav1.3 channel subtype, such as isradipine, can delay the onset of PD-like signs and symptoms, slow their progression, and/or prevent their development in model systems. Genetic mutations have been identified in familial PD, but the majority of cases of PD are sporadic. Substantial epidemiological evidence suggests a role for environmental contaminants in PD, but, to date, no specific environmental agent has been shown unequivocally to be causative or act as a risk-factor. Methylmercury (MeHg) accumulates in the basal ganglia and may distort DAergic neuronal functioning in the SNpc and efferent projection regions (e.g., striatum). We hypothesize that chronic, adult-onset exposure to MeHg facilitates development of NSDA and SNpc dysfunction, potentially leading to

PD-like effects. Given the well-known psychophysical properties of interval timing and the sensitivity of the processes underlying interval timing to degeneration and dysfunction of DAergic-related and Ca^{2+}-mediated processes in the SNpc, a timing preparation could be an exemplary method to quantitatively assess the potential mechanisms by which the above factors may affect the underlying neurobiological and behavioral processes. In the present experiments, the effects of chronic, adult-onset exposure to either 0 ppm or 5 ppm MeHg on the accuracy and precision of interval timing as assessed under the PIC procedure were examined using retired breeder, BALB/c mice that were about 9 months old at beginning of exposure. To investigate the potential role of Ca^{2+} homeostasis/regulation, the effects of concurrent, chronic adult-onset exposure to either 0 ppm or 2 ppm of the L-type Ca^{2+} blocker, isradipine (ISR) on PIC performance by the aged BALB/c mice. Phase 1 assessed *PIC* timing *early* into exposure (weeks 10 – 20) using target durations of 8-s (*short*) and 32-s (*long*), that is, widely spaced (1:4 relative difference). Phase 2 assessed *PIC* timing *later* in exposure (weeks 22 – 32) and the target durations were changed to 12-s (*short*) and 24-s (*long*), that is, spaced closer to one another (1:2 relative difference). In both phases, a model-comparison approach**,** integrating the theories and assumptions of the Behavioral Theory of Timing (BeT), Killeen, Weiss, and colleagues' pseudo-logistic model (PLM), and more recent Bayesian models**,** was employed to assess the validity of different models. During Phase 1, MeHg caused the *short* target duration to be overestimated and the *long* to be underestimated, conforming to Vierordt's law and qualitatively similar to that observed in PD patients. During Phase 2, while MeHg again caused the *long* target duration to be underestimated, again conforming to Vierordt's law and similar to PD patients, the *short* target duration was also grossly underestimated. In both phases, MeHg increased the relative variability in PI timing. Importantly, ISR eliminated all MeHg-induced effects on the PI timing precision, the rightward migration of the *short* in Phase 1 and leftward migrations of the *long* target durations in both phases. In accord with the PLM-comparison, these MeHg-induced distortions of timing occurred by greatly slowing pacemaker speed and

increasing the variability in its regulation during both phases and this was hypothesized to result in the migration-like effects observed during each Phase. In sum, Chronic, adult-onset MeHg exposure distorted both the accuracy and precision of PI timing at the *short* and *long* target durations arranged in each phase. Co-exposure to ISR alleviated or protected against most of the MeHg-induced distortions in accuracy and all in the precision of PI timing. The degree and direction of distortion by MeHg and protection by ISR in the accuracy and precision of PI timing were qualitatively similar in the two phases despite differences in the timing parameters used and the duration of exposure. These results are the first to our knowledge to show that chronic, adult-onset MeHg exposure disrupts interval timing and time perception, thus adding to the literature concerning the compound's neurobehavioral toxicity. Additionally, these results add further evidence that one potential way in which MeHg exerts its neurobehavioral toxicity is by disrupting Ca^{2+} functioning in DA neurons of the SNpc and that many of the MeHg-induced disruptions of interval timing and time perception can be attenuated by co-administration of ISR.

Acknowledgements

I would like to offer my gratitude to my advisor Chris Newland for his support of my research interests over the past five years. I would also like to express my appreciation to my committee members, Drs. Katz, Robinson, and Rapp, for their valuable input and guidance during my major area paper and dissertation as well as Dr. Mark Carpenter for his help reviewing this dissertation, and Dr. Peter Killeen for providing his unrequited support and guidance throughout my career. All my achievements are, first, the direct result of the stimulating and wonderful upbringing provided by my parents; I am forever indebted to them. I would also like to thank my friends and colleagues, Drs. Andrew Shen, Blake Hutsell, Duncan Amegbletor, Brandon Johnson, and Kelly Zuromski from whom I was fortunate enough to receive tremendous support and guidance, alongside rousing discourse, throughout my time at Auburn. Lastly, I would like to acknowledge and thank the all of the philosophers, scientists, musicians, writers, and artists who have shaped the ways in which I think and interact with the world and, importantly, the continued and everlasting inspiration each provides; these include, but are not limited to: Aristotle, Friedrich Nietzsche, Charles Darwin, Jean-Baptiste Lamarck, Albert Einstein, Malcolm X, Martin Luther King Jr., Karl Marx, Friedrich Engels, Bernie Sanders, L.L. Thurstone, Ernst Weber, Gustav Fechner, Edward Lorenz, B.F. Skinner, S.S. Stevens, R. Duncan Luce, Roger Shepard, Benoit Mandelbrot, Peter Killeen, John Gibbon, Anthony Dickinson, Gilbert Ryle, Daniel Dennett, Jimi Hendrix, Tupac Shakur, Kendrick Lamar, Killer Mike, Danny Brown, Gertrude Stein, Virginia Woolf, William Shakespeare, Jane Austen, Hunter S. Thompson, Edgar Allen Poe, Langston Hughes, Alexander Pushkin, JK Rowling, Quentin Tarantino, Wes Anderson, Stanley Kubrick, Woody Allen, Spike Lee, Kathryn Bigelow, Nic

Pizzolatto, Claude Monet, Donatello, Leonardo Da Vinci, Pablo Picasso, Michelangelo Buonarroti, Bansky, and Jean-Michel Basquiat.

The text formatting for Chapters 2 and 3 is based on the style guide for the journal *Behavioural Brain Research*.

.

Table of Contents

List of Tables

Chapter 2: Phase 1

Chapter 3: Phase 2

List of Figures

Chapter 1

Chapter 2: Phase 1

Chapter 3: Phase 2

CHAPTER 1: INTRODUCTION

The present thesis builds on the premise of several decades of research regarding the neurobehavioral effects of methylmercury (MeHg) exposure. Specifically, the thesis herein explores the potential neurobehavioral effects of chronic, adult-onset exposure to low levels of MeHg, as might occur by regular seafood consumption, and especially interactions between MeHg exposure and consequences for neurobehavioral processes during normal aging. Focus is placed on the potential for such MeHg exposure to affect nigrostriatal dopamine (NSDA) neuronal function in the substantia nigra pars compacta (SNpc) because these neurons, and their associated afferent and efferent projection regions, are well-known to play a role in the development and severity of many age-related diseases (ARDs) and neurodegenerative disorders (NDs), most notably, Parkinson's Disease (PD). Genetic mutations have been identified in familial PD, but the majority of cases of PD are sporadic (Schapira, 2008). Substantial epidemiological evidence suggests a role for environmental contaminants in PD (Weiss, 2008, 2011; Weiss et al., 2002; see Chin-Chan et al., 2015 for a review), but, to date, no specific environmental agent has been shown unequivocally to be causative or act as a risk-factor. MeHg accumulates in the basal ganglia, a region associated with motor timing, motor speed, and a variety of cognitive/behavioral processes (Artieda et al., 1992; Malapani et al., 1994; Malapani et al. 1998, 2002; Pastor et al., 1992; Pastor et al., 1992), and may distort NSDA neuronal functioning in the SNpc (Faro et al., 2002; Moller-Madsen, 1991). It is the premise of this paper that chronic, adult-onset exposure to low-levels of MeHg may facilitate development of NSDA and SNpc dysfunction, leading to PD-like effects, especially in subjects with genetic or age-related susceptibility (i.e., acts as a risk-factor).

Given the well-known psychophysical properties of interval timing and the sensitivity of the processes underlying interval timing to degeneration and dysfunction of DAergic-related and Ca^{2+}-mediated processes in the SNpc, a timing preparation could be an exemplary method to quantitatively assess the potential mechanisms by which the above factors may affect the underlying neurobiological and behavioral processes. The present experiments examined the effects of chronic, adult-onset exposure to either 0 ppm or 5 ppm MeHg – an environmentally relevant level – on interval timing and time perception as assessed under the bi-peak interval (PI) or peak-interval choice (PIC) procedure using retired breeder (i.e., aged; 9 months) BALB/c mice. To investigate the potential role of Ca^{2+} homeostasis/regulation and elucidate possible mechanisms of protection or prevention of MeHg's potential neurotoxic effects on performance, the present study also examined the effects of concurrent chronic, adult-onset exposure to either 0 ppm or 2 ppm of the L-type Ca^{2+} blocker, Isradipine on PIC performance by the aged BALB/c mice. Finally, to isolate potential behavioral

mechanisms of MeHg's action and/or ISR's protection on PIC performance, theoretical and quantitative models of interval timing based on Killeen and Fetterman's Behavioral Theory of Timing (BeT; 1988, 1993) and Killeen, Fetterman, & Bizo's (1997) Signal Detection/Dispersion Model of timing were applied to the data. The effects of MeHg and/or ISR on the parameters of these models were determined using an information-theoretic, model comparison approach (Burnham & Anderson, 2002).

1.1 OVERVIEW OF THE BACKGROUND AND LITERATURE REVIEW

Section 1.2 will provide the context for subsequent descriptions and interpretations of interval timing data obtained under the PI and PIC procedures.

Section 1.3 will review the different preclinical procedures used to assess interval or immediate timing, while section 1.4 will review the robust behavioral properties of temporal responding under these procedures.

Section 1.5 will review one of the most prominent theories of interval timing, the Behavioral Theory of Timing (Killeen & Fetterman, 1988, 1993), in relation to the behavioral properties discussed in section 1.4. Due to the limitations of BeT in predicting some results obtained under the PI and PIC procedures, section 1.6 will discuss a relatively new model of interval timing, the Signal Detection/Dispersion Model (SDTD; Killeen et al., 1997), which builds on BeT, and circumvents many of the problems and limitations with most current theories and models of timing.

Subsequently, section 1.7 will review the defining signs and symptoms of PD and discuss the neurobiology underlying the disruptions observed in this disorder. Section 1.8 will examine PD in relation to the general aging process, discuss neuropharmacological ways in which PD can be delayed, attenuated, and potentially prevented, and offer interacting mechanisms responsible for the origin of PD.

Section 1.9 and 1.10 will discuss the potential role of exposure to the environmental neurotoxicant MeHg in the etiology of PD, while section 1.11 will review the neurobiology of MeHg's toxicity. Finally, section 1.12 will reexamine the structural and functional similarities in neurobiological and behavioral dysfunction between MeHg and PD, which provides a context for section 1.13: The aims and predictions of the two proposed experiments.

Section 2.1 provides information regarding the first phase of an experiment in which the effects of chronic, adult-onset exposure to either 0 ppm or 5 ppm MeHg on PIC performance of retired breeder (i.e., aged; 9 months) BALB/c mice was assessed early into exposure and when the target durations under a PIC procedure were 8-s (*Short*) and 32-s (*Long*), respectively. Further, to investigate the potential role of Ca^{2+} homeostasis and elucidate possible mechanisms of protection or prevention of MeHg's potential neurotoxic effects on performance, the present experiments also examined the effects of concurrent chronic, adult-onset

exposure to either 0 ppm or 2 ppm of the L-type Ca^{2+} blocker, Isradipine on PIC performance by the aged BALB/c mice. Thus, the first phase of the experiment assessed the effects of *early* MeHg exposure and potential protective effects by ISR on PIC performance by the aged BALB/c mice when the target durations were widely spaced (1:4 relative difference). Finally, to determine the underlying mechanisms by which *early* MeHg and ISR exposure potentially affect interval timing under the PIC procedure with widely spaced *short* and *long* target durations, a description of how the SDTD model of timing will be applied to the data will be provided.

Section 3.1 provides information regarding the second phase of the experiment in which the same mice and design were used, but the effects of chronic, adult-onset exposure to either 0 ppm or 5 ppm MeHg and 0 or 2 ppm ISR on PIC performance of retired breeder (i.e., aged; 9 months) BALB/c mice was assessed much later into exposure and when the target durations were changed to 12-s (*short*) and 24-s (*long*), respectively. Thus, the second phase experiment assessed the effects of *later* and *continued* MeHg exposure and potential protective effects by ISR on PIC performance by the even more aged BALB/c mice when the target durations were more closely spaced (1:2 relative difference). Again, a description of how the SDTD model of timing will be applied to the data will be provided, along with predictions and potential interpretations.

INTERVAL TIMING AND TIME PERCEPTION

1.2 TIME'S CAUSES

"*So, the question is: What is time? That we can buy it, find it, bide it, give it, kill it – in the right order – and measure it. It's a strange beast especially when you think in terms of measurement, because measurement historically means putting two things side by side and seeing if one sticks over the edge of the other. It is enigmatic because we are looking for things rather than things that hold things. These are accomplished facts; how can we put the past decade in correspondence with the past day? Even if we were to do that, how could we say that they are about the same length in time, but that one only seems longer than the other?"* (Quotes from a presentation given by Peter Killeen at the Society for the Quantitative Analysis of Behavior, 1999).

The present thesis will deal with time, how we as researchers measure it and interpret it, and why it is so often used to investigate underlying neurobehavioral mechanisms of action. Focus will first be placed on the nature of time, in particular, its fundamental relativity. Then it will be turned to the percepts that arise from time, that is subjective time or 'behavior's time:' How does an organism's behavior change as a function of physical time or what is the relation between changes in physical time with changes in an organism's

temporal percepts or subjective time? To help answer these questions, the foundation for theoretical and quantitative models relating physical time to changes in temporal percepts or behavior's time will be provided.

In the next few sections, focus will be placed on the proximate *whys* and *likes* of timing. In addressing the question of *whys* – reinforcing events –and of *likes* – theories and models – a survey of the landscape of contemporary interval timing theory is provided and then detailed consideration of a few leading theories will be discussed. First, an overview of the methods by which interval timing and time perception are assessed will be provided, with focus primarily placed on immediate timing procedures that require subjects to differentiate or distribute their responses in time in order to match a previously learned standard or target duration and those that require subjects to categorically scale their behavior/responses with respect to multiple target durations simultaneously available.

1.3 TIMING METHODOLOGY

The processes that allow animals to adjust their behavior to the temporal regularities of the environment have been studied using different procedures that model the relationship between physical elapsed time and behavior's perceptual or subjective time. Killeen and Fetterman (1988) proposed a taxonomy of interval timing based on the subject's location in time with respect to the temporal stimulus being timed. When an organism judges or classifies the duration of an elapsed temporal stimulus/interval the timing is termed retrospective (e.g., interval bisection); when the organism responds during an elapsing duration/interval the timing is immediate (e.g., PI and PIC procedures); and, finally, when it chooses between outcomes that are delayed in the future the timing is prospective (e.g., inter-temporal choice). Here, focus will be placed on the procedures designed to assess immediate interval timing or time perception.

1.3.1 Immediate Timing Procedures

In the human timing literature, when participants are asked to delay engaging in some response (e.g., depress a button) in order to match a previously learned standard or target duration, it is called temporal production or reproduction. Under Killeen and Fetterman's taxonomy, when a non-human organism responds during an elapsing target duration(s), the timing is immediate. In immediate timing procedures, the origin floats from the start of the temporal stimulus to the end, and the subject must continually estimate whether they are in the first, second, third, or etc. portion of the interval. The two types of immediate timing procedures relevant to the present thesis are the peak-interval (PI) and the categorical scaling or peak-interval choice (PIC) procedure, which are extensions of the fixed-interval (FI) schedule of reinforcement. The PI procedure involves ongoing timing of a single target duration, while the PIC procedure involves simultaneous timing of two or more target durations.

1.3.1.1 Fixed-Interval (FI) Schedule of Reinforcement. Under an FI schedule, responding delivers reward at a fixed interval after the offset of a 'warning' or trial onset signal, commonly called the conditional stimulus (CS); the duration of the interval between CS offset and the time after which responding produces reward is called the target duration. There are a number of ways in which the temporal control over FI responding has been characterized, including the latency to first response (the postreinforcement pause (PRP)) and the point during the FI when substantial responding begins (the break-point, break-run- or high-state of responding; see Killeen & Fetterman, 1988 for a review).

As noted many times before, neither the PRP nor solely the breakpoint is an ideal measure of timing (Killeen & Fetterman, 1988); they were originally designed simply to describe schedule performance (Platt, 1979). As shown empirically by Sanabria and Killeen (2009), which was originally proposed by Stubbs and Dreyfus (1981), FI schedules provide no standardized contingencies to discourage early or "untimed" responses (Gallistel, King, & McDonald, 2004). A more efficient measure of temporal control in these situations is to specify the entire distribution of responses over time, so as to calculate the mean and variance of the onset of responding or some other measure of its temporal pattern. Unfortunately, the direct calculation of these indices requires that such an entire distribution be available, uninterrupted by the deliveries of reinforcement. Two solutions to this inconvenience have been used: One is to use theory to determine a mean of the right descending limb of the distribution based on only the left ascending limb of the distribution; the other, the PI procedure, is to probabilistically reinforce responding at a target duration(s) and record data for the right limb of the distribution on nonreinforced probe or peak trials directly. The present study focuses on only the second method, as the first misses important aspects of the data at hand (see Killeen & Fetterman, 1988).

1.3.1.2 Single Peak Interval (PI) Procedure. The most frequently used, and most thoroughly analyzed, experimental paradigm for the study of temporal control over behavior is the single PI procedure (Catania, 1970; Cheng & Westwood, 1993; Cheng, Westwood, & Crystal, 1993; Church et al., 1994; Killeen & Fetterman, 1988; Roberts & Church, 1978). In the PI procedure, subjects are first trained to respond on a FI X-s across several sessions. Once reliable responding and clear temporal control over behavior has emerged, reinforcers are omitted on some trials, called peak interval (PI) trials. On these trials, the organism is permitted to respond beyond the standard FI target duration allowing for the rising and falling portions of the response distribution to be characterized. Usually PI trials last two- or three times the FI duration. On PI trials, organisms begin responding at some time before the previously learned target duration and stop responding at some point after that target duration has past, meaning responding on PI trials brackets the

previously learned target duration.

1.3.1.3 Peak Interval Choice (PIC) Procedure. Following the pioneering work on single PI procedures, it was necessary to expand the methodologies used to provide additional insights into the mechanisms of immediate interval timing. The peak interval choice (PIC) or categorical scaling procedure was first described by Killeen and Fetterman (1993) and elaborated in more detail in Fetterman and Killeen (1995). In their version of the procedure, three FI schedules ran concurrently so pigeons partitioned time across three target durations: Responses to one key were reinforced after a relatively short duration, to a second key after a relatively intermediate duration, and to a third key after a relatively long duration. This procedure is identical to the single PI procedure, but it requires subjects to simultaneously time multiple target durations, allowing for a complete response distribution to be characterized at multiple target durations on a trial-by-trial basis. In this procedure, reinforcement is primed for responding at only one of the three target durations on each trial, with reward opportunities equally distributed among the multiple operandum-target duration alternatives (see also Stubbs, 1976; Platt & Davis, 1983). After sufficient training, the subject begins by responding on the short target duration, and after sometime switches to the intermediate target duration, and finally, after additional time, switches to the long target duration. Thus, the temporal pattern of responding comes under a high degree of control by the spatiotemporal contingencies. Following sufficient training, PI trials are interspersed within each session, such that responding at any target duration does not result in reinforcement and the trials end after two to three times the longest target duration arranged. Identical to the single PI procedure, this allows for the characterization of the entire response distribution, but at each of the multiple and simultaneously available arranged target durations.

1.4 BEHAVIORAL PROPERTIES OF PI AND PIC TIMING

Under both the PI and PIC procedures, the peak strength or probability of conditioned behavior during PI trials summits at approximately the time at which reinforcement has usually been delivered in the past under the standard FI trials (Bevins et al., 1997; Bolles & Moot, 1973; LaBarbera & Church, 1974; Roberts & Church, 1978; White et al., 2000), which implies control by reinforcement latency over current behavior, as a result of experience with the procedure (Fantino, 1969; Gibbon, Church, & Meck, 1984; Killeen, 1975; Savastano & Miller, 1998). This peak response distribution commonly exhibits both systematic error in the mean and trial-to-trial variability (Gibbon et al., 1984). These parameters of the behavior differ from subject to subject (Gallistel & Gibbon, 2000), suggesting their utility in genetic screening and susceptibility to age-related declines, toxicological, pharmacological, and environmental manipulations.

1.4.1 Single PI Procedure

Original analyses of PI and PIC timing were concerned with changes in response rates as a function of PI trial time at a given target duration: Response rates on individual PI trials were binned into, most frequently, 1 – 3-s intervals as function of PI trial time and then averaged across many of those individual trials to produce a mean response rate distribution at a particular target duration. As recognized by many researchers in the late 80's and early 90's, although it is necessary for a theory/model to accurately account for these mean PI response rate functions, analyzing PI performance in this way obscures the underlying structure of interval timing that occurs on a trial-by-trial basis. As demonstrated by Schneider (1969; *cf.* Hanson & Killeen, 1981), performance on individual standard FI trials is well-characterized by a 'low-high' or 'break-run' pattern of responding and, likewise, performance on PI trials is well-characterized by a 'low-high-low' or 'break-run-break' pattern of responding (Cheng & Westwood, 1993; Cheng et al., 1993; Church, Gibbon, & Meck, 1984; Gibbon & Church, 1990, 1992; Hanson & Killeen, 1981). Specifically, on any given PI trial, PI responding can divided into three mutually exclusive and exhaustive intervals: 1) an initial duration during which the subject is disengaged from responding more often than engaged, 2) a 'run' duration during which the subject is responding more often than not, and 3) a final duration during which the subject is again disengaged from responding more often than engaged. The duration during which responding occurs at a high-rate corresponds to the 'run' of high frequency, discrete responses identified by Schneider and later in the pioneering work of Hanson and Killeen (1981) and Church et al. (1994) in the analysis of individual trials in the PI procedure. As demonstrated here, the smooth, bell-shaped mean response rate functions obtained under PI procedures are then the result of averaging many uniform start and stop distributions which occur on a trial-by-trial basis.

Using the individual PI trial analysis, performance on each PI trial can be characterized by the time at which the subject begins to respond at a high rate – the start time of a run – and the time at which the subject ceases to respond at a high-rate – the stop time of a run. From this, researchers can define the middle or center of the run state, c = [(start + stop)/2] and the duration of the run state, s = (stop – start), called the *dwell* time or *spread*, on each individual PI trial. Calculating the start, stop, center, and spread of a run on each individual PI trial then yields distributions of starts, stops, centers, and spreads of runs at a particular target duration. Once these distributions have be obtained for a particular target duration, the mean start, stop, center, and spread of runs can be calculated, in addition to the variability, standard deviation, and coefficient of variation (CV; standard deviation/mean) of each of these distributions. Normalized peak curves, showing the probability a run was in progress as a function of PI trial time, can then be calculated by subtracting the cumulative distribution of stops (falling phase) from the cumulative distribution of stops (rising

phase) obtained from individual PI trials at a particular target duration. In the mouse, as in the pigeon, the rat, and the human, the start and stops of runs on PI trials vary from trial to trial. Thus, when averaged over many PI trials, the probability that a run is in progress rises to nearly unity when some proportion of the target duration has elapsed, then returns to near zero as the duration of the PI trial becomes considerably greater than the target duration.

Using mean, normalized peak curves, researchers have identified near ubiquitous properties of interval timing under the single PI procedure. Notably, normalized peak curves from sessions arranging different target durations nearly superpose when plotted against the elapsed proportion or relative/normalized PI trial time (Gibbon, 1977; Killeen & Fetterman, 1988; Gallistel et al., 2004). In accordance with Weber's psychophysical law for time, as the physical, to-be-timed target duration increases the mean of the start and stop distributions, and, thus, the center of the peak curve, and their standard deviations each increase proportionally, so that peak curves from different target durations overlap or superpose when plotted on relative axes (see Gibbon et al., 1997 for an example). This relationship between length of a target duration and both the center and spread of peak curves is known "Scalar Property." This means that both the locations (central tendency) and spreads (standard deviation) of the start and stop distributions, and, thus, the resulting peak curves, are nearly fixed proportions of the target durations. Scalar variability – variability of start and stop distributions and the spread of peak curves proportionate to the target duration – is a ubiquitous feature of timing under the PI procedure using this analysis (Gibbon, 1977, 1991, 1992; Killeen & Weiss, 1987). Scalar variability is most often demonstrated by calculating the coefficient of variation (CV) – the standard deviation of the start/stop distribution or spread of the peak curve divided by its respective mean – at different target durations. Accordingly, if variability or the spread of start/stop distributions and peak curves is scalar, start/stop/center CVs remain constant across different target durations (Gibbon, 1991).

A second ubiquitous finding is that the superposed peak curves are not centered directly about the target durations (which is at 1 on the normalized axis). This means that the average center of peak curves deviate from the target duration; systematic error in the control over timed behavior by the target durations. Interestingly, this systematic error is also usually proportional to the target duration, a phenomenon known as 'scalar error.' The difference between systematic error and trial-to-trial variability in timing is the same as the distinction between systematic and random error in, for example, statistical variables. It is the distinction between the location of the mean response rate function relative to the target time and its spread.

Figure 1 shows normalized peak curves from a C57Bl/6 mouse run in our laboratory's version of the PI procedure. Trial onset was signaled by an auditory stimulus in an operant chamber modified to

accommodate mice. A lever-press triggered the insertion of a dipper into the chamber at or after the target duration had elapsed. Once reliable responding at each target duration was established, PI trials were arranged across blocks of several sessions. The same subject was tested in blocks of multiple sessions at each of four different target durations – 8, 12, 24, and 32-s, respectively (order of presentation was 8-s, 32-s, 12-s, & 24-s). These normalized peak curves from sessions with different target durations nearly superpose when plotted against the elapsed proportion of the target duration (relative or normalized trial time) (Gibbon, 1977; Killeen & Fetterman, 1988; Gallistel et al., 2004). This means that both the peak locations (central tendencies) and the spread (standard deviation) of the start and stop distributions and resulting peak curves were nearly fixed proportions of the target durations, demonstrating scalar variability, which is Weber's law for time (Gibbon, 1977). Also as with mean response rate functions, the superposed plots are not centered about the target duration (which is at 1 on the normalized axis). This means that the average center of a run, the halfway between start and stop, deviated significantly from the target duration; in the case of the C57Bl/6 mouse, all target durations tested tended to be slightly overestimated (later than 1 on relative axis in Figure 1). Again, this phenomenon is called systematic error in the temporal control of behavior and this systematic error was also proportional to the target duration, known as scalar error. In sum, under the single PI procedure, scalar timing is a robust finding, no matter how the data are analyzed. As will be discussed below, there are some exceptions to these findings when more fine-grained analyses are used. These and similar results are discussed in more detail below.

1.4.2 PIC Procedure.

In the original article, Killeen & Fetterman (1995) trained pigeons on a tri-PIC procedure; in doing so they simultaneously reproduced many of the findings observed under the single PI procedure, mentioned above, and introduced new findings, some of which contradict Weber's law for time and scalar timing. First, they showed that absolute and relative response rates on each of the three keys were an orderly function of time, showed approximately proportional changes with changes in the target durations, consistent with Weber's law and scalar timing, and showed small systematic, but scalar errors. Contra to Weber's law and scalar timing, however, the standard deviations of the times at which subjects switched between successive keys increased more slowly within a base of three target durations, where the average rate of reinforcement in the context was constant, but across bases arranging three different target durations, where the average rate of reinforcement changed, standard deviations increased proportionally, as predicted by Weber's law and scalar timing. Importantly, they also showed that increases and decreases in reinforcement probability/density produced both transient and longer lasting changes in the PI psychometric functions.

Specifically, when the probability/density of reinforcement in the context was increased, it produced an abrupt leftward shift in the peak curves – underestimation of the target durations – while decreases in reinforcement probability/density shifted response distributions rightward – overestimation of the target durations. Interestingly, after approximately 15 sessions of exposure to these changes in reinforcement probability/density, the pigeons adjusted or recalibrated their timing. For example, the initial leftward shifts in the peak curve induced by an increase in reinforcement probability/density were followed by a readjustment of the peak curves rightward towards the pre-shifted baseline. These and similar results are discussed in more detail below.

1.5 THEORIES AND MODELS OF INTERVAL TIMING

Many models of timing posit a special-purpose pacemaker-counter or clock mechanism (e.g., Treisman, 1963; Church et al., 1992). In these systems, one component of the clock, the pacemaker, emits pulses and another, the counter, accumulates said pulses. Percepts of elapsed time or subjective time, referred to wholly as '*behavior's time,'* are represented as a tally of pulses in a count register, with temporal responses based on a reading of this tally. Such neurobehavioral clocks somehow provide information to organisms and researchers by indicating when and where events occur and where in the order of the occurrence of events organisms are located. To keep these events organized, labels with intrinsic ordinal properties are invoked. It is easier to know that 4 comes after 3 than it is for Kendrick Lamar to come after Tupac Shakur; numbers are better than names when it comes to clocks and time. Thus, when researchers are interested in time or timing, they are interested in how events or behavior in a temporal context change with time. Clocks point to these labels, but what happens between these labels; what happens between one event and the next for a particular neurobehavioral clock? Further, how does physical time change as a function of changes in the percepts of time represented by neurobehavioral clocks or *visa versa*?

The following section will review and discuss one of the most important and well-tested theories of immediate timing that has sought to answer the above questions, the Behavioral Theory of Timing (Killeen & Fetterman, 1988; BeT). Much research has clearly demonstrated that organisms embody and emit regular processes that can be correlated with standard time: Heartbeats, respiration, theta rhythms, neuronal firing, lever-pressing, key-pecking, etc., all fulfill the aforementioned statement. As such, organisms must have what could properly be called clocks and these clocks give rise to the percepts of time and govern the subjective or behavioral scale of time for the organisms under study. Further, research has also shown that under PI and PIC procedures, in which no external stimuli are arranged in a functional manner with time, PI responding is better predicted by time, or the subject's behavior in time, than by any other external stimuli in the

environment because that environment has been rendered barren (Killeen & Bizo, 1990). This strongly suggests that some component(s) of the neurobehavioral clock must be internal in nature. Accordingly, the theory and model discussed below (BeT), assumes that some sort of pacemaker-counter or clock system governs the subjective and behavioral time of organisms under study. As mentioned briefly in section 1.4, research definitively illustrates that subjective or behavioral time is relative; relative to the contingencies/contexts of reinforcement with which researchers ask subjects to read their clocks. Thus, the theories and models discussed below specify which internal clock governs subjective or behavioral time and posit if and when the nature or class of the neurobehavioral clock depends on the contingencies of reinforcement for timing and the concurrent neurobiological state of the organism.

1.5.1 The Behavioral Theory of Timing (BeT)

As the name hints, BeT places a special emphasis on the role of behavior – different response classes, nontarget and target – unfolding throughout a temporal interval in mediating timing. These different nontarget response classes are presumed to act as conditional/discriminative stimuli for subsequent nontarget responses and, finally, the target response (i.e., FI/PI responding) – they are digits on the counter. BeT's core assumptions were heavily influenced by research on so-called adjunctive (i.e., nontarget behavior), beginning with the seminal work of Staddon and Simmelhag (1971). Although not reviewed here, it is important to note than many researchers now agree that what had previously been referred to as adjunctive behavior is actually nontarget behavior that has been strengthened, via the delay of reinforcement gradient, by its proximity to reinforcement delivered for target responding. Effectively this means that classes of so-called adjunctive behavior are indeed classes of operant behavior that are just not the target response (see Killeen & Pellón, 2013 for a discussion). Regardless, what has become clear is that behavior measured by switch closures (target behavior) constitute only part of the behavioral repertoire strengthened by various schedules of reinforcement, especially period schedules such as FIs. After researchers began to open up the chambers and watch their subjects behave, we observed a) that animals engaged in a panoply of different behavioral classes, nontarget and target, and b) that these classes of behavior were highly regular in time and could be described by simple quantitative models (Killeen, 1975). In accord with BeT, such structure affords the possibility that a subject's behavior may come to serve as discriminative/conditional stimuli that help predict the subject's position in time relative to upcoming reinforcement.

As in most theories of timing – specifically, pacemaker-counter or clock theories modeled after Creelman (1962) and Treisman (1963) – transitions between different behavioral states are caused by pulses from a Poisson pacemaker. The underlying Poisson process means that there is a constant probability that

an organism will move from one behavioral state to the next that is uniform across states, but several such pulses or transitions may be necessary to arrive at a new class of behavior. That is, each of the behavioral states may be of variable duration, a single response class may be correlated with just one or several states, and the rate of the response classes in the state(s) may be of variable duration. A pulse from the Poisson pacemaker might occur before the organism even has a chance to emit the behavior characteristic of a particular state, thus making behavioral states propensities to response, but not the different classes of observed responses themselves. The proximity among a mediating class of behavior, the target timing response, and reinforcement evolves with repeated exposure to a target duration; classes of behavior that facilitate timing and thus aid the acquisition of reinforcement will become more strongly conditioned than those classes of behavior that are less proximate to reinforcement.

To summarize, when the rate of reinforcement and other sources of arousal are constant, the speed of the pacemaker is also constant and the central tendencies and variability of peak responding are governed by Poisson timing. If, however, the rate of reinforcement is varied, there is a concomitant change in pacemaker rate then the central tendencies and variability of peak responding each grow proportionally with time and target duration and, thus, while governed by a Poisson process, result in scalar timing or Weber's law. In order to achieve pure Weber and scalar timing, BeT assumes that the changes in pacemaker rate are proportional to the changes in reinforcement rate. As noted briefly above, this is seldom precisely true. How can the flatter linear relation observed between inferred pacemaker speed and reinforcement rate be reconciled? Killeen et al. (1997) first noted that pure Weber or scalar timing under PI and PIC procedures is also the exception; there is usually only a linear relation between the standard deviation of PI responding and the intereinforcement interval, in which case a linear relation between pacemaker rate and reinforcement rate is the predicted mechanism. Second, if there is any constant error in peak responding – for example, in estimating the criterion to start, stop, or switch – variability will grow more slowly than proportionate to the rate of reinforcement or target duration to-be-timed. Killeen et al. (1997) assumed that this constant error is proportional to the criterion in question (e.g., start or stop) and, thus, the additive constant will be larger when investigating stops than starts and each larger at longer than shorter target durations. This source of criterial error is very similar to the error in accessing reference memory posited in SET. Third, Killeen and Weiss (1987) showed that Weber-like error in timing may derive from Weber-like error in the counter. In relation to BeT, this means that sometimes subjects must skip a mediating state; and sometimes they remain in a state for more than one counted pulse (see Reid et al., 1993). Moreover, to obtain Weber-like variance in peak responding, the magnitude of these counter errors must increase with the number of counts (i.e., longer

target durations). Alternatively, it is plausible that as a PI trial wears on, arousal decreases, causing a within-trial decrease in pacemaker speed. Indeed, Fetterman and Killeen (1995) showed that response rates were lower for longer target durations than shorter ones. Poisson changes in timing plus linear changes in arousal and pacemaker speed within a PI trial could lead to the parameters found appropriate for these data in Killeen et al. (1997). Thus, Weber-like error will dominate at intermediate and long intervals, when pacemaker speed, and, thus, pacemaker error, is small, and when the rate of reinforcement in the context is changed. At short to intermediate durations and/or when the rate of reinforcement in the context is constant and multiple target durations are required to be timed, Poisson error will dominate; at very short target durations, constant error will rule.

1.5.1.1 Limitations of BeT. Although the augmented version of BeT (Killeen & Fetterman, 1993) resolved many of the limitations of the original version (Killeen & Fetterman, 1988), the first limitation to this theory is the consistently observed less-than-proportionate changes in pacemaker speed with reinforcement rate and arousal. Although Killeen and colleagues have posited several ways such less-than-proportionate changes may occur, nearly all remain to be tested. Second, although the augmented version of BeT predicts the negative start-spread correlation of peak responding, some studies have shown that the inclusion of a movement latency or transit time parameter does not improve fits or predictions enough to justify its inclusion, which implies that different behavioral states or classes may have different such latencies, with different variability, which would complicate the model. Third, BeT has not specified the well-documented, differential sensitivity of start and stop times and start/stop variability to changes in target durations or under the single PI vs. PIC procedure (Gallistel et al., 2004). As noted by Killeen himself, there is no obvious map relating changes in overall reinforcement or changes in target durations with the observed differential sensitivity of start and stop times and start/stop variability to these factors. That is, while BeT more than adequately predicts and accounts for changes in the peak curve with nearly all manipulations discussed, because the model is inherently concerned with the run or dwell distributions of different classes of behavior, carried by *n*, the criterial count, it would be necessary to include a criterial count for the start of peak responding and a separate criterial count for the stop of peak responding and potentially different start and stop criterial counts for different target durations or under different procedures, as mentioned above. While this is a plausible way to reconcile this limitation, it clearly adds several free parameters than may not increase the goodness-of-fit enough to justify their inclusion.

Finally, and probably the biggest limitation to BeT, as in SET, is that BeT assumes the worst possible pacemaker – a purely random pacemaker driven by a Poisson process – and the most accurate counter – all

pulses from the pacemaker are accumulated/counted; none are dropped or added. As mentioned above, this type of Poisson clock becomes more accurate the faster the rate of the pacemaker and, if the rate of reinforcement controls the rate of the pacemaker in a linear manner, then increasing the target duration, thus decreasing the rate of reinforcement, slows the pacemaker and decreases the accuracy of the clock. This is how BeT arrives at Weber's law for time or scalar timing. Further, when the rate of reinforcement is constant, as in the PIC procedure, then BeT predicts that the rate of the pacemaker should be constant and, thus, the relative accuracy of timing increases as the number of counts increases. That is, the standard deviation of a temporal estimate grows as the square root of its duration according to Poisson timing and, thus, variance in timing a target duration grows more slowly as it increases than predicted by Weber's law and scalar timing. Real clocks, however, do not become more accurate the faster the emit pulses, nor does relative accuracy increase with time counted. Instead, with real clocks, as with subjects' biological clocks whose pacemaker rate changes with target duration and rate of reinforcement, the relative error is approximately constant; real clocks demonstrate Weber's law and scalar timing. Thus, random pacemakers emitting pulses according to a Poisson process cannot generate scalar timing unless the rate of the pacemaker is tied to changes in the rate of reinforcement. Additionally, it is highly unlikely that the counter – the behavioral states in BeT – is perfectly accurate. Because it is implausible that the worst possible pacemaker – a Poisson pacemaker – drives the best possible counter – a perfectly accurate counter – even when assuming that the rate of the pacemaker is tied to the rate of reinforcement, the necessary variance to generate scalar timing and to result in a biologically more plausible clock for interval timing must be found in the counter. Biological timing, that referred to as immediate timing here, is most accurate for a narrow range of pacemaker speeds (Fetterman & Killeen, 1990), above which it shows proportionally increasing error or scalar timing, most notably under single PI procedures. Killeen (2002) showed that stochastic counters – counters that add or drop counts with an exponentially increasing probability as a function of the number of counts, time, or use – provide a mechanism for scalar timing that is lacking in both the perfectly accurate counters of BeT and SET. Although this sort of model is beyond my knowledge, Killeen et al. (1997) provided a simpler model that can account for both scalar and Poisson timing, in addition to our sources of error in biological systems, which will be discussed next.

1.6 A GENERAL MODEL FOR PACEMAKER-COUNTER ERROR

1.6.1 Signal Detection Theory

In any type of discrimination, including the temporal discriminations of interest here, researchers arrange for subjects to respond to one or more alternatives corresponding to the state of the environment as

they sense it. In FI/PI procedures, we train subjects to begin responding on an alternative when the time reinforcement has been delivered in the past 'close enough' and stop responding when that time is 'far enough' away. This results in two ways for the organism to be 'correct' and two ways for the organism to be 'incorrect:' if a FI/PI trial is presented and the organism responds at the appropriate time, reinforcement will be delivered or peak curves will bracket the target time (HIT); if no trial is signaled and the organism does not respond, then no reinforcement will be lost and accurate timing will be upheld (CORRECT REJECTION); if a trial is presented and the organism responds at an inappropriate time, reinforcement will not be delivered and peak curves will not bracket the target time (MISS); if a trial is not presented and the organism responds, reinforcement will be lost and timing may become distorted (FALSE ALARM). This recognition that there are two ways to be 'correct' and two to be 'incorrect' under PI procedures is the hallmark of Signal Detection Theory (SDT).

1.6.2 Percepts and Discriminal Dispersions

Let's denote the physical length of a temporal stimulus or target duration as S_n and the location on a physical scale that corresponds to a subjective criterion (i.e., start/stop/switch) as S_x. Then let P_n and P_x be the subjective perceptions ('percepts') corresponding to these physical stimuli. Under PI and PIC procedures, the subject evaluates the percepts of current time relative to the percepts corresponding to the start/stop criterion, which are determined by the percepts generated by the physical target duration(s) arranged, and this determines peak responding. Under PIC procedures only, the subject may just evaluate the percepts of current time relative to the percepts corresponding to physical lengths of the *short* and *long* target duration and responds at the *long* target duration whenever the percept exceeds some criterion (i.e., switch criterion). In any case, if the physical target durations or criteria gave rise to equally precise and replicable percepts, peak responding would be perfect, but this is almost never the case. Whence, then, is the error in timing? There is error in the physical characteristics of the contextual stimuli: Perceptions of visual wavelengths near absolute threshold, phase and ramp in auditory stimuli, etc. There is also 'actual' error that occurs when a biological system is required to time a temporal stimulus or target duration, with some instances of P_i shorter than the target duration that gave rise to it, and on other occasions more characteristic of longer times. Thurstone (1927, a, b; see also Guilford, 1954) called the totality of such processes that give rise to a distribution of different percepts in the presence of the same stimulus the *discriminal process*. He redefined the scale of the x-axis so that the distribution of the percepts fit a predefined (most often normal) distribution, whose standard deviations he called *discriminal dispersions*. Elevating a distribution of error to the status of an international standard of measurement was an amazingly bold and seminal idea.

1.6.2.1 Three Models of Discrimination on a Metathetic Continuum. How can an organism respond under PI and PIC procedures in order to maximize a variable such as the information regarding the precision and accuracy of timing to the experimenter or the reinforcement provided for such? For simplicity, let's consider a bi-PIC procedure; under a bi-PIC procedure, call the shorter target duration S_1, the longer target duration S_2, the criterion to switch from responding on the *short* to responding on the *long* S_c; and call the percepts for the shorter target duration P_1 the longer duration P_2, and the criterion P_c. One strategy under this bi-PIC procedure would entail responding on the longer target duration (S_2) whenever the percept for current time is greater than the average percept (P_1) for the shorter target duration (S_1); this strategy is suboptimal, as half of the time the shorter target duration itself will generate percepts that exceed P_1. If reinforcement is provided equally for responding on each alternative, symmetry suggests that the subject performs best if it responds on the longer target duration whenever the percept for current time exceeds the point on the perceptual dimension at which the densities of percepts for the shorter and longer target duration cross (P_c). If, however, reinforcement is greater (lower) for responding on the shorter than the longer target duration, the subject should move the criterion (P_c) for responding at the longer target duration to the right (left) or later (earlier) in time.

In Thurstone's original analyses, carried forward by nearly every researcher that has fitted a normal distribution to PI-type data, the discriminal dispersions of percepts at different target durations or different times were proposed to fall on a metathetic or qualitative continuum (Stevens & Ganter, 1957), where the standard deviation of the percepts is constant across changes in physical time. Figure 2 (continuous curves) shows the discriminal dispersions on a metathetic temporal continuum, where the standard deviation of the percepts arising from an 8-s (*short*) target duration is equal to the standard deviation of percepts arising from a 16-s (*long*) target duration. If reinforcement has been distributed equally for responding on the two alternatives and the subject is unbiased, the temporal continuum will be partitioned at 12-s (the *Point of Subjective Equality* [PSE]), with percepts <12-s categorized or responded with respect to as "*short*" and percepts >12-s categorized or responded with respect to as "*long*."

In accord with these original analyses, once the criterion for switching from *short* to *long* (P_c) is established (the *PSE*; located at 20-s in Figure 2), it is represented as a distribution on the perceptual continuum, usually with zero variance; invariant bisections of the axis represented by a single, vertical line at the point at which the percept densities for each target duration cross. If there is no variance in the criterion, then the probability of responding at the long target duration as a function of time – the psychometric function – can be derived from the integral of the temporal percepts' densities, shown in the top panel of Figure 3.

If the perceptual continuum remains metathetic, as many would propose it does, then the previous model is equivalent to another, quite different model: There is no variance in the percepts of time, but there is fluctuation and variance in the criterion to switch from responding *short* to responding *long* (bottom Panel of Figure 3). Note that, because these discriminal dispersions are not observed, the two models – variance in the percepts, but not the criterion, or variance in the criterion, but not the percepts – are empirically indistinguishable on the basis of simple psychometric functions.

Finally, both of the previous models are equivalent to a third model in which there is variance in both the percepts of the target duration and the percept of the criterion. As noted by Killeen et al. (1997), as long as a metathetic continuum is proposed to underlie these dispersions – one where the standard deviations of percepts are constant across changes in target duration and criterion – these three models are empirically equivalent.

1.6.3 The Psychometric Function

In general, the psychometric function for timing data relates the cumulative probability of making a certain response at a particular target duration (e.g., start or stop) as a function of PI trial time. In the above examples, under the both the single PI and PIC procedures, psychometric functions can be mapped out for the probability of both the starts of responding and the stops responding at one or more target durations. Using a bi-PIC procedure, a psychometric function is often mapped out only for the probability of responding at the longer target duration as a function of PI trial time. Under both types of procedures, the difficulty of the particular discrimination of interest is given by the flatness of the ogives, as measured for the distance required for the curves to extend from the mediation to the 75^{th} percentile, known as the traditional difference limen (DL), or the 84^{th} percentile, which is a DL of one standard deviation if the fitted distribution is normal. The Weber fraction, a measure of relative inaccuracy, is the DL of one standard deviation (84^{th} percentile) divided by the mean of the ogive, in which case it is also known as the CV. As mentioned several times above, Weber's law states that the Weber fraction and CV are invariant over changes in time or the target duration.

1.6.4 The Dispersion Function

Fetterman and Killeen (1992) showed that the standard deviation of temporal estimates is relatively constant below target durations of 0.20-s, but at target durations greater than this point, the standard deviation of temporal estimates grows proportionally to the length of the target durations. Thus, Weber's Law – proportionality of the standard deviation of temporal estimates to its mean – holds for moderate to long target durations. There is an important inconsistency in the above formulation of the great psychophysicists

such as Thurstone and Fechner: The phi-gamma hypothesis posits that the temporal percepts fall on a metathetic continuum or that the standard deviations of temporal percepts are constant across increases in time or target durations; yet Weber's law posits, and nearly all timing data demonstrate, that the standard deviation of temporal percepts grows proportionally with increases time or target durations. Thus, the above discussions, and many psychophysics and timing researchers, have applied models based on the phi-gamma hypothesis (e.g., normal distribution), that is, those appropriate for a metathetic continuum to time, which by virtue of Weber's law and analysis is demonstrably a prothetic continuum. Because the data show that Weber's law holds true, the phi-gamma hypothesis and proposition of an underlying metathetic continuum must be false. The discriminal dispersions of temporal percepts are not congruent with time (as in Figures 2 and 3), but the standard deviations of these dispersions grow proportionally with time and target duration (a prothetic continuum as shown in Figure 4) according to the dispersion function:

$$\sigma_t = \sqrt{(\omega t)^2 + \rho t + c^2} \qquad Eq.\,2\ (Killeen\ et\ al.,\ 1997).$$

Equation 2 was derived by Killeen and Weiss (1987) as a general model of variance in interval timing that is generated by any sort of pacemaker-counter system. The parameter ω is the Weber Fraction, and Killeen and Weiss (1987) showed that its value is determined solely by error in the counter. For intermediate to long durations ωt dominates so that changes in the standard deviation of peak responding become proportional to changes in t: $\sigma_t \approx \omega t$. This is Weber's Law for time or scalar timing. The parameter ρ reflects the speed of the pacemaker and magnitude of pacemaker variability, and also some components of counter variability, such as if counts are added or dropped according to a Bernoulli process. If the pacemaker emits pulses according to a Poisson process, as assumed in BeT, there is a constant probability a pulse will be emitted at any instance in time. Then the interpulse interval is exponentially distributed, with a standard deviation equal to the average period of the pacemaker. It follows that ρ would equal 1 (assuming no other sources of variance); if the pacemaker is more regular than a Poisson emitter, then p will be less than 1. Note, however, that as long as p is greater than 0, and ω is small, the standard deviation of the pacemaker's period is proportional to its period, and the error in the pacemaker follows Weber's law. As mentioned above, however, because the pacemaker's growth in error follows Weber's law does not ensure than the clock system of the subject as a whole will also. According to Eq. 2, BeT would predict that the value of p changes proportionally with the rate of reinforcement and, in this case (if ω is small), increases in the value of p with increases in target duration would predict proportional growth in the standard deviation of temporal estimates, thus fulfilling Weber's law and scalar timing. If the rate of reinforcement remains constant and multiple target durations are to-be-timed, as in the PIC procedure, and p is greater than 0 and ω small, then the standard

deviation of temporal estimates will show less than proportional growth relative increases in t: $\sigma_t = \sqrt{pt}$. This is Poisson timing.

The constant c in Eq. 2 reflects a constant error in the counter, such as that stemming from mapping discrete counted pulses onto the temporal continuum or synchronizing counts at the start and end of a PI trial, and may also include constant variance caused by inconsistency in the location of start/stop or switch criteria. This constant error, c, dominates at very short target durations, so that the standard deviations of temporal estimates are approximately constant below these very short target durations. Rather than treat c as a free parameter, however, Killeen et al. (1997) assumed that it was comprised primarily of error in estimating the location of start/stop or switch criteria, and subject to the same dispersion function as the estimation of real time. According to this assumption, its contribution to the standard deviation is simply the Weber fraction parameter, ω, times the location of the criterion, μ, and/or, under certain conditions, it may be the square root of the Poisson parameter, ρ, times the location of the criterion, μ. As noted by Killeen et al. (1997), either of these methods may underestimate the true value of c because fractional error in the counter arising from the synchronization of the beginning and end of intervals is left out, and reasons it may overestimate the value, such that its error could decrease by the inverse square rule as a function of experience (Gibbon & Church, 1990). In various applications of the dispersion function (Eq. 2), however, the above assumptions have proven more parsimonious and close enough to the fits achieved with c as a free parameter. Thus, by setting the constant error proportional to the time of the start/stop criteria, within either a Poisson, Weber, or combination of the two PLM, the additive constant will be larger for stop criteria than start criteria and each larger, overall, when peak responding at longer target durations is assessed.

1.6.5 The Pseudo-Logistic Model (PLM)

In order to achieve a coherent analysis and accurate description/prediction of psychometric and peak functions under the PI and PIC procedures, only dispersions whose standard deviation increases proportionally with time/target duration according to Eq. 2 are fitted. One method involves calculating the probability corresponding to the deviations of each percept (P) at time t or target duration T (e.g., target duration) from a criterion (C; e.g., start/stop or switch) divided by the standard deviation of each percept at time t. This logic requires multiple discriminal dispersions, one centered over time point t or target duration T). The equation it generates, however, is equivalent to a single psychometric function centered at the criterion, C; this method calculates the probability corresponding to the same deviation mentioned above, with the mean of that single ogive now located at the criterion C, rather than over each of the percepts at time t or target duration T (Figure 4):

$$p = \left[1 + e^{\left(\frac{\mu - t}{0.55\sigma_t}\right)}\right]^{-1}, \qquad Eq.3 \text{ (Killeen et al., 1997)}.$$

The multiple-densities treatment is most vital: it asserts that there is variance in the percepts of all temporal durations and that variance follows Eq. 2.

1.6.6 Applications of the PLM to Single PI and PIC Data

To apply the PLM to peak responding and predict normalized peak curves from the single-PI procedure first requires that Eqs. 2 and 3 be fitted to both the cumulative start and stop distributions at a particular target duration. To generate normalized peak curves from predicted start and stop distributions using Eqs. 2 and 3, one subtracts the PLM predicted distributions of stops from the PLM predicted distribution of starts, identical to the calculation of obtained normalized peak distributions (discussed in 1.4 above).

In summary, there is very good evidence for the behavioral processes assumed by BeT to exist and these are embodied in the parameters *p* and μ in the equations of the PLM. Other processes may also be necessary to predict changes in timing, such as changes in arousal level and error in the counter and start/stop criteria. The dispersion function (Eq. 2; Killeen & Weiss, 1987) is a simple model that accounts for changes in the variance of peak data under PI and PIC procedures depending on changes in different parameters, and, coupled with Eq. 3, the PLM provides a simple model of psychometric functions and peak curves that is consistent with the dispersion function and gives the various underlying processes expression, allowing for precise comparisons among different models of the PLM.

PARKINSON'S DISEASE (PD)

Parkinson's disease (PD) is a disabling neurodegenerative disorder that is strongly associated with aging, increasing exponentially in incidence above the age of 65 years (de Rljk et al., 1997; de Lau et al., 2004). The incidence of PD is expected to increase dramatically worldwide as life expectancy increases, but the cause of PD is unknown and currently there is no preventative or curative therapy.

1.7 DEFINING SIGNS AND SYMPTOMS

Overall slowing, in both motor (bradykinesia) and cognitive domains (bradyphrenia), is widely reported as the major behavioral deficits in PD (Benecke et al., 1986; Bloxham, Dick, & Moore, 1987; Evarts, Teravainen, & Calne, 1981; Flowers, 1976; Frith, Bloxam, & Carpenter, 1986; Hallet & Khoshbin, 1980; Malapani et al., 1994; Obeso, Rodriguiz, & DeLong, 1997; Worringham & Stelmach, 1990). However, interference and/or switching between alternative motor plans or classes of behavior or deficits in switching between different cognitive/behavioral strategies have also been linked to the major motor and cognitive Parkinsonian symptoms (Flowers, 1976; Malapani et al., 1994; Taylor, Saint-Cyr, & Lang, 1986). Said differently, bradykinesia and bradyphrenia may not be solely a general cognitive slowing, but rather a

consequence of interference from competing environmental events, classes of behavior, or 'memories.' One important feature of motor pattern execution that may contribute to difficulty in acquiring new motoric patterns or classes of behavior in PD is the necessity to inhibit previously learned alternatives. For instance, PD patients consistently err in psychological tests requiring switching between different motor programs/responses or cognitive/behavioral strategies (Benecke et al., 1986; Malapani et al., 1994; Robertson & Flowers, 1990; Taylor et al.,1986). Patients with PD also exhibit deficits in executing a designated sequence of behavior while at the same time suppressing an alternative, currently inappropriate or incompatible sequence (Frith et al., 1986; Worringham & Stelmach, 1990). Of special pertinence to the present paper, is that an early sign and symptom of PD are dysfunctions in temporal processing, timing, and time perception.

1.7.1 The Neurobiology of PD

The aforementioned motoric, cognitive, and behavioral signs of PD are clearly linked to the degeneration and death of substantia nigra pars compacta (SNpc) dopamine (DA) neurons (Hornykiewicz, 1966; Riederer & Wuketich, 1976), which subsequently results in lower levels of DA in the striatum (Marsden, 1992). Hence, DA deficiency in the SNpc and efferent projection regions may induce both cognitive/behavioral slowing and interference associated with competing and previously learned motor programs or classes of behavior. The efficacy of the clinical gold-standard treatment for PD, L-DOPA – a precursor to DA – is testament to the centrality of the DAergic system in the signs and symptoms of PD. As discussed later, intact DAergic functioning in the striatum underlies normal temporal processing, interval timing, and temporal perception and, thus, any impairment in this system would impact these processes (see Balci et al., 2009; Meck, 1996; Meck et al., 2007 for reviews).

1.7.1.1 Theories of Selective Vulnerability. The mechanisms responsible for the preferential loss of DA neurons in PD have been debated for decades. A widely held theory implicates DA itself, suggesting that oxidation of cytosolic DA (and its metabolites) leads to the production of cytotoxic free radicals, which are highly toxic and can cause cell death (Greenamyre & Hastings, 2004; Sulzer, 2007). There are problems with this hypothesis, however, including the fact that there is considerable regional variability in the vulnerability of DA neurons in PD, with some areas being completely lacking of pathological markers (Damier et al., 1999; Ito et al., 1992; Kish et al., 1988; Matsuk & Saper, 1985; Saper et al., 1991). Moreover, L-dopa administration, which treats PD by *elevating* levels of DA, does not appear to accelerate the progression of PD (Fahn, 2005), suggesting that DA itself is not a significant source of reactive oxidative stress (ROS), at least over a short-time span. Sulzer and colleagues have recently demonstrated that Ca2+ entry through L-type channels

stimulates DA metabolism in SNpc DAergic neurons, pushing cytosolic DA concentrations into a toxic range with L-DOPA loading (Mosharov et al., 2009). Thus, the general death or phenotypic decline of a variety of non-DAergic neurons in PID argues that DA itself is not likely the principle culprit producing the signs of the disease.

What has yet to be discussed, however, is why, in relation to PD, SNpc DA neurons should be more and selectively vulnerable to mitochondrial or ER dysfunction than any other neuronal type. Interestingly, there is no heterogeneity in these organelles across cell types and no evidence of selective regional expression of genes associated with familial forms of PD that are predictive of the progression and severity of the signs and symptoms of the disease (Moore et al., 2005b). One possible explanation, put forth by Surmeier et al. (2009, 2011), is that intracellular environment of these organelles exacerbates or activates the pathological potential of genetic mutations, environmental toxicants, and/or aging. A corollary explanation is the fact that SNpc DA neurons possess a unique phenotypic function that adjudicates them more vulnerable to disruptions in another pathway in comparison with other neurons. This explanation will be discussed in detail, next, in relation to Ca^{2+} functioning.

1.7.1.2 Ca^{2+} Functioning in SNpc DAergic Neurons. As discussed in detail elsewhere, Ca^{2+} regulation, in particular $[Ca^{2+}]$ homeostasis, is a common element that may act as a unifying mechanism resulting in the degradation and dysfunction of SNpc DA neurons observed in PD. Indeed, DA synthesis is stimulated by Ca^{2+}; as seen by the neurotoxic impact that can result from L-DOPA loading (Mosharov et al., 2009), and Ca^{2+} a chief modulator of the functions of mitochondria and the ER. Recent work has revealed that SNpc DA neurons exhibit a unique feature in the way they utilize Ca^{2+}. Unlike the vast majority of neurons in the brain, SNpc DA neurons are autonomously operational; conferring pacemaking activities that generate regular bursts of broad, slow action potentials in absence of synaptic input (Grace & Bunney, 1983). Such pacemaking activity is thought to be pivotal in maintaining ambient levels of DA in efferent regions innervated by SNpc neurons, in particular, the striatum (Romo & Shultz, 1990). SNpc DA neurons also engage ion channels that allow extracellular Ca^{2+} to enter the cytoplasm, while most other neurons rely singularly on monovalent cation channels (e.g., Na^{+}) to drive such pacemaking activity (Bonci et al., 1998; Ping & Shepard, 1996; Puopolo et al., 2007). For SNpc DA neurons, the above process thus leads to large elevations in $[Ca^{2+}]$ concentrations (Chan et al., 2007; Wilson & Callaway, 2000).

To be more specific, the SNpc DA neurons have distinctive Cav1.3, voltage-gated, L-type Ca^{2+} channels, that deliberate their pacemaking activities (Chan et al., 2007; Striessnig et al., 2006). This type of voltage-gated, L-type Ca^{2+} channel is relatively rare, constituting approximately 10% of all L-type Ca^{2+}

channels found in the brain (Sinnegger-Brauns et al., 2009). L-type Ca^{2+} channels with the Cav1.3 subunit differ from other L-type channels in that they open at a relatively hyperpolarized state, allowing them to contribute to the mechanisms underlying the autonomous pacemaking activity (Chan et al., 2007; Guzman et al., 2009; Puopolo et al., 2007). Based on studies illustrating the ability of L-type Ca2+ channel blockers to freeze such pacemaking activity, it was posited that L-type Ca2+ channels were essential for the SNpc DA neuron pacemaking activity, which rendered them less than ideal drug targets if such pacemaking was necessary to maintain neurobiologically important DA levels in target structures (Mercuri et al., 1994; Nedergaard et al., 1993). Recent evidence, however, has shown that at the concentrations necessary for such L-type Ca2+ blockers to terminate pacemaking, it also results in the antagonism of other L-type subunits and, further, other ion channels (e.g., Na^{+}), thus complicating the interpretations of previous studies.

At lower, channel-specific concentrations of L-type Ca2+ blockers, pacemaking endures in an unaltered rate and regularity, despite near total antagonism of the L-type channels (Guzman et al., 2009). Thus, the sustained pacemaking activity of SNpc DA neurons under these circumstances reflects the heartiness of the multichannel pacemaking system and that the Cav1.3 L-type Ca^{2+} channels play at least a supportive, if not pivotal role in such a process.

It is unclear why Cav1.3 L-type Ca2+ channels are found in significantly higher density in SNpc DA neurons than in neighboring DAergic neurons found in the ventral tegmental area (VTA) (Guzman et al., 2009; Khaliiq & Bean, 2010; Puopolo et al., 2007). These channels also participate in the postsynaptic response to synaptic activation and spiking of glutamatergic neurons, but it is modest in comparison with NMDA receptors (Blythe et al., 2009; Deister et al., 2009). As noted previously, it is plausible that entry of Ca^{2+} through L-type channels helps to regulate an adequate level of DA synthesis (Mosharov et al., 2009), but, as with burst spiking, this modulation seems not to be of major functional significance to the neurobiological system.

What is clear, however, is that the pacemaking activity resulting from sustained engagement of Cav1.3 L-type Ca^{2+} channels results in an obvious metabolic cost to the SNpc DA neurons. $[Ca^{2+}]$ is under very tight homeostatic control, due to its involvement in processes ranging from regulation of enzyme activity to apoptosis, with a cytosolic set point near 100 nM – 10,000 times lower than the extracellular concentration of Ca^{2+} (Berridge et al., 2000; Orrenius et al., 2003). When Ca^{2+} enters neurons, it is rapidly sequestered or pumped back across the steep concentration gradient of the plasma membrane, a process that requires energy stored in ATP and/or in ion gradients maintained with ATP-dependent shuttles. As might be inferred, utilization of $[Ca^{2+}]$ in cellular processes is several magnitudes more energetically taxing on a per charge

basis than monovalent ions, such as Na+, whose transmembrane concentration ratio is ~10X. In most neurons, however, this straining of energetic processes is not a significant issue as opening of Ca^{2+} channels is a relatively rare event, occurring primarily during very brief action potentials. Because of this, it makes the use of Ca^{2+} and its metabolic price easily manageable. That is, in SNpc DA neurons, where Cav1.3 L-type Ca^{2+} channels are open the majority of the time, the magnitude and spatiotemporal extent of Ca2+ influx is orders larger than in the majority of other neurons (Wilson & Callaway, 2000).

Recent work by Surmeier et al. (2009, 2011) and Guzman et al., (2009) illustrated that sustained opening of these Ca^{2+} channels in SNpc DA neurons creates basal oxidant stress within mitochondria (Guzman et al., 2010). With transgenic mice, these studies have illustrated that engagement of the CaV1.3 L-type Ca^{2+} channels during normal, autonomous pacemaking activity created mitochondrial oxidative stress and this was specific to the vulnerable SNpc DA neurons and not apparent in neighboring DAergic neurons of the VTA.

1.8 PD AND AGING: FUNCTIONAL SIMILARITIES AND UNANSWERED QUESTIONS

Cell loss and dysfunction associated with aging, and, age-related diseases is widely viewed to be a direct consequence of accumulated mitochondrial DNA and organelle damage produced by ROS and relative reactive molecules generated by the ETC during the course of oxidative phosphorylation. The work reviewed here, and as suggested by Surmeier et al. (2011), predicts that an acceleration in this decline in SNpc DA neurons because of their higher basal metabolic rate driven by the pacemaking activity of the unique CaV1.3 L-type Ca^{2+} channels. Indeed, research concerning the aging primate brain provides strong support for this notion (Collier et al., 2007). DAergic neurons in the primate ventral SNpc show clear phenotypic downregulation with advanced age in addition to signs of oxidant damage, where as neurons in the dorsal SNpc or VTA show little or no decline. Moreover, this distribution matches that seen in PD patients and in animal models following administration of MPTP or 6-hydroxydopamine (Collier et al., 2011). Importantly, this suggests that the mechanisms underlying the cell loss associated with normal aging and those underlying PD are, at the very least, similar and correspond to hypotheses that everybody would get PD if they lived long enough.

1.8.1 Can PD be Attenuated, Delayed, or Prevented?

Although there are several factors governing the loss and dysfunction of SNpc DA neurons, most of them cannot be manipulated or changed. The exception is the engagement of L-type Ca2+ channels. Thus, if PD is a consequence of Ca2+-accelerated aging in SNpc DA neurons, then reducing Ca2+ flux through L-type channels should delay the onset of PD signs and symptoms and slow its progression. These channels

are antagonized or blocked by orally deliverable dihydropryidine (DHP) L-type Ca2+ channel blockers (CCBs), drugs that have good bioavailability and a long record of safe use in humans (Becker et al., 2008). CCBs, including those used in nonhuman studies, are used in clinical practice to treat hypertension, which has created a database to be mined. A case-control study of hypertensive patients found a significant reduction in the observed risk of PD with CCB use, most notably isradipine (Striessnig et al., 1998), but not with medications that reduce blood pressure in other ways (Becker et al., 2008). More recently, these findings were extended by showing that only DHPs such as isradipine that cross the blood-brain barrier (BBB) are associated with reduced PD risk (~30%) (Becker et al., 2008; Marras et al., 2012; Pasternak et al., 2012; Ritz et al., 2010). Given the short period of treatment in many cases (~2 years), variable dosing, and low relative affinity of DHPs for Cav1.3 Ca2+ channels compared with Cav1.2 channels (Eisenberg et al., 2004; Kupsch et al., 1996; Mannhold et al., 1995), this is a surprisingly strong association and lends further credence to the notion that a BBB permeable and potent Cav1.3 L-type CCB could be a very effective neuroprotective agent against PD.

In absence of a selective Cav1.3 CCB, the DHP isradipine has been the most attractive drug used in preclinical research and clinical trials (Illijic et al., 2011; Kang et al., 2012; Simuni et al., 2010; Simuni et al., 2013). Isradipine has a relatively higher affinity for Cav1.3 Ca2+ channels than all other DHPs and has good brain availability (Dragicevic et al., 2014; Kang et al., 2012; Koschak et al., 2001; Mangoni et al., 2003; Parkinson's Study G, 2013; Sinnegger-Brauns et al., 2004; Scholze et al., 2001; Schuster et al., 2009; Surmier et al., 2011; see Csoti et al., 2016 for a recent review). At the doses used to treat hypertension, this drug has relatively few and minor side-effects (Fitton & Benfield, 1990), but the question will be whether it will prove neuroprotective in PD at doses tolerated by the general population. For example, in the MPTP model of drug-induced Parkinson's Disease, Surmeier et al. (2011) showed that plasma concentrations of isradipine necessary to protect mice against systemic MPTP administration are very close to those achieved in humans with a well-tolerated daily dosing, suggesting such neuroprotection is achievable. A more recent study using an intrastriatal 6-hydroxydopamine model has shown that systemic administration of isradipine produces a dose-dependent protection of both SNpc DA axon terminals and cell bodies at plasma concentrations in a similar range (IC50 4 – 8 ng/ml) (Ilijic et al., 2011). The plasma concentrations required for significant protection against this acute challenge were greater than those needed in the more specific, chronic MPTP model, but were still near the range achievable in humans. It is noteworthy that these studies suggest that protection is afforded by partial antagonism of Cav1.3 channels, minimizing any complications that might attend near complete disruption of these channels. Indeed, isradipine is currently being used in clinical trials

to determine its neuroprotective efficacy in treating/delaying PD (Parkinson's Study G, 2013; see Poetschke et al., 2015 for a recent review)

The ideal candidate for DHP therapy would be in the very early stages of SNpc loss, before the onset of symptoms. Unfortunately, there are no biomarkers that would allow the identification of presymptomatic PD patients. As a consequence, the most likely subjects for a clinical trial are those that have been recently diagnosed with PD. In these early-stage patients, SNpc DA cell loss is substantial (60%), and the remaining neurons might be compromised in ways not seen in healthy tissue. Nevertheless, disease progression could be tracked in a longitudinal study to determine whether treated patients exhibit a slower rate of motor deficit progression. There is growing evidence that inflammation could have an important impact on disease progression at this stage (Hirsch & Hunot, 2009). Antagonism of L-type channels might be helpful but not enough to significantly slow progression if this is the case.

1.8.2 Interacting Causes of PD

The number of years lived is indubitably the single strongest risk factor for PD (Caine & Langston, 1983; Gibb & Lees, 1991); all humans would develop PD if they lived forever, but, alas, humans do not. Therefore, the question then turns to whether the trajectory of cell loss in the SNpc leads to passage across the PD symptomatic threshold (~75% loss) before some other system causes cell death and, clearly, there is considerable individual variation in this point. Certainly, genetic predispositions could account for a large part of this variation (Calne & Langston, 1983; Moore et al., 2005a; Sulzer, 2007), perhaps by resulting in increases or decreases in the rate at which vulnerable neurons age by compromising or enhancing ER and/or mitochondrial function. Other factors, like brain trauma or elevated inflammatory responses could also alter the trajectory of cell loss (Klegeris et al., 2007). Finally, and of primary interest to the present thesis, are other environmental factors, in particular, exposure to heavy metal neurotoxicants, most notably, MeHg (Ho et al., 2012; Shao et al., 2015).

THE ROLE OF ENVIRONMENTAL TOXICANT EXPOSURE IN THE ETIOLOGY OF PD

The impact of PD, and other NDs, will increase as the incidence of ARDs and NDs rises in step with the aging population. Many gene-environment interactions have been postulated for sporadic PD, but to date no specific neurotoxicant has been linked unequivocally to PD. Further, PD lacks an obvious 'pre-clinical' state and, in the majority of cases, does not exhibit specific genetic linkage. This makes it difficult to identify specific environmental stressors/toxicants/events that contribute to the disease, but also reinforces the notions that environmental toxicant exposure is, nonetheless, a key element and/or risk-factor in the etiology of PD. Few studies have focused on long-term, postdevelopmental exposures to neurotoxic metals, leaving a

large void that needs to be filled. Postdevelopmental effects of neurotoxic metals is an important yet underappreciated and under-researched area. So-called 'multi-hit' types of toxicity can occur posdevelopmentally and can involve both occupational and environmental exposures. These can synergize with processes normally associated with senescence, diseases, and lifestyle to speed up the onset of neuronal demise.

1.9 METHYLMERCURY EXPOSURE

The following sections explore the hypothesis that chronic, adult-onset exposure to low-levels of the neurotoxicant methylmercury (MeHg) acts as a risk-factor for the development, onset, and severity of PD. This direction is unique in that the developmental effects of MeHg exposure on the nervous system are clearly accepted, but much less is known about its' propensity to cause neurobehavioral dysfunction in the mature and aging organism and its potential role in the etiology of PD.

Several natural and man-made sources of mercury constitute the vast majority of Hg in the atmosphere. In particular, Hg vapor resides in the Earth's atmosphere for ~1 year, due to its high stability, and can, thus, then be distributed globally. Mercury vapor present in the upper atmosphere is then oxidized to water-soluble ionic mercury and is then returned to the Earth's surface in the form of rainwater (Clarkson, 2002) – a 'toxic rain; this rain enters surface bodies of water, which contributes to the major source of human mercury exposure: the consumption of fish and other seafood from Hg-polluted waters. Specifically, MeHg bioaccumulates in the aquatic food chain, beginning with micro-organisms that methylate Hg to plankton to small fish, and finally, to large predatory fish such as shark and other fish-consuming marine mammals (Change, 1991; Clarkson, 2002). Through this process MeHg is biomagnified, with the highest levels of MeHg found in those large predatory organisms, where concentrations are highest in the liver, brain, kidney, and muscle tissue (Morel et al., 1998).

In accordance, the type of exposure hypothesized to act as a risk-factor for PD in the present paper approximates the condition portrayed by regular seafood consumption over the lifespan, one of contemporary concern. The fundamental premise is that such a pattern of exposure might hasten the onset of the neurodegenerative changes in the brain associated with aging and PD.

1.10 MEHG EXPOSURE: AN ORIGIN OR RISK FACTOR FOR PD?

In 1995, Geir Bjorklund suggested that chronic, adult-onset exposure to the neurotoxicant methylmercury (MeHg) might play a role in the etiology of PD. His suggestion was based on a case-control study among the multiethnic population of Singapore carried out by Ngim and Devathasan (1989). They tested the hypothesis that high levels of body-burden MeHg is associated with an increased risk of PD. In 54

cases of idiopathic PD and 95 hospital-based controls, detailed interviews were conducted. The researchers found a clear monotonic dose-response association between blood mercury levels and PD, even after adjusting for several potential confounding factors. Indeed, tremor is a classical motoric symptom of MeHg toxicity, as it is in PD, and although they differ in frequency and magnitude, it is conceivable that chronic, postdevelopmental exposure to low-levels of MeHg might be capable of producing PD-like signs and symptoms.

On a similar note, Weiss. Clark, and Simon (2002; see also Weiss & Simon, 1975) noted a similarity in the long latency period between chronic, postdevelopmental low-level exposure to MeHg and the onset of clinical neurobehavioral MeHg toxicity and the process presumed to underlie PD. Latency periods following such types of MeHg exposure, in both humans and nonhumans, can extend from months to years, depending on species. Thus, a toxic dose of MeHg will cause an initial cell loss/dysfunction, which may or may not reduce the number of target cells to the point at which overt signs and symptoms appear. Over time, the aging process will further reduce the number of cells until those that remain are too few to sustain adequate functioning; at this point, overt effects of MeHg erupt. In this situation, the higher the initial dose, the greater the loss of cells due to the action of MeHg and this will, in turn, reduce the latency period due to aging. Now notice how this latency period of MeHg's toxicity associated with chronic, low-level postdevelopmental exposure mimics the development and onset of the signs and symptoms of PD. Most observers agree that the appearance of clinical signs of PD is merely the ultimate phase of a neurodegenerative process whose inception might even be traced to events during early development, but certainly to events that occurred during adulthood. The clinical signs of PD are believed to emerge after the death of 60-90% of the DAergic neurons in the SNpc. The long latency is attributed to the ability of the remaining DAergic cells in this region to compensate for the functions of the vanished DAergic cells. Thus, in both MeHg toxicity induced by chronic, postdevelopmental low-level exposure and in the onset of PD, it is more than plausible that in the period of time preceding overt signs and symptoms of MeHg toxicity or PD, brain structures were undergoing continuous degeneration. In both cases, only after the compensatory mechanisms begin to fail under their burden, does the extent of the destruction assert itself in an overt manner.

Keeping the above ideas in consideration, the following sections will examine the similarities between the molecular, cellular, and structural mechanisms causing MeHg's toxicity and PD's signs and symptoms.

1.11 THE NEUROBIOLOGY OF MEHG'S TOXICITY

1.11.1 MeHg and ROS

Exposure to MeHg has been shown to increase ROS levels. For example, when exposed to MeHg, human monocytes (Insug et al., 1997); T-cell (Shenker et al., 1998), and various rodent neurons (e.g., Ali et al., 1992; Yee & Choi, 1994) all showed increases in ROS. *In vitro* application of MeHg has shown that ROS increases as a function of time since exposure and, simultaneously, cell viability decreases, each in a dose-dependent fashion (Chen et al., 2006). Localization of ROS has been shown in brain regions specifically sensitive to the effects of MeHg, most notably the cerebellum (LeBel et al., 1990, 1992).

Interestingly, as in PD, the increased level of ROS induced by MeHg exposure has been hypothesized to result from alterations in the functioning of mitochondria. Indeed, MeHg accumulates heavily in the mitochondria, which leads to decreases in the rate of oxygen consumption, alterations in the ETC, and a lower induction of the MMP (Bondy & McKee, 1991; Castoldi et al., 2000; Insug et al., 1997; Shenker et al., 1999). The studies mentioned here indicate a role of mitochondrial alterations and induction of ROS in MeHg's toxicity, not unlike those processes mentioned above in relation to PD.

1.11.2 MeHg and the Functioning of the ER and Mitochondria

An important component of Ca^{2+} homeostasis is the specialized intracellular organelles known as [Ca^{2+}] stores, which act as a Ca^{2+} buffering system (Friel & Tsien, 1992; Neter, 1998; Toescu, 1998) as well as a source of Ca^{2+}. As mentioned above, there are two types of these stores: the ER and mitochondria. Chronic exposure to MeHg inhibits mitochondrial enzymes and depoloraizes the mitochondrial membrane, thus reducing ATP production and the buffering capacity of Ca^{2+}. This reduction in Ca^{2+} buffering alters [Ca^{2+}] homeostasis in such a way that excess concentrations of [Ca^{2+}] accumulate. For instance, Levesque and Atchison (1991) showed that mitochondria isolated from rat forebrain, when exposed to MeHg, released mitochondrial-associated calcium ions, and at the same time prevented uptake of calcium ions by the mitochondria. Further, shown both *in vitro* and *in vivo,* decreases in mitochondrial respiration occurred as a result of MeHg -nduced inhibition of the citric acid cycle or tricarboxylic acid (TCA) cycle (Fox et al., 1975; Verity et al., 1975; Yoshino et al., 1966).

In more recent years, MeHg exposure has also been shown to cause apoptotic cell death through opening of the mitochondrial permeability transition pore (Limke & Atchinson, 2002; Limke et al., 2003, 2004). Further studies have suggested that the above process could result in squandering of the MMP, potentially resulting in latter efflux of mitochondrial Ca^{2+} ions and inhibition of mitochondrial Ca^{2+} ion uptake (Denny et al., 1993; Hare et al., 1993; Komulainen & Bondy, 1987). The dissipation of the MMP could be due to two, independent or interacting mechanisms: 1) excessive accumulation mitochondrial [Ca^{2+}] and/or 2) the production of ROS and depletion of ATP (Bernardi et al., 1998). Finally, the role of [Ca^{2+}] stores, like the

mitochondria, in Ca^{2+} buffering are also important to MeHg's toxicity because of the role of the mitochondria in neuro-excitotoxicity, or prevention thereof (Keelan et al., 1999; Nicholls & Budd, 1998). When stimulated, glutamate neurons that demonstrate a large mitochondrial depolarization will preserve elevated levels of $[Ca^{2+}]$ and the subsequent delayed Ca^{2+} deregulation culminates in neuronal death.

1.11.3 MeHg, DA, and DAergic Neurons

MeHg accumulates and can produce lesions in the basal ganglia, a region associated with regulating motoric and psychological timing and speed (Weiss, 2002). As mentioned above, this region and those behavioral processes are also affected in PD. Although little is known about the functional consequences of chronic, postdevelopmental low-level MeHg exposure on functions mediated by DA and DAergic pathways, there is some evidence that the adult DA systems are vulnerable to adult-onset MeHg toxicity. MeHg has been shown to accumulate in the SNpc and striatum during chronic exposure to drinking water (Møller-Madsen, 1991), but the functional cognitive/behavioral consequences of MeHg exposure in the SNpc are not known. In the striatum, however, direct infusions of relatively high concentrations of MeHg results in a 9X increase in extracellular striatal DA (Faro, et al., 2003, Faro, et al., 2007). At low micromolar concentration, MeHg increases the spontaneous release of DA (and GABA) (Minnema, et al., 1989), which reflects an increase in $[Ca^{2+}]$.

Further, chronic exposure to a low (0.1 mg/kg/day for three months) or high (2 mg/kg/day for 1 month) increases extrasyaptic DA and increased DA metabolites, HVA, and DOPAC in behaving rats, as measured with microdialysis (Faro, et al., 2002). A negative correlation between brain mercury and DA D2 receptor binding was reported in striatum of captured river mink and otters exposed to environmental levels of MeHg due to fish consumption (Basu, et al., 2005a, Basu, et al., 2005b). More recently, MeHg has been shown to decrease tyrosine hydroxylase, the rate-limiting factor in DA synthesis, neurons expressing the DA transporter protein (reuptake), as well as overall DA levels and DA metabolites such as MAO-B in a manner similar to MPP^+ (Shao et al., 2015a), a neurotoxin known to cause PD-like symptoms in preclinical and epidemiological studies (Eberhardt & Schultz, 2003; Petit-Paitel et al., 2009). Further, MeHg exposure and MPP^+ change gene and protein expressions in similar manners, indicating that these neurotoxins disrupt similar signaling DAergic pathways, cause mitochondrial dysfunction, and effected proteins involved in phosphorylation and other important functions resulting in energy deficits, ultimately leading to the pathogenesis of PD (Shao et al., 2015b). The functional behavioral/cognitive relevance of these changes, however, is unknown.

Thus, accumulation of MeHg in the basal ganglia and SNpc resulting from chronic, postdevelopmental

low-level MeHg exposure could facilitate development of NSDA dysfunction leading to PD-like effects, especially in organisms with genetic or age-related susceptibility. This conclusion is in part based of the further similarities between MeHg toxicity and PD in regards to Ca^{2+} alterations, discussed next.

1.11.4 MeHg, Ca2+, and Downstream Effects

Years of recent research have implicated MeHg-induced neurobiological dysfunction in post-exposure disruptions in synaptic function (Yuan & Atchison, 2007). Atchison and colleagues have described two specific alterations in neurotransmitter release that occur as a result of bath-applications of MeHg. Both of these alterations are mediated by Ca^{2+} processes and include alterations in nerve-evoked neurotransmitter release and in spontaneous release of neurotransmitter. Specifically, a block of nerve-evoked, synaptic neurotransmitter release occurs following high concentrations of *in vitro* MeHg bath-application; an effect, as discussed below that is, in part, due to MeHg blocking voltage-gated Ca^{2+} channels (see Atchison & Hare, 1994; Atchison, 2003). The MeHg-induced nerve-evoked release is blocked and the regularity of spontaneous neurotransmitter release are affected simultaneously, but in two distinct phases. The first phase involves an initial stimulation in spontaneous release of neurotransmitter that is then followed by a second stage of complete suppression of the spontaneous release, both involving regulation of free [Ca^{2+}] (Atchison, 2003; Atchison & Hare, 1994; Yuan & Atchison, 2007). Using the electrophysiology technique called whole-cell path clamp to study multiple ion channels over the membrane range of entire cells and record currents of those channels and confocal imaging of Ca^{2+} channels to measure the cell layer concentrations of Ca^{2+}, Yuan and Atchison (2007) demonstrated several important effects of MeHg exposure. These included 1) a significant increase in [Ca^{2+}] levels in the molecular and granule layers of the cerebellum as well as the dendrites of Purkinje cells in rodent brains following all doses of the MeHg-bath application; 2) MeHg-induced elevation of presynaptic terminal Ca^{2+} correlated both temporally and spatially to the initial increases in frequency of spontaneous release of neurotransmitter – representing the early stimulatory effects on spontaneous synaptic responses induced by MeHg – and; 3) the 2) effect was shown to occur in all cell types examined, demonstrating the generality of the MeHg-induced motivation of spontaneous neurotransmitter release.

Further, other *In vitro* experiments utilizing Fura 2AM have identified a specific pattern of MeHg's effects on Ca^{2+} homeostasis, which, in turn, likely contribute to the alterations described above as neurotransmitter release. Specifically, these studies have shown that MeHg exposure induces a biphasic alteration of [Ca2+] in the neuron terminal due to 1) rapid, but relatively small release and increases in [Ca^{2+}] likely the result of Ca^{2+} release from stores in mitochondria and the ER (Bearrs et al., 2001; Limke et al.,

2003) and 2) slower, longer-lasting and very large increases in [Ca^{2+}] entry into the cells via L-, N-, and/or Q-type voltage-gated calcium-channels (Marty & Atchison, 1997). The overall elevations in [Ca^{2+}] as a result of this biphasic effect of MeHg disrupts Ca^{2+} signaling, alters neuronal excitability and neurotransmitter release, and can cause cell death (see Bailey et al., 2013). As suggested by Atchison and Hare (1994), because Minnema et al. (1989) demonstrated that MeHg exposure can increase the permeability of the synpatosomal membrane to small molecules, these may include the Ca^{2+} ion. As discussed above with PD, these studies suggest that MeHg-induced neurotoxicity can be attributed to a component that is Ca^{2+}-dependent.

One hypothesis that has been suggested to explain both the decreased nerve-evoked release and increased spontaneous release of neurotransmitter that occurs with MeHg exposure is that such exposure causes nerve terminal depolarization (Atchison & Hare, 1994). Such a depolarization would 1) decrease the effectiveness of the presynaptic action potential in eliciting neurotransmitter release and, 2) open membrane Na^{+} and Ca^{2+}, thereby increasing cation influx and leading to spontaneous neurotransmitter release. In support of this hypothesis, Hare & Atchison (1992) have shown that MeHg depolarized the plasma membrane of rat brain synaptosomes (i.e. terminal of neuron) and Minnema et al. (1989) showed that MeHg increases synpatosomal membrane permeability to small molecules.

The above discussions and studies focused on cerebellar dysfunction, as it is a common and widely described effect of postdevelopmental MeHg exposure. In particular, specific populations of cells in the cerebellum, the granule cells, exhibit remarkable susceptibility to MeHg-induced toxicity. This effect has been recapitulated *in vitro* and appears to result from disruption of intracellular Ca2+ regulation as well as effects on L-type voltage-gated Ca2+ channels. The ability of MeHg to affect distinct populations of neurons and to do so by alterations of Ca2+ raises the possibility that other subsets of neurons with vulnerability that depend on Ca2+ regulation could also be sensitive to MeHg. Indeed, the combination of the long period of time Cav1.3 L-type Ca2+ channels remain open, coupled with their rhythmicity, means that SNpc DA neurons are constantly being exposed to pulses of elevated [Ca2+]. For this reason, it is highly plausible, coupled with the above data, that chronic, postdevelopmental low-level MeHg exposure can facilitate NSDA neuronal damage by interaction with L-type Ca2+ channels, disturbing mitochondrial function and elevating [Ca2+] and, importantly, in a manner similar to that observed in PD. Thus, because increased [Ca2+] is associated with PD and aging in the brain and MeHg consistently increases [Ca2+], it could be that chronic, adult exposure to low-levels of MeHg enhances the severity or accelerates aging-dependent disruption of [Ca2+], in a manner again consistent with PD. Because of the unique dependence of SNpc DA neurons on cyclical changes in [Ca2+], mediated through pacemaking or rhythmic firing and mediated by Cav1.3 L-type Ca2+ channels, this

places these cells at risk for both PD and MeHg-induced damage and alteration.

1.11.5 Can MeHg's Neurotoxicity be Attenuated, Delayed, or Prevented?

As with PD, although there are several factors governing MeHg's neurotoxicity, most of them cannot be manipulated or changed. Also as with PD, and the mechanism hypothesized to underlie MeHg's neurotoxicity, the exception is the engagement of L-type Ca2+ channels. Thus, in a nearly identical fashion as discussed with relation to PD, if MeHg's neurotoxicity is a consequence of increased [Ca2+], then reducing Ca2+ flux through L-type channels should attenuate, delay, or prevent the signs of MeHg-induced toxicity. Indeed, VGCCBs delay both the first and second-phases of MeHg-induced Ca2+ entry *in vitro.* Moreover, several studies using rats have demonstrated that MeHg induced [Ca2+] elevations were not a result of direct excitotoxic insult, because inhibition of excitatory amino acid receptor-activated channels did not prevent MeHg induced elevations in [Ca2+] (Marty & Atchison, 1997; 1998). In contrast, when VGCCs were blocked with known calcium ion channel blockers like nifedipine, the time of onset of MeHg mediated increase in [Ca2+] was delayed both in NG108-15 neuroblastoma (Hare & Atchison, 1995b) and primary cerebellar granule cell cultures (Marty & Atchison, 1997). The response of granule cells to MeHg-induced elevation of [Ca2+] was found to be approximately 10 times that of NG108-15 neuroblastoma cells (Hare & Atchison, 1995a). These data suggest that MeHg causes increased [Ca^{2+}] via the activation of VGCCs, but not via excitatory ligand-gated channels.

The in vitro reports have been confirmed recently *In vivo.* VGCCBs protect against behavioral impairment associated with various Ca^{2+}-induced CNS damage, like that caused by aging, brain ischemia, brain trauma, and, as mentioned above, animal models of PD. Sakamoto et al. (1996) reported that L-type CCBs improved survival of cerebellar granule cells exposed to MeHg in culture and prevented weight-loss in adult rats exposed orally to MeHg. An experiment carried out in our laboratory, using sophisticated behavioral endpoints, tested the hypothesis that chronic, adult-onset MeHg neurotoxicity results from disruption of [Ca^{2+}] homeostasis by examining the neuroprotective effects of the L-type Ca^{2+}blocker, Nimodipine, alongside chronic, daily consumption of 15 ppm MeHg, on survival and neurobehavioral functions in mice. Importantly, Bailey et al. (2014) showed that when Nimodipine was added to the rodents' daily diet, it delayed or, depending on dose, completely prevented *in vivo* neurobehavioral effects of the neurotoxicity associated with chronic consumption of water laced with up to 15 ppm of MeHg. In sum, the well-described ability of an L-type Ca^{2+} channel blocker to delay, attenuate, or completely prevent the severity of MeHg-induced neurobehavioral toxicity *in vivo* and delay MeHg-induced, Ca^{2+}-mediated cell death *in vitro* suggests that MeHg exposure may disrupt NSDA function through interactions with Cav1.3 L-type Ca2+ channels and

altering intracellular Ca2+ homeostasis.

1.12 MEHG AND PD RECONSIDERED: NEUROBIOLOGICAL AND BEHAVIORAL PERSPECTIVES

1.12.1 Similarities in Neurobiological Dysfunction.

Ca^{2+} dyshomeostasis has long been thought to be important in the neurodegeneration and, recently, shown to be important in neurodegeneration due to both PD- and MeHg-induced toxicity. Most often, however, these disruptions in Ca^{2+} have been viewed as late-stage consequences of organelle damage inflicted by some other burden. The inimitable reliance of SNpc DAergic neurons on voltage-gated L-type Ca^{2+} channels that convene autonomous pacemaking activity indicates that neuronal entry of Ca^{2+} and dyshomeostasis could be a cause of their selective vulnerability to both PD and MeHg, rather than merely a late stage consequence. This hypothesis is consistent with the centrality of mitochondria and the ER, key organelles in the regulation of Ca^{2+} homeostasis, in prevailing models of pathogenesis in PD and the neurobehavioral toxicity of MeHg exposure. The additional metabolic cost placed upon these organelles by the demands coupled with sustained Ca^{2+} entry could accelerate their aging and enhance the vulnerability of SNpc DAergic neurons to genetic and environmental challenges, including those posed by MeHg exposure. Although plausible and reliable with regional deficits seen in normal aging, PD, and exposure to MeHg, the proposition that Ca^{2+} entry during pacemaking compromises or yields vulnerable mitochondrial and ER function remains to be fully tested. Nevertheless, the evidence clearly demonstrating that L-type VGCCBs can attenuate or delay the signs and symptoms of PD and the neurobehavioral signs of MeHg-induced toxicity suggests the plausibility of the connection between Ca^{2+}, loss of SNpc DAergic neurons in PD, and potential loss or damage of these neurons resulting from MeHg exposure. Therefore, based on the plethora of data provided above, the experiments proposed herein focus on the hypothesis that chronic, low-level, postdevelopmental exposure to MeHg enhances or accelerates aging-dependent disruption of $[Ca^{2+}]$ and distortion of NSDA functioning, which may play a role in the etiology of PD or lead to PD-like effects, especially in those with genetic- or age-related susceptibility. Further, these experiments further test the above hypotheses by assessing the ability of the L-type CCB isradipine to mitigate this dysfunction.

1.12.2 Are there Similarities in Behavioral Dysfunction?

Dysfunction of temporal processing, interval timing, and time perception has been demonstrated to be an early sign/symptom of ARDs and NDs, as intact NSDA functioning underlies normal temporal processing, interval timing, and time perception and, thus, any impairment in this system, due to the processes leading to PD or MeHg exposure, should impact these behavioral processes.

1.12.2.1 Timing and Time Perception in PD. The striatum and efferent projections from SNpc DA

neurons to the striatum are vital for interval timing and time perception (Mattel & Meck, 2004; Meck, 2006). The DAergic-related depletion in these areas and slowing and disruption of Ca^{2+} regulation n PD have been related to an underlying distortion of the perception and production of temporal intervals/durations (Artieda et al., 1992; Ivry & Keele, 1989; Nakamura et al., 1978; O'Boyle, Freeman, & Cody, 1996; Oprisan & Buhusi et al., 2011, 2013; Pastor et al., 1992a, 1992b; Volkmann et al., 1992). This hypothesis is consistent with extensive non-human animal work that emphasizes the role of DAergic systems and the NSDA-frontal circuitry in timing and time perception (see Meck, 1996 for a review). Specifically, the output of DAergic neurons originating in the SNpc and projecting to the striatum are thought to act as the pacemaker/clock required for interval timing and time perception. Indeed, under the PI procedure, the DA transporter (DAT) knockout mouse, which has elevated levels of synaptic DA, show higher response rates and peak curves shifted leftward (underestimation) relative to wild-type controls over a range of target durations. This effect has been attributed to an increase in pacemaker speed in these mutant mice and/or the hyper-DAergic state resulting in reduced variability in pacemaker speed between trials, resulting in both a leftward-shifted and narrower distribution of remembered or reinforced times of reinforcer delivery during standard trials. Moreover, these results are consistent with the effects of low to moderate doses of DA agonists, including amphetamine and methamphetamine, which produce leftward shifts compatible with an increase in pacemaker speed, while DA antagonists, including haloperidol, produce the inverse effect, rightward-shifts in peak curves compatible with a decrease in pacemaker speed (Meck, 1986). Additionally, 6-OH DA lesions of the striatum eliminate normal interval timing and time perception in rodents that does not recuperate after intrastriatal infusion of L-dopa. In contrast, disrupted timing and time perception is restored by L-dopa administration in animals with SNpc damage, suggesting that those DAergic neurons responsible for pacemaking activity that endure the lesion act effectively following administration of L-dopa (Hinton & Meck, 1997).

It was proposed that damage to the SNpc and striatum produces distortions in timing and time perception, effectively slowing down the speed of the pacemaker. Focal lesions in, and neurodegenerative diseases of, the basal ganglia and NSDA neurons, as in PD, cause subjects to overestimate target durations under the single PI procedure (Malapani et al., 1994; Pastor et al., 1992a, 1992b). Moreover, this overestimation of target durations (right-ward shifts in peak curves) was related to DA depletion in the human brain, as this alteration was found to be accentuated in PD patients when tested under the single PI procedure without L-dopa replacement treatment (Pastor et al., 1992a, 1992b).

If slowing in monitoring current time – the SNpc pacemaking activities and projection to the striatum –

due to DAergic deficiency in PD was the culprit for understanding the motoric, cognitive, and behavioral slowing experienced by these patients, then one might expect interval timing to be overestimated with different time ranges and under both the single PI and PIC procedures (Gibbon et al., 1997). However, shortened or simply more variable timing of temporal durations have been shown in PD patients, but PD-induced distortions of timing and time perception that result in over- or underestimation are most often attenuated by DA replacement therapies (Malapani et al., 1998; O'Boyle et al., 1996; Pastor et al., 1992a, 1992b; Wing et al., 1984).

Of special pertinence to the present paper, is an additional DA-dependent distortion in interval timing with a unique pattern (Malapani et al., 1998; Malapani et al., 2002) in PD patients responding under the PIC procedure. Specifically, Malapani et al. (1998) showed that when PD patients were tested under the PIC procedure with DA replacement therapy (hereafter referred to as the 'ON drug' group), performance was equal to or better than age-matched controls. When tested without DA replacement therapy (referred to as the 'OFF drug' group), the same patients overestimated the shorter of two target durations (8-s) and underestimated the longer of the two (21-s), a pattern termed the "migration effect." Importantly, in this study, the migration effect was observed in every patient tested OFF drug, suggesting that the underlying behavioral mechanisms/processes were extremely dependent on intact SNpc and NSDA functioning.

Given the observation in Malapani et al. (1998) that intermittent feedback did not correct the migration effect in PD patients OFF drug over the course of testing, the migration effect was hypothesized to reflect a dysfunction in the times reinforced or remembered, rather than a disruption in the speed of the pacemaker. Nonhuman-animal data collected under the PI and PIC procedures indicate that such a dysfunction in the times reinforced or stored in memory can be inferred with such inaccuracies in timing target durations is relatively permanent and unaffected by intermittent corrective feedback during testing (Meck, 1996). In contrast, the classic error caused by changes in pacemaker speed, due to DAergic manipulations (Meck, 1996) is an initial rapid shift in the peak curves that gradually returns to veridical accuracy followed by a rebound-effect in the opposite direction when the DAergic manipulation is discontinued. Peak curves of animals originally trained without administration of a DA agonist show rapid leftward shifts (underestimation) that continue under influence of the DA agonist. Over training and time, however, peak curves gradually return to veridical accuracy as new subjective times of reinforcement overlay previously learned reinforced times for target durations learned without the administration of the DA agonist. Thus, a faster (or slower) pacemaker might generate a faster (or slower) subjective time of reinforcement, but as long as the training and testing conditions remain identical, behavioral tolerance can occur and this same faster (or slower)

subjective time will be reproduced at the appropriate, veridical, objective target duration. On those grounds, Malapani et al. (1998) concluded that alterations in pacemaker speed monitoring current, subjective time could not induce the migration effect because PD patients OFF drug were trained and tested under identical conditions.

Interestingly, the underestimation or leftward shift in the peak curve at the longer target duration was not systematic in PD patients OFF drug, occurring only under the PIC procedure, but not the single PI procedure; that is, when responding at two target durations is reinforced and must be remembered. Under the single PI procedure, PD patients overestimated or showed rightward shifts in peak curves at the long, 21-s target duration, strongly suggesting that the migration effect was dependent on timing two target durations simultaneously. When PD patients are tested under the PIC procedure, reinforced or remembered timing at the shorter target duration appear to affect the timing of the reinforced or remembered timing at longer target duration, by causing a migration of reinforced or remembered times for each target duration toward each other. Thus, the permanent migration effect observed in PD patients OFF drug was ascribed to a dysfunction in the reinforced timing or memory of the target durations during training (i.e., 'storage') and/or the subsequent timing based off of those reinforced or remembered times during PI trials.

1.12.2.2 Timing and Time Perception Following MeHg Exposure. To knowledge, no studies of the effects of chronic, low level, adult-onset MeHg exposure on PI or PIC timing and time perception have been conducted. Further, studies of gestational, prenatal, or development exposure to MeHg have been limited to strict FI schedules. For instance, Rice (1992) showed that monkeys exposed gestationally and postnatally to MeHg, and tested as infants, showed FI response distributions that were shifted leftward (underestimation) relative to controls. Similarly, Reed and Newland (2007) used FI schedules that were either clocked (i.e., auditory stimuli associated with different portions of the FI) or unclocked (i.e., standard FI schedule; no stimuli) to assess the effects of *in utero* MeHg. The authors showed that MeHg-exposed rats demonstrated overall higher response rates and that, in some groups, also showed slight leftward shifts in the FI response rate function (i.e., underestimation). These results, however, may have little or no relation to performance under PI or PIC schedules of rodents exposed chronically in adulthood.

1.13 THE CURRENT STUDY: AIMS AND PREDICTIONS

Because no data are available regarding chronic adult-onset exposure to MeHg and its effects on timing and time perception under the PI or PIC procedure, only goals can be offered and predictions made. Based on the neurobiological dysfunction seen in PD and as a result of MeHg exposure, the main question is: does chronic exposure to a low-level of MeHg in adulthood produce effects similar to those seen in PD under

the PIC procedure and does the L-type CCB isradipine attenuate, protect, or prevent such potential effects? Specifically, does such MeHg exposure result in the migration of timing a short target duration with that of a long target duration or does MeHg exposure produce unidirectional shifts in timing at both target durations and does ISR exposure delay, attenuate, and/or prevent against such disruptions. Further, does the time-course of exposure and absolute target durations, and their relative difference, modulate any of MeHg's effects and potential protection by ISR?

REFERENCES

Artieda J, Pastor MA, Lacruz F, and Obeso JA (1992) Temporal discrimination is abnormal in parkinson's disease. Brain 115(Pt 1):199-210.

Basu N, Klenavic K, Gamberg M, O'Brien M, Evans D, Scheuhammer AM, and Chan HM (2005a) Effects of mercury on neurochemical receptor-binding characteristics in wild mink. Environ. Tox. Chem. 24:1444-50.

Basu N, Scheuhammer A, Grochowina N, Klenavic K, Evans D, O'Brien M, and Chan HM (2005b) Effects of mercury on neurochemical receptors in wild river otters (lontra canadensis). Environmental Sci. Tech. 39:3585-91.

Bergman H, Feingold A, Nini A, Raz A, Slovin H, Abeles M, Vaadia E (1998) Physiological Aspects of Information Processing in the Basal Ganglia of Normal and Parkinsonism Primates. TINS 21:32.

Bloxham CA, Dick DJ, and Moore M (1987) Reaction times and attention in parkinson's disease. J Neuro. Neurosurg. Psych. 50:1178-83.

Bonci A, Grillner P, Mercuri1 NB, and Bernardi G (1998) L-Type calcium channels mediate a slow excitatory synaptic transmission in rat midbrain dopaminergic neurons. J Neurosci 18(17): 6693-6703.

Braak H and Braak E (2000) Pathoanatomy of Parkinson's disease. J Neurol 247: II3-10.

Budd SL and Nicholls D (1996) Mitochondria, calcium regulation, and acute glutamate excitotoxicity in cultured cerebellar granule cells. J Neurochem 67(6): 2282-2291.

Burke WJ, Li SW, Williams EA, Nonneman R, Zahm DS (2003) 3,4-Dihydroxyphenylacetaldehyde is the toxic dopamine metabolite in vivo: implications for Parkinson's disease pathogenesis. Brain Res 989:205 - 213.

Cagiano R, De Salvia MA, Renna G, Tortella E, Braghiroli D, Parenti C, Zanoli P, Baraldi M, Annau Z, and Cuomo V (1990) Evidence that exposure to methyl mercury during gestation induces behavioral and neurochemical changes in offspring of rats. Neurotoxicol. Teratol. 12:23-8.

Church RM and Deluty MZ (1977) Bisection of temporal intervals. J Exp Psychol Anim Behav Proc. 3(3):216-28.

Church RM, Meck WH, and Gibbon J (1994) Application of scalar timing theory to individual trials. J Exp Psychol Anim Behav Process. 20(2):135-55.

Cuomo V, Ambrosi L, Annau Z, Cagiano R, Brunello N, and Racagni G (1984) Behavioural and neurochemical changes in offspring of rats exposed to methyl mercury during gestation. Neurobehav. Toxicol. Teratol. 6:249-54.

Dauer, W. and Przedborski S. (2003) Parkinson's disease: mechanisms and models. Neuron 39: 889-909.

De Lau LM, Giesbergen PC, de Rijk MC, Hofman A, Koudstaal PJ, Breteler MM (2004) Incidence of parkinsonism and Parkinson disease in a general population: the Rotterdam Study. Neurology 63:1240-1244.

Demarest KT and Moore KE (1979) Comparison of dopamine synthesis regulation in the terminals of nigrostriatal, mesolimbic, tuberoinfundibular and tuberohypophyseal neurons. J Neural Transm 46:263-277.

Denny MF and Atchison WD (1994) Methylmercury-induced elevations in intrasynaptosomal zinc concentrations: an 19F-NMR study. J Neurochem 63(1):383-6.

Donlin WD and Newland MC (Under Review). The effects of chronic methylmercury and selenium on the acquisition of high-rate behavior in the rat. Neurotoxicol. Teratol.

Drolet RE, Behrouz B, Lookingland KJ, and Goudreau JL (2006) Substrate-mediated enhancement of phosphorylated tyrosine hydroxylase in nigrostriatal dopamine neurons: evidence for a role of alpha-synuclein. J Neurochem 96:950-959.

Fahn S (2003) Description of Parkinson s Disease as a Clinical Syndrome. Ann N Y Acad Sci 991: 1-14. Faro LR, do Nascimento JL, Alfonso M, and Duran R (2002) Mechanism of action of methylmercury on in vivo striatal dopamine release. Possible involvement of dopamine transporter. Neurochem Int. 40(5): 455- 65.

Faro LR, Duran R, do Nascimento JL, Perez-Vences D, and Alfonso M (2003) Effects of successive intrastriatal methylmercury administrations on dopaminergic system. Ecotoxicol Environ Saf. 55(2):173-177.

Faro LR, Rodrigues KJ, Santana MB, Vidal L, Alfonso M, Duran R (2007) Comparative effects of organic and inorganic mercury on in vivo dopamine release in freely moving rats. Braz J Med Biol Res. 40(10):1361-5.

Fetterman JG, Killeen PR (1995) Categorical Scaling of Time: Implications for Clock-Counter Models. J Exp Psych: Ani Beh Proc, 21(1): 43 – 63.

Filipov NM, Norwood AB, and Sistrunk SC (2009) Strain-specific sensitivity to mptp of c57bl/6 and BALB/c mice is age dependent. Neuroreports 20:713-717.

Freire MAM, Oliveira RB, Picanço-Diniz CW, and Pereira JA (2007) Differential effects of methylmercury intoxication in the rat's barrel field as evidenced by nadph diaphorase histochemistry. NeuroToxicology 28:175-181.

Gibbon J (1977) Scalar Expectanyc Theory and Weber's law in animal timing. Psych Review. 84:279- 325.

Gibbon J (1981) On the form and location of the psychometric bisection function for time. J Math Psych. 24:58-87.

Gibbon J (1991) Origins of Scalar Timing. Learning and Motivation. 22:3- 38.

Gibbon J (1992) Ubiquity of scalar timing with a Poisson clock. J of Math Psych. 36:283- 293.

Gibbon J, Church RM (1984) Sources of variance in an information processing theory of timing. In H. L. Roitblatt, T. G. Bever, & H. S. Terract (Eds.), *Animal Cognition,* pp. 465 – 488. Hillsdale, NJ: Erlbaum.

Gibbon J, Church RM (1990) Representation of time. Cognition, 32, 23 – 54.

Graham DG (1978) Oxidative pathways for catecholamines in the genesis of neuromelanin and cytotoxic quinones. Mol Pharmacol 14:633-643.

Graham DG, Tiffany SM, Bell WR, Jr., and Gutknecht WF (1978) Autoxidation versus covalent binding of quinones as the mechanism of toxicity of dopamine, 6-hydroxydopamine, and related compounds toward C1300 neuroblastoma cells in vitro. Mol Pharmacol 14:644-653.

Hajela, RK, Peng SQ, and Atchison WD (2003) Comparative effects of methylmercury and Hg^{2+} on human neuronal N- and R-type high-voltage activated calcium channels transiently expressed in human embryonic kidney 293 cells. J Pharmacol Exp Ther 306(3):1129-36.

Heikkila RE and Manzino L (1984) Behavioral properties of GBR 12909, GBR 13069 and GBR 13098: specific inhibitors of dopamine uptake. Eur J Pharmacol 103:241-248.

Hornykiewicz O (1963) The tropical localization and content of noradrenalin and dopamine (3-hydroxytyramine) in the substantia nigra of normal persons and patients with Parkinson's disease. Wien Klin Wochenschr. 75:309-12.

Johnson JE, Pesek EF, and Newland MC (2009) High-rate operant behavior in two mouse strains: A response-bout analysis. Behav. Proc. 81:309-315.

Killeen, P. R. (1981b). Learning as causal inference. In M. L. Commons & J. A. Nevin (Eds.), Quantitative analyses of behavior (Vol. I): Discriminative properties of reinforcement schedules. Cambridge, MA: Ballinger, 1981.

Killeen, P. R. (1985b). Incentive theory: IV. Magnitude of reward. *Journal of the Experimental Analysis of Behavior, 43*, 407 – 417.

Killeen, P. R. (1991). Behavior's time. In G. H. Bower (Eds.) The psychology of learning and motivation (pp. 295 – 334). New York: Academic Press.

Killeen, P. R. (2001a). Modeling games from the 20th century. *Behavioural Processes, 54,* 33-52.

Killeen, P. R. (2001b). Writing and overwriting short-term memory. *Psychonomic Bulletin & Review, 8*(1), 18-43.

Killeen, P. R. (2005). Gradus ad parnassum: Ascending strength gradients or descending memory traces? *Commentary in Behavioral Brain Sciences, 28*(3), 432 -434.

Killeen, P. R. (2009). An additive-utility model of delay discounting. *Psychological Review, 116*(3), 602 – 619.

Killeen, P. R. (2011). Models of trace decay, eligibility for reinforcement, and delay of reinforcement gradients, from exponential to hyperboloid. *Behavioral Processes*, 87, 57–63.

Killeen, P. R. (2013). The structure of scientific evolution. *The Behavior Analyst, in press.*

Killeen, P.R. (2013). Absent without leave; a neuroenergetics theory of mind-wandering. *Frontiers in Psychology, 4*(373).

Killeen, P. R. & Fantino, E. (1990). Unification of models for choice between delayed reinforcers. *Journal of the Experimental Analysis of Behavior, 53,* 189-200.

Killeen PR, Fetterman JG (1988) A behavioral theory of timing. Psych. Rev. 95:274-95.

Killeen PR, Fetterman JG (1993) The behavioral theory of timing: Transition Analyses. J Exp Anal Of Behav, 59, 411 – 422.

Killeen PR, Fetterman JG, Bizo LA (1997) Time's Causes. In C. M. Bradshaw & E. Szabadi (Eds.), Time and Behavior: Psychological and Neurobehavioural analyses (pp. 79 – 131). Amsterdam: Elsevier Science.

Killeen, P. R., Russell, V. A., & Sergeant, J. A. (2013). A behavioral neuroenergetics theory of ADHD. *Neuroscience & Biobehavioral Reviews 37*(4),

Killeen, P. R. & Sitomer, M. T. (2003). MPR. *Behavioural Processes, 62,* 49 – 64.

Killeen & Smith (1984). Perception of contingency in conditioning: Scalar timing, response bias, and erasure of memory by reinforcement. *Journal of Experimental Psychology: Animal Behavior Processes, 10*(3), 333-345.

Killeen PR, Weiss N (1987) Optimal Timing and the Weber Function. Psych Review, 94, 455 – 468.

LaVoie MJ and Hastings TG (1999a) Peroxynitrite- and nitrite-induced oxidation of dopamine: implications for nitric oxide in dopaminergic cell loss. J Neurochem 73:2546-2554.

LaVoie MJ and Hastings TG (1999b) Dopamine quinone formation and protein modification associated with the striatal neurotoxicity of methamphetamine: evidence against a role for extracellular dopamine. J Neurosci 19:1484-1491.

Malpani C, Rakitin B, Meck WH, Deweer B, Dubois B, and Gibbon J (1998) Coupled temporal memories in parkinson's disease: A dopamine-related dysfunction. J Cognit. Neurosci.10:316-331.

Mason JN, Farmer H, Tomlinson ID, Schwartz JW, Savchenko V, DeFelice LJ, Rosenthal SJ, Blakely RD (2005) Novel fluorescence-based approaches for the study of biogenic amine transporter localization, activity, and regulation. J Neurosci Methods 143:3-25.

Matell MS and Meck WH (2004) Cortico-striatal circuits and interval timing: Coincidence detection of oscillatory processes. Cognit. Brain Res. 21:139-70. Mattson MP (2007) Calcium and neurodegeneration. Aging Cell 6:337- 350.

McNaught KS and Olanow CW (2003) Proteolytic Stress: a unifying concept for the etiopathogenisis of Parkinson's Disease. Ann Neurol. 53: S73-84.

McNaught KS, Olanow CW, Halliwell B, Isacson O, Jenner P (2001) Failure of the ubiquitin-proteasome system in Parkinson's disease. Nat Rev Neurosci 2(8): 589-94. Meck WH (1996) Neuropharmacology of timing and time perception. Cognit. Brain Res. 3:227-242.

Meck WH (2006) Neuroanatomical localization of an internal clock: A functional link between mesolimbic, nigrostriatal, and mesocortical dopaminergic systems. Brain Res. 1109:93-107.

Mercuri NB, Bonci A, Calabresi P, Stefani A, and Bernardi G (1995) Properties of the hyperpolarization-activated cation current Ih in rat midbrain dopaminergic neurons. Eur J Neurosci 7(3):462-9.

Minnema DJ, Cooper GP, and Greenland RD (1989) Effects of methylmercury on neurotransmitter release from rat brain synaptosomes. Toxicol. App. Pharmacol. 99:510-21.

Møller-Madsen B (1991) Localization of mercury in CNS of the rat. Iii. Oral administration of methylmercuric chloride (ch3hgcl). Fund. App. Toxicol. 16:172-87.

Nass R, Hall DH, Miller DM, 3rd and Blakely RD (2002) Neurotoxin-induced degeneration of dopamine neurons in Caenorhabditis elegans. Proc Natl Acad Sci USA 99, 3264-9.

Nedergaard S, Flatman JA, and Engberg I (1993) Nifedipine- and omega-conotoxin-sensitive Ca conductances in guinea-pig substantia nigra pars compacta neurones. J Physiol. 466:727-47.

Newland MC and Rasmussen EB (2003) Behavior in adulthood and during aging is affected by contaminant exposure in utero. Curr. Dir. Psych. Sci. 12:212-217.

O'Boyle DJ, Freeman JS, and Cody FW (1996) The accuracy and precision of timing of self-paced, repetitive movements in subjects with parkinson's disease. Brain 119:51-70.

Olanow CW, Obeso JA, and Stocchi F (2006) Continuous dopamine-receptor treatment of parkinson's disease: Scientific rationale and clinical implications. Lancet Neuro. 5:677-87.

Peng S, Hajela RK, and Atchison WD (2002) Effects of methylmercury on human neuronal L-type calcium channels transiently expressed in human embryonic kidney cells (HEK-293). J Pharmacol Exp Ther 302(2):424-32.

Puopolo M, Raviola E, and Bean BP (2007) Roles of subthreshold calcium current and sodium current in spontaneous firing of mouse midbrain dopamine neurons. J Neurosci 27(3):645-656.

Rasmussen EB and Newland MC (2001) Developmental exposure to methylmercury alters behavioral sensitivity to *d* amphetamine and pentobarbital in adult rats. Neurotoxicol Teratol 23:45-55.

Reed MN and Newland MC (2009) Gestational methylmercury exposure selectively increases the sensitivity of operant behavior to cocaine. Behav. Neurosci. 123:408-417.

Roy EA, Saint-Cyr J, Taylor A, and Lang A (1993) Movement sequencing disorders in parkinson's disease. Intern. J of Neurosci. 73:183-94.

Schroeder U, Kreutz MR, Schroeder H, and Sabel BA (1997) Amphetamine induces hypermotility in mptp-lesioned mice. Pharmacol. Biochem. Behav. 56:281-285.

Schuster S, Doudnikoff E, Rylander D, Berthet A, Aubert I, Ittrich C, Bloch B, Cenci MA, Surmeier DJ, Hengerer B, and Bezard E (2009) Antagonizing L-type Ca2+ channel reduces development of abnormal involuntary movement in the rat model of L-3,4-dihydroxyphenylalanine-induced dyskinesia. Biol Psych. 65(6):518-26.

Shafer TJ and Atchison WD (1989) Block of 45Ca uptake into synaptosomes by methylmercury: Ca and Na dependence. J Pharmacol Exp Ther. 248(2):696-702.

Shull RL, Gaynor ST, and Grimes JA (2001) Response rate viewed as engagement bouts: Effects of relative reinforcement and schedule type. J. Exp. Anal. Behav. 75:247-274.

Stubbs A (1968) The discrimination of stimulus duration by pigeons. J Exp. Anal. Behav.11:223-238. Surmeier DJ (2007) Calcium, ageing, and neuronal vulnerability in Parkinson's disease. Lancet Neurol. 6(10): 933-8.

Yuan Y and Atchison WD (1994) Comparative effects of inorganic divalent mercury, methylmercury and phenylmercury on membrane excitability and synaptic transmission of CA1 neurons in hippocampal slices of the rat. Neurotoxicology 15(2):403-411.

Yuan Y and Atchison WD (1999) Comparative effects of methylmercury on parallel-fiber and climbing-fiber responses of rat cerebellar slices. J Pharmacol Exp Ther 288(3):1015-1025

Yuan Y and Atchison WD (2005) Methylmercury induces a spontaneous, transient slow inward chloride current in Purkinje cells of rat cerebellar slices. J Pharmacol Exp Ther 313(2):751-64.

Yuan Y and Atchison WD (2003) Methylmercury differentially affects GABA(A) receptor-mediated spontaneous IPSCs in Purkinje and granule cells of rat cerebellar slices. J Physiol 550(Pt 1):191-204.

Figures Captions

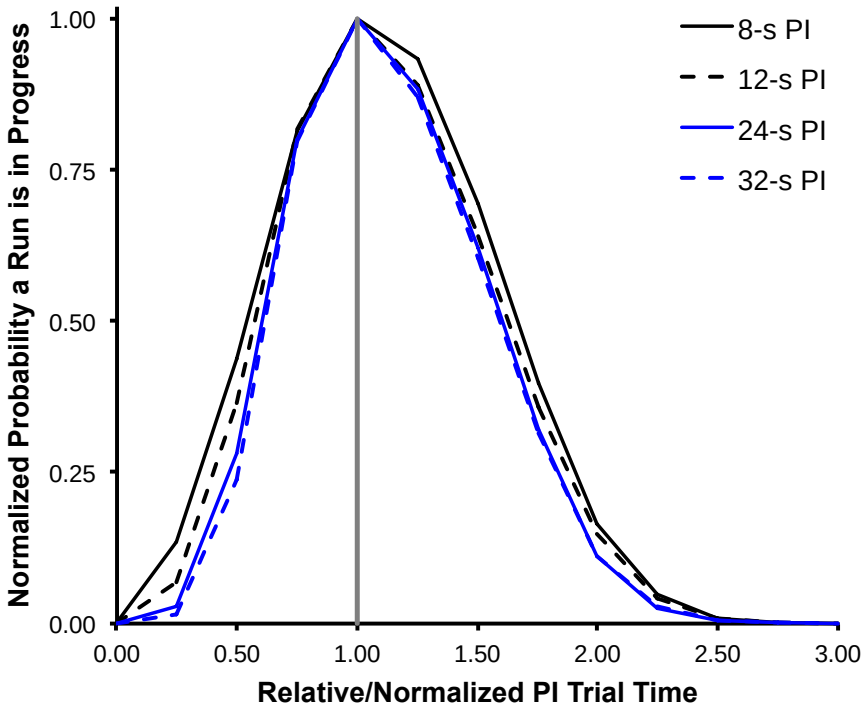

Figure 1. Data obtained under our laboratory's version of the bi-PIC procedure. The graph shows the normalized probability that a run was in progress versus the normalized/relative PI trial time in an individual C57Bl/6 mouse obtained over 250 PI trials at four different target durations. The target durations arranged across multiple blocks of different sessions were 8-s, 32-s, 12-s, and 24-s (in that order). These plots are called normalized peak curves. The rising phase is the cumulative probability of starts and the falling phase is the inverse of the cumulative probability of stops.

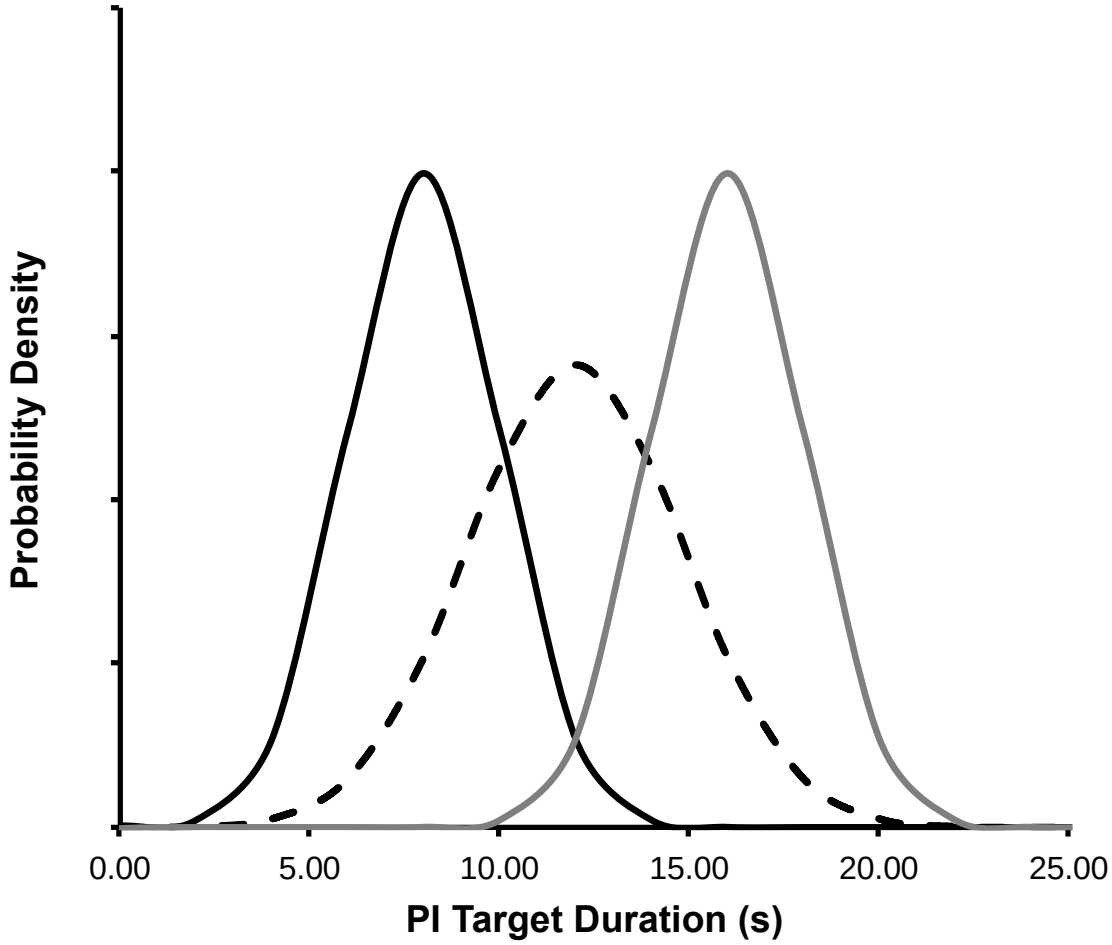

Figure 2. Distributions of percepts corresponding to target temporal durations located at 8-s and 16-s (continuous lines). These distributions are called “discriminal dispersions” and have equal variance on a metathetic continuum. Also shown is another dispersion, located at 20-s (dashed line) and having a variance equal to the sum of the constituent variances.

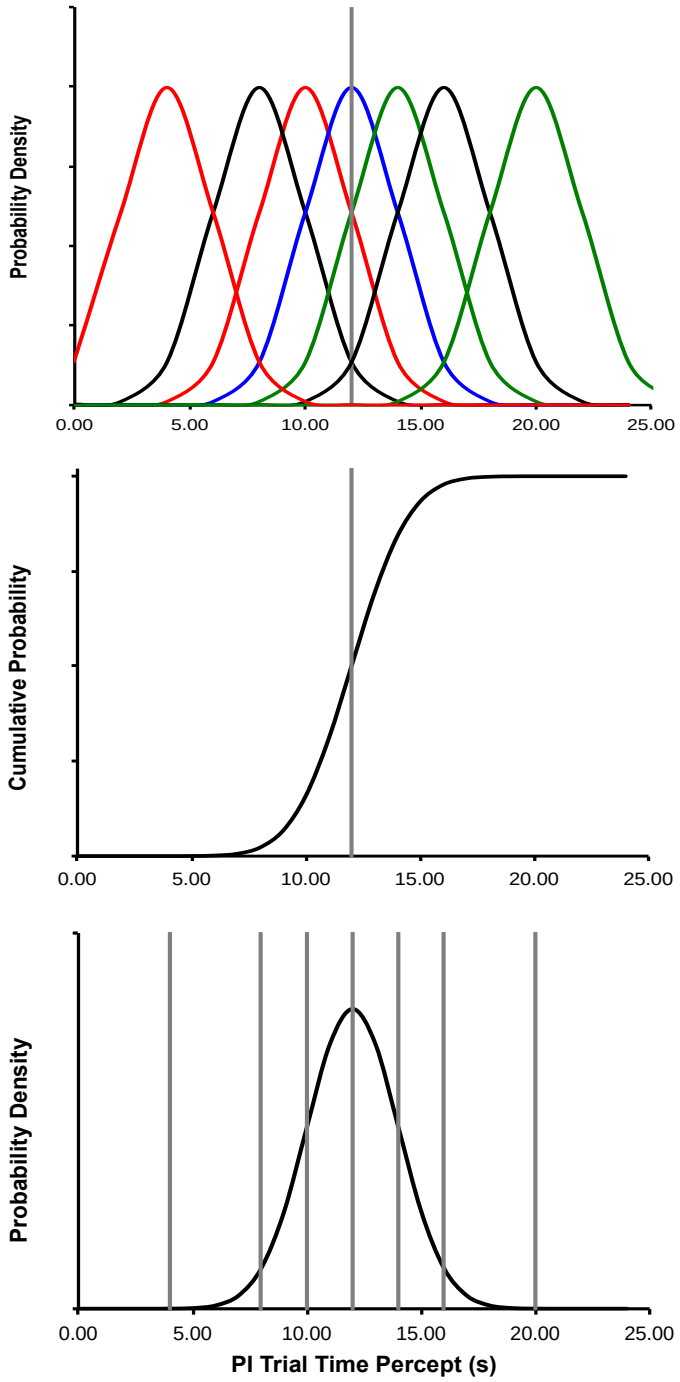

Figure 3. TOP PANEL. Discriminal processes (continuous lines) corresponding to different times into a PI trial (*t*). The solid vertical grey line is the criterion (PSE) dividing the shorter temporal percepts that should be called "short" from the longer temporal percepts that should be called "long," located at 12-s. The solid black lines represent discriminal dispersions for the trained 8-s and 32-s target durations, while the solid red lines represent discriminal dispersions for time at different durations < 12-s into a PI trial during testing and the solid green lines represent discriminal dispersions for time at different durations > 12-s into a PI trial during testing, respectively. MIDDLE PANEL. The area under each density to the right of the criterion in the top panel gives the cumulative probability of responding "long," the psychometric function. BOTTOM PANEL. Sampling the processes from left to right is equivalent to moving the criterion from right to left through a single density located at the PSE (12-s), and thus establishes the curve in the middle panel as a cumulative density, that is, as a distribution function. It is clear that the psychometric function in the middle panel could equivalently have arisen from variable percepts for time and a single cut through the continuum made by the precise criterion (top panel) or from a variable criterion and multiple cuts made through it by precise temporal percepts (bottom panel).

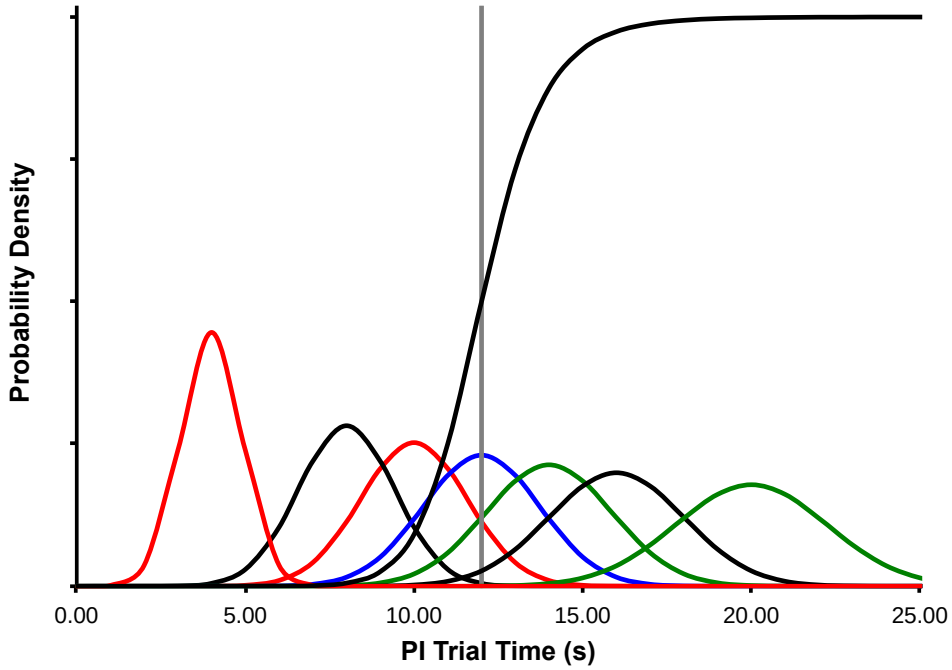

Figure 4. Distributions of percepts arising from time into PI trial of duration 4, 8, 10, 12, 14, 16, & 20-s when the subject was trained to respond at target durations of 8-s (short) and 16-s (long). These discriminal dispersions have increasing variance on prothetic continua, including time or temporal duration. The area under the tail of these densities to the right of the criterion (PSE; 12-s), gives the probability of responding "long" as a function of PI trial time. That probability is given by the rising ogive, which is a pseudo-distribution function given by Eqs.2 and 3 (see text for details).

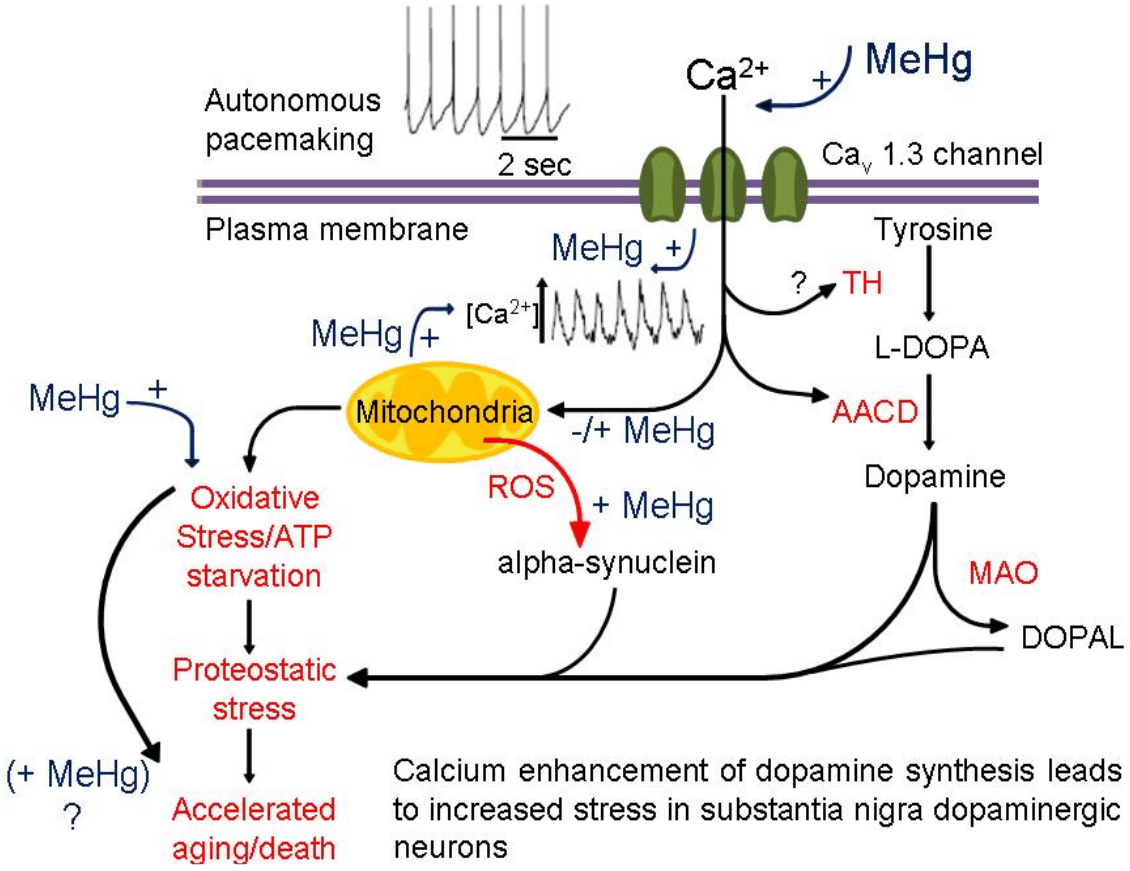

Figure 5. A modified version from Surmeier et al. (2010, 2011) illustrating the proposed cascade by which NSDA neurons in the SNpc exhibit enhanced vulnerability to oxidative damage mediated by increased intracellular $Ca2^{+}$. This figure indicates sits at which MeHg may interact and, as shown, may be numerous.

CHAPTERS 2 & 3

Distortions in bipeak interval timing by chronic methylmercury exposure are attenuated by the L-type Ca++ channel blocker isradipine: Effects of relative and absolute target duration and duration of exposure.

To be submitted to Behavioral Brain Research

Authors: Derek A. Pope, Andrew N. Shen, Blake A. Hutsell, Daniel Hoffman, Megan Arnold, & M. Christopher Newland

ABSTRACT

Nigralstriatal dopamine neurons have a unique, Cav1.3, L-type Ca^{2+} channel that exhibits rhythmic oscillations in Ca^{2+}, conferring pacemaking activities. This may make them vulnerable to Parkinson's Disease (PD) or methylmercury (MeHg) exposure, as both are linked to disrupted Ca^{2+} regulation. Isradipine (ISR), an L-type Ca++ blocker, prevents PD in model systems. Distortions in interval timing, including the migration effect and gross deviations from the scalar property, are behavioral correlates of PD. In the present experiments, timing was assessed in retired breeder, BALB/c mice (~9 months) using the bi-peak interval choice (PIC) procedure. To assess MeHg-induced distortions in timing and investigate the potential role of Ca^{2+} regulation, mice were chronically exposed to 0 or 5 ppm MeHg and 0 or 2 ppm ISR. During Phase 1, *early* into exposure and arranging target durations of 8-s and 32-s, MeHg caused the *short* target duration to be overestimated and the *long* to be underestimated, conforming to Vierordt's law. During Phase 2, *later* in exposure and when target durations were 12-s and 24-s, MeHg caused both target durations to be grossly underestimated. In both phases, MeHg increased the relative variability in timing and caused greater deviations from the scalar property. Importantly, ISR eliminated all MeHg-induced effects on timing variability and any migration effects in timing accuracy. A model-comparison approach, employing theory from the Behavioral Theory of Timing, the Pseudo-Logistic Model, and recent Bayesian models, revealed that these MeHg-induced distortions were due to large reductions in pacemaker/clock speed and increased variability in its regulation. These results add further evidence that one potential way in which MeHg exerts its toxicity is by disrupting Ca^{2+} functioning in nigrostriatal DAergic-neurons and suggest that PD and MeHg may disrupt similar neurobehavioral systems.

CHAPTER 2: INTRODUCTION

The fidelity of time perception in the seconds to minutes range, known as interval timing, is subject to distortion by environmental and pharmacological factors ***(1 – 5)***. The most frequently used experimental procedure for studying interval timing in nonhuman and human animals is a modified version of the fixed interval (FI) schedule called the peak interval (PI) procedure ***(6 – 9)***. Under a PI procedure, responding during standard trials delivers reward at a FI *T*-s after the onset of a warning signal or trial, where *T* is called the target duration. During *peak* trials, reinforcement is withheld and responding is monitored for 2-3 times the target duration. Killeen and Fetterman ***(10, 11)*** extended the single PI procedure by requiring subjects to respond to, or time, multiple, simultaneously elapsing target durations within the same trial. In its simplest form, this peak interval choice (PIC) procedure requires subjects to time two target durations, called a bipeak interval procedure, with reinforcement primed for responses to only of the target durations on each trial; responses on one lever can be reinforced after a *short* duration (e.g., 8-s) and on another after a *long* duration (e.g., 32-s). Under both procedures, subjects begin responding well before the target duration(s) on a given peak trial and stop responding at some point after the target duration(s) has past; thus, responding during peak trials usually brackets the target duration(s). In all species, the starts and stops of responding at a given target duration vary from trial to trial. Averaging over many trials, the probability of making a response as a function of PI trial time, the peak curves, rises to near unity after some proportion of the target duration(s) has elapsed, then returns to near zero as the duration of the peak trial becomes considerably greater than the target duration(s) ***(9, 12)***.

Under the single PI procedure, peak curves from conditions arranging different target durations very nearly superpose when plotted against the relative elapsed proportion of the target duration, that is, when this time is normalized to the absolute peak trial time. This means that both the central tendencies and the spread of the start and stop distributions are nearly fixed proportions of the target durations. Superposition is a manifestation of Weber's psychophysical law, which holds the mean response duration and its variability increase proportionally to increase in target duration, a relationship known as the scalar timing ***(12 – 14)***. The scalar property is a ubiquitous feature of single PI timing data in nonhumans and humans ***(12 – 17)***. Similarly, absolute and relative response rates at each of the arranged target durations under the PIC procedure are an orderly function of time, and show approximately proportional changes with changes in the target duration, consistent with Weber's law and scalar timing.

However, as demonstrated best in the original Killeen and Fetterman PIC studies ***(10, 11)***, the growth in error, expressed as a standard deviation of response distributions, increases in proportion to the square root of the increase in target duration. This is slower than in the single PI procedure and represents a phenomenon known as Poisson timing. This means that the difference in *temporal context* between the single PI and PIC procedures heavily affects the precision of timing. Interestingly, temporal context can also influence the accuracy of interval timing under PIC procedures generally ***(18 – 25)***. For instance, when subjects are required to learn multiple target durations under the PIC procedure, they tend to bias their PI responding towards the mean of *all* target durations presented during FI training by overestimating *short* durations and underestimating *long* durations – a relationship known as Vierordt's law ***(23, 26 – 28).***

Alterations in PI and PIC timing induced by environmental, pharmacological, lesion, or stimulation techniques or by particular disorders and diseases are postulated to be diagnostic of the underlying neuropsychological processes ***(29 – 35)***. Of particular interest here are the persistent distortions in interval timing linked to dopamine-related (DA) dysfunction in the basal ganglia, as epitomized in patients with Parkinson's disease (PD) ***(31, 32, 36 – 39)***. PD is an age-related neurodegenerative disorder characterized by the degeneration of DAergic neurons in the substantia nigra pars compacta (SNpc) that project to the striatum – a region of the brain of critical importance to motor function as well as to interval timing ***(26, 29 - 39).***

Malapani et al. ***(40, 41)*** demonstrated that when PD patients given DA-replacement therapy (ON-drug) are trained and tested under the bi-PIC procedure, the accuracy and precision of PI timing is equal to age-matched controls. Conversely, when PD patients are tested under PI trials OFF-drug, the *short* target duration (6-s or 8-s) is grossly overestimated and the *long* target duration (17-s or 21-s) is underestimated both relative to when ON drug and in the absolute sense. This distortion has been characterized as a 'migration effect,' as though there is a mutual attraction or coupling of previously reinforced response times at the *short* and *long* target durations. Because the migration effect was demonstrated whenever PD patients were tested under PI trials OFF drug, the authors attributed it to a DA-dependent dysfunction in the processes governing the performance of previously reinforced response classes that had been correlated with the target durations during PI trial training, and not a dysfunction in the original learning of those response classes during original FI trial training. Indeed, when PD patients were trained under FI trials OFF-drug, but tested under PI trials ON-drug, this OFF-ON group substantially overestimated both target durations. Apparently, restoring DA functioning during PI testing eliminates the DA-dependent dysfunction in performance processes (migration effect) and unmasks a second, DA-dependent dysfunction in the

processes governing original learning during FI trial training, suggesting a slowing of temporal perception ***(41)***.

DA-dependent distortions in learning (FI training) and performance (PI testing) processes are also distinguishable by changes in the pattern of variability in PD patients ON and OFF drug. In PD patients tested OFF-drug, the migration effect was accompanied by a violation of the scalar property, with the width of the 8-s peak curve being relatively broader than that of the 32-s peak curve. This means that the coefficient of variation (CV), the standard deviation of PI response distributions divided by their mean, was higher at the *short* than the *long* target durations in PD patients tested under PI trials OFF drug. In contrast, the DA-dependent overestimation of both target durations during FI training for the OFF-ON group was linked to timing variability that adhered to the scalar property, with CVs constant across target duration ***(40, 41)***.

At the neurobiological level, a question that remains is why Substantia Nigra Pars Compacta (SNpc) DAergic neurons are vulnerable and succumb in PD, but DA neurons in the Ventral Tegmental Area are relatively spared ***(42 – 46)***. One clue comes from evidence that the DA neurons of the SNpc display intrinsic, autonomous pacemaking activities that depend on the engagement of the relatively rare CaV1.3 subtype of L-type, voltage-gated Ca^{2+}channels ***(44 – 53).*** The engagement of these pacemaking Ca^{2+}channels elevates the sensitivity of SNpc DA neurons to mitochondrial toxicants, suggesting that increased Ca^{2+}entry is a factor in the selective vulnerability of SNpc DA neurons to PD ***(54-58)***. Reducing Ca^{2+}flux via administration of L-type, voltage-gated Ca^{2+}channel blockers, such as isradipine, that cross the blood-brain-barrier (BBB) and have a high affinity for the Cav1.3 channel subtype can delay the onset of PD-like signs and symptoms, slow their progression, prevent their development in model systems ***(48, 55, 59-64)*** and is associated with reduced PD-risk in humans ***(59, 62).*** Several investigators have hypothesized that the main factor driving the neurobehavioral and neurodegenerative changes in PD is the metabolic stress created by sustained Ca^{2+} entry and that this risk is exacerbated by genetic predisposition or environmental challenges that compromise proteostatic competency or protection against oxidation ***(45, 46, 65).***

Genetic mutations have been identified in familial PD ***(55, 56, 66 – 70)***, but the majority of cases of PD are sporadic ***(69, 71)***. Substantial epidemiological evidence suggests a role for environmental contaminants in PD ***(72 – 76)***, but, to date, no specific environmental agent has been shown unequivocally to be causative or act as a risk-factor. Methylmercury (MeHg) accumulates in the basal ganglia ***(77 – 81)*** and may distort functioning in DA neurons, whose cell bodies lie in the SNpc and whose efferent projections include the striatum ***(79 – 82)***. We hypothesize that chronic, adult-onset exposure to MeHg facilitates development of NSDA dysfunction, such as those that lead to PD-like effects. While MeHg could contribute to

SNpc dysfunction or risk of PD, as might arise in a multi-hit model, there is no direct evidence that MeHg is a direct causal factor in the disorder. As such, our hypothesis is grounded in observations that the autonomous pacemaking activity of SNpc DAergic neurons is dependent upon the presence of the CaV1.3 L-type voltage-gated Ca^{2+} channels and, thus, may yield these neurons vulnerable to disruption via aging, PD, or MeHg ***(23, 45, 46, 79 – 82)***. Interestingly, different populations of neurons, in particular, granule cells in the cerebellum, are remarkably susceptible to MeHg exposure due to its disruption of intracellular Ca^{2+}regulation via L-type, voltage-gated Ca^{2+}channels ***(83 – 95)***. Moreover, the well-described ability of L-type, voltage-gated Ca^{2+}channel blockers to delay, decrease, or prevent MeHg-induced neurobehavioral toxicity *in vivo* ***(96, 97)*** and Ca^{2+}-mediated degeneration *in vitro* ***(88)*** suggests that MeHg exposure could disrupt SNpc DA function through interactions with L-type Ca^{2+}channels and altering intracellular Ca^{2+}homeostasis ***(45, 46, 82),*** perhaps in a manner similar to PD.

Both the empirically derived principles of PI and PIC timing and observed deviations described above have influenced the development of theoretical, highly quantitative models of interval timing, most of which posit a special-purpose pacemaker-counter or clock mechanism ***(8, 15 – 17, 98)***. While some current explanations of the timing process implicate internal operations as the basis of the subject's perception of time ***(3-5, 7, 9, 12-14)***, there is much empirical support for the view that behavior mediates temporal control ***(8, 11, 12, 99).*** For instance, Killeen ***(8)*** measured the way in which behavior changes throughout the interval between two reinforcers, describing such processes as a cascade of behavior involving transitions between different classes of behavior as a function of time until reinforcement.

Killeen and Fetterman formalized this notion in their Behavioral Theory of Timing (BeT) ***(8, 11, 12, 99)***, a nuanced theory that describes how subjects respond under timing procedures. BeT first assumes that biologically-important events, like reinforcers and stimuli that signal their availability, activate responses. The resulting responses may be the particular target response(s) of interest or nontarget response classes. As in most pacemaker-counter theories of timing, BeT holds that temporal transitions among *n* different response classes occur with constant probability and are treated as coincident with pulses emitted from an neurobehavioral pacemaker. That is, these pulses could represent events nested within a different level of analysis than the particular events under investigation. These nested events could be classes of behavior or action patterns occurring at a smaller time scale or even patterns of covert, neurobiological events ***(38).*** .

BeT then presumes that the different response classes unfolding during an interval may come to serve as discriminative stimuli for subsequent responses; the organism's sequence of response classes itself becomes the "counter." For instance, when an organism is required to time target durations of different

lengths under a PI procedure, temporal perception may be driven by the ready-made behavioral counter: If the target duration is *short*, then as the time of reinforcement approaches the organism is likely to be engaged in one nontarget response class, such as pacing the left wall of the chamber, but as the *short* time of reinforcement becomes imminent, the pacing transitions to a target response class, such as pressing the left lever in the chamber. If the target duration is *long*, then the organism is likely to engage in a different nontarget response class, such as checking the feeder, before transitioning to another target response class, such as pressing the right lever. If responding *short* on the left lever at a time when they had been pacing the left wall is highly correlated with reinforcement, and responding *long* at a time when they had been checking the feeder is highly correlated with reinforcement, through conditioning processes these nontarget response classes should become discriminative stimuli for the appropriate *short* or *long* target response.

One of the mathematically simplest models of the behavioral transition process in BeT is one in which the pacemaker is maximally random. This is the constant-probability model of BeT, which is called a Poisson process or a Poisson pacemaker. The average period of a Poisson pacemaker, ρ, is also equal to its variance. In contrast to most other theories of timing, however, BeT assumes that the speed and variability of the Poisson pacemaker are a function of the prevailing density of reinforcement: High densities increase pacemaker speed and decrease variability, while low densities decrease speed and increase variability. This way, BeT predicts the ubiquity of Weber's law and scalar timing under the single PI procedure by assuming that changes in the estimation of different target durations are accomplished by proportional changes in the speed of the pacemaker, not by varying the number of behavioral states or criterial pulses registered by the counter ***(8, 11, 12, 99)***.

Under the PIC procedure, subjects time two or more target durations in the same context, so the prevailing overall reinforcement density is constant, Therefore, BeT predicts that the period of the pacemaker also remains constant. Under these conditions, because target durations of different lengths are estimated by varying the number of behavioral states or criterial pulses tallied by the counter, n, the clock system as a whole will manifest less than proportional growth in the standard deviation of peak response distributions, constituting Poisson timing. Thus, a pacemaker that displaying Weber error (which increases linearly with target duration) can still be a component of a clock system whose error grows more slowly with time, as the $\sqrt{n}$, if longer target durations are mensurated by increasing n, that is, by increasing the number of behavioral states or criterial counts ***(11, 12)***.

BeT provides a sound theoretical and quantitative theory of interval timing but it provides no obvious map for predicting start, stop, and center times and CVs under PI procedures or the observed differential

sensitivity of these measures to various procedural and contextual factors ***(9, 100)***. Killeen, Weiss, and colleagues have provided such a map in a general model of error in temporal perception that is generated by any sort of pacemaker-counter system. Importantly, this general model, the dispersion function, allows for BeT, and related models, to be embedded directly, thus building and expanding on the ability to predict interval timing ***(15, 101).*** According to this model ***(15)***, the variability in subjective temporal estimation, and resulting response distributions (σ_t), grows as a function of time, *t*, or target duration, *T*, according to the following equation:

$$\sigma_t = \sqrt{(\omega t)^2 + pt + c^2} \qquad Eq.1\ (\mathbf{15, 101}).$$

In Eq. 1, a dispersion function, the parameter ω governs Weber error and is called the Weber fraction. With $\omega > 0$ and no other sources of error are involved (p & $c = 0$), Eq. 1 rearranges to $\sigma_t = \omega t$; which is the classic formulation of *Weber's Law and scalar timing*; the standard deviation of temporal estimates is proportional to the magnitude of temporal stimulus, *t*. Killeen and Weiss ***(15)*** showed that the parameter ω, represents one form of error in the counter of a clock system alone. BeT presumes that $\omega > 0$ when predicting the growth in error of peak response distributions arranging different overall rates of reinforcement, such as across conditions under the single PI procedure. Pure Weber error, however, seems to be the exception, not the rule under PIC procedures ***(8, 9, 11, 12, 101)***

The parameter ρ in governs Poisson error; with $p > 0$ and no other sources of error involved (ω & $c = 0$), Eq. 1 rearranges to $\sigma_t \approx \sqrt{pt}$, which is *Poisson Dispersion or Poisson Timing*. Here, the standard deviation of temporal estimates is proportional to the square root of the magnitude of the time point, *t.* Killeen and Weiss showed that the parameter *p* primarily reflects the magnitude of pacemaker variability ***(10, 15, 101)***. Accordingly, it can be assumed that the value of *p* represents both the period and the variability of the pacemaker ($1/p$ = pacemaker rate), with higher values of *p* indicative of slower pacemakers with longer periods and greater variability. Killeen and Weiss also showed, however, that ρ may represent error in the counter or the transitioning between behavioral states, such as might occur if the counter occasionally adds or drops a pulse with a probability of $1 - p$, which constitutes Bernoulli error in the counter. In relation to BeT, this means that an organism may occasionally fail to transition to the next behavioral state or skip over one behavioral state and transition to a latter state. Because a Poisson pacemaker and Bernoulli counter have equivalent and indiscriminable effects in this model, and the evidence supporting a mechanistic neurobehavioral role for a Poisson pacemaker far outweighs that for a Bernoulli counter, it is assumed here that *p* primarily reflects the processes of a Poisson pacemaker. BeT presumes that $p > 0$ when predicting the

growth in error of peak response distributions at different target durations in a context with a constant overall reinforcement rate, such as under the PIC procedure.

Finally, the parameter *c* reflects a constant error in the clock system that occurs when pulses from the pacemaker must be accumulated by the counter; the variance associated with this switch would appear as a source of constant error ($c > 0$). This could be motoric latency that occurs in transitioning from one response class to another or a fractional count, as would occur when a free-running pacemaker is wedged in the center of a cycle when the interval begins, introducing an error proportional to the period of the pacemaker it multiplies. In this formulation, it means that *c* is equal to the product of the synchronization error or error in setting the start or stop criterion, μ, and the period of the pacemaker, *p.*

While the dispersion function adeptly describes, predicts, and offers a mechanistic explanation of the precision of temporal perception and response distributions, Eq. 1 provides no direct way to predict temporal accuracy. Killeen and colleagues ***(101)*** provided a model in which the dispersion function can be embedded into a separate process and, thus, attain a coherent analysis of both the precision and accuracy of start and stop psychometric functions and peak response distributions under the PIC procedure. The method used here calculates probabilities based on deviation of a subjective criterion, such as the start and stop time, μ, from objective time point *t* or target duration *T,* divided by the estimated standard deviation, derived from the dispersion function in Eq. 1, at objective time point *t* or target duration *T*:

$$p = \left[1 + e^{\left(\frac{\mu - t}{0.55\sigma_t}\right)}\right]^{-1}, \qquad Eq.2\ (\mathbf{101}).$$

Equation 2 is called the Pseudo-Logistic Function and in combination with Eq. 1, the Pseudo-Logistic Model (PLM) ***(101)***. The PLM asserts that there is variance in the perception and estimation of time and that variance follows the dispersion function. The single ogive given by Eq. 2 traces the area to the right of a criterion, μ, which is equivalent to the criterial behavioral state or count, *n,* in BeT, for each time point or target duration.

The BeT-PLM model hypothesizes that the PD-induced distortions in PIC timing are due to an overall slowing in motor and behavioral domains in the form of, respectively, bradykinesia and bradyphrenia. These, which may occur together or separately, and are thought to result from DA-depletion in the SNpc. In relation to the BeT-PLM model, such DA-dependent slowing would be reflected by an increase in the period of the pacemaker and the variability in its regulation, *p* in Eq. 1, and, according to the real-time criterion view of constant error, also an increase in *c*. While such a prediction by the PLM model accounts for the overall greater variability in temporal perception and response distributions as well as the violations of the scalar property and adherence to Poisson error in PD patients tested OFF drug under the PIC procedure, it also

predicts all target durations to be overestimated. This is clearly not the case for PD patients tested OFF drug, as strong migration and inaccuracy is also observed.

The well-established psychophysical properties of interval timing, their sensitivity to degeneration and dysfunction of DAergic systems, and the role of Ca^{2+}-mediated processes in these systems in the SNpc, indicate that a timing preparation could be an exemplary method to quantify the mechanisms underlying behavioral neurotoxicity. In the present experiments, the effects of chronic, adult-onset exposure to 5 ppm MeHg on the accuracy and precision of interval timing as assessed under the PIC procedure was examined using retired breeder, BALB/c mice that were about 9 months old at beginning of exposure. The MeHg dose was selected so that neurotoxicity would unfold slowly. To investigate the role of Ca^{2+} homeostasis/regulation, concurrent, chronic adult-onset exposure was provided to either 0 ppm or 2 ppm of the L-type Ca^{2+} blocker, isradipine (ISR). Phase 1 assessed *PIC* timing <u>*early*</u> into exposure (weeks 10 – 20) using target durations of 8-s (*short*) and 32-s (*long*), that is, widely spaced (1:4 relative difference). Phase 2 assessed *PIC* timing <u>*later*</u> in exposure (weeks 22 – 32) and the target durations were changed to 12-s (*short*) and 24-s (*long*), that is, spaced closer to one another (1:2 relative difference). A model-comparison approach ***(102),*** integrating the theories and assumptions of BeT ***(8, 10, 11)***, the PLM ***(15, 101)***, and more recent Bayesian models of interval timing ***(23),*** was employed to assess the validity of different models.

EXPERIMENT 1

2.1 PHASE 1

2.1.1 Materials and Methods

<u>*2.1.1.1 Subjects*</u>. Fifty-eight, approximately nine-month-old, experimentally naïve, adult male, BALB/c mice were purchased as retired breeders from Harlan Laboratories and pair-housed in clear, polycarbonate Optimax cages with woodchip bedding located in an AAALAC-accredited facility. The Optimax cages were attached to an OptiMICE® HVAC quality air controller that provides separate airflow to each cage. A Plexiglas barrier located in the meridian of the cage served to separate cage-mates, who were always in the same exposure group, effectively creating single-housing. This was necessary because adult BALB/c mice frequently display lethal aggression against each other.

The vivarium was temperature- and humidity-controlled and maintained on a 12-h light-dark cycle (lights on at 06:00). All animals were maintained at approximately 24 g by feeding a measured quantity of food daily (usually 3.0 g). Thus the mice did not acquire excess fat, which can accumulate MeHg and the daily dose of ISR was relatively constant. Two MeHg water concentrations and two ISR diets produced a 2 (MeHg) X 2 (ISR) full factorial design with 14 or 15 mice in each of the 4 exposure groups. Mice were

assigned to treatment groups such that they were indistinguishable on pre-exposure evaluation of free-feeding body mass, performance on rotorod, and autoshaping of lever-pressing.

2.1.1.2 MeHg and ISR Exposure. Mice were exposed chronically to 0 or 5 ppm of mercury as methyl mercuric chloride, dissolved in their only source of drinking water. Water consumption was measured daily for several weeks at various times during exposure to determine the approximate dose of MeHg per day. Within each MeHg exposure group, mice were exposed chronically to 0 or 2 ppm of the L-type calcium channel blocker, ISR, in their chow. These doses corresponded to approximately 0 and 0.2 mg/kg/day of ISR, based on consumption calculations. Chow was manufactured by Purina Test Diets and based on a 5LL2 laboratory chow diet. Methyl mercuric chloride was purchased from Alfa-Aesar (Ward Hill, MA) and ISR from Sigma-Aldrich (St. Louis, MO). Exposure to both MeHg and ISR began about 2 weeks after the mice arrive to the vivarium, when the mice were ~36 weeks of age.

2.1.1.3 Apparatus. Experimental sessions were conducted in 11 operant conditioning chambers manufactured by Med Associates (Med Associates Inc., St. Albans, VT, model # MED ENV-007, 12.0" L x 9.5" W x 11.5" H) enclosed in sound-attenuating cabinets and modified to accommodate mice. The rear wall in each chamber was equipped with two Sonalert® tone generators located at the top of the chamber equidistant (L and R) from a centrally positioned houselight. The front wall of each chamber was equipped with two retractable response levers (ENV-312-2R). Above each lever, a LED light was available to be illuminated and responses to each lever exceeding approximately 0.05 N were counted as effective responses. A liquid dipper system (ENV-302W-SX) located equidistant from the two response levers delivered sweetened condensed milk. Liquid reinforcement consisted of 0.1 cc presentations of a 3:1 solution of water: milk. Two SONALERT tone generators were located on the back wall of the chamber equidistant from one another. In an adjacent room, a Windows® computer with Med Associates® IV programming and interface system controlled experimental events and collected data with a temporal resolution of 0.01 s.

2.1.1.4 Criteria for Euthanasia. Animals were inspected daily and body weight was recorded five days per week. If an animal appeared ill or moribund, as defined by weight loss, failure to eat, failure to locomote when placed on an open surface, the attending veterinarian was consulted. An effort was undertaken to keep an animal alive, providing it did not prolong distress. Animals meeting predefined criteria for euthanasia were euthanized using procedures approved by the Auburn IACUC.

2.1.2 General Procedure

Mice were weighed prior to each session, and then placed in the operant chambers. Mice responded under a peak-interval choice procedure, adapted from Fetterman & Killeen ***(10, 11)*** in which responding was reinforced under a mixed, concurrent FI *short*-s EXT, EXT FI *long*-s schedule. That is, subjects could respond on either of two concurrently available levers. Responses on one were sometimes reinforced following a relatively *short* target duration. With equal probability, responses on the second lever were reinforced following a relatively *long* target duration. Subjects could, and almost always did, begin responding on the "short" lever and then transition to the "long" lever if no reinforcer was delivered after a period of time. Sessions under this two-lever choice procedure lasted 50 trials or 90 minutes, whichever occurred first. Which lever was correlated with the *short* and *long* FIs was counterbalanced across-subjects and within-exposure groups.

During Phase 1, the target durations for the *short* and *long* target durations were 8-s and FI 32-s respectively. That is, mice responded under a mixed, concurrent FI 8-s EXT, EXT FI- 32-s schedule, a relative difference of 1:4 and absolute difference of 24 s. Phase 1 was designed to assess performance of each group under two widely spaced intervals early into exposure.

2.1.2.1 Standard Trials. Subjects were initially trained on standard FI trials that always arranged reinforcement for responding under the 8-s or 32-s target durations during the first 3 of the 10 weeks of exposure in Phase 1 (weeks 10 – 13). Trial onset was signaled by the illumination of the houselight for 10-s followed by a 2-s presentation of a high-tone, low-tone alternation. Then both the left and right levers were inserted into the chamber and the LED located above each lever was illuminated. One half of the trials arranged reinforcement for responding on the lever correlated with the *short,* FI 8-s (left or right lever depending on counterbalancing), while the remaining trials arranged reinforcement for responding on the lever correlated with the *long,* FI 32-s. Reinforcement was assigned with equal probability to the levers in a quasi-random fashion such a manner that reinforcement from a particular lever did not occur on more than three consecutive trials. On a given trial, responding could have occurred on either of the concurrently available levers, but the first response on the *long* lever, usually a switch from responding on the *short* lever to the *long* lever, resulted in the retraction of the *short* lever. If the trial arranged reinforcement for responding on the *short* lever, the first press following 8-s resulted in the reinforcement cycle comprising retraction of both levers, extinguishing of both LEDs, and access to 3-s of dipper presentation. If the trial arranged reinforcement for responding on the *long* lever, the first press after 32-s resulted in the same reinforcement cycle.

Trials included a limited hold on the availability of reinforcement by restricting the availability of

reinforcement to a window ranging from the programmed time of reinforcement to 150% of that time. Thus, if no response occurred after 12-s for the *short* and 48-s for *long* lever during a trial, the lever retracted and the trial ended. Trials were separated by a 15-s ITI during which the chamber was dark, and then a new trial began. The limited hold ensured that programmed and obtained time intervals were in close accord. No correction procedure was used; success or failure in obtaining reinforcement on one trial had no effect on the requirements for subsequent trials. Succeeding reinforcer delivery was a 15-s blackout ITI, followed by the trial onset stimuli. Sessions ended after 50 trials were completed.

2.1.2.2 Peak Interval (PI) Trials. Peak interval (PI) trials were interspersed within each session during the final 7 of the 10 weeks of exposure in Phase 1 (weeks 13-20 of exposure). During PI trials, all conditions were the same as a standard trial, except that reinforcement was withheld at the usual FI target durations for both *short* and *long* lever responses. These trials permitted subjects to respond well after the usual to-be-timed intervals. When the target durations were 8-s and 32-s, these PI trials lasted on average 80-s (2.5 times the *long* FI). The length of PI trials varied quasi-randomly from trial-to-trial around an average of 2.5 times the *long* target duration to discourage the resurgence of responding on an available alternative(s) at the end of PI trials ***(100)***.

During PI sessions, 30 of the 50 trials were PI trials and the remaining 20 were standard trials, split evenly between the *short* and *long* target durations. During PI sessions, PI and standard trials were selected in a quasi-random fashion, such that out of every 10 trials, two trials primed reinforcement for responding on the *short* lever, two trials primed reinforcement for responding on the *long* lever, and the remaining six trials were PI trials ending in nonreinforcement for responding at both the *short* and *long* target durations.

2.1.3 PI Data Analysis: Raw Data

For each subject, the last 250 PI trials from the final 9 consecutive sessions in Phase 1 were selected for analysis. These 250 PI trials occurred during weeks 17-20 of exposure. During nearly all of these PI trials contained at least one lever press, and typically many, so that on the vast majority of trials there was a visually obvious run of more or less sustained responding that bracketed each of the *short* and *long* to-be-timed target durations.

Under PI choice procedures, a smooth, bell-shaped response function that summits around the arranged target duration(s) and whose ascending and descending limbs rise and fall around that summit typically appears but this smooth curve is an artifact of averaging many uniform start and stop response distributions across individual PI trials ***(7, 9, 16)***. Such averaging obscures the underlying structure of interval timing and temporal generalization on a trial-by-trial basis, which is usually characterized by an abrupt onset

and offset of a high-rate of responding at the arranged target duration(s) ***(6, 7, 9, 16)***. Therefore, a more detailed analysis of the microstructure of timed behavior on each trial was undertaken. For individual subjects, performance on individual PI trials was modeled as a break-run-break pattern of responding. The algorithm for finding 'start' and 'stop' times on each PI trial was adapted from Church, Meck, and Gibbon ***(7)*** and applied on a trial-by-trial basis for each individual subject independently for responding at the *short* and *long* target durations. Specifically, responding at each target duration was divided into three mutually exclusive and exhaustive intervals: 1) an initial duration during which the mouse was disengaged from lever-pressing (i.e., *short* or *long*) more often than engaged, 2) a run duration during which the animal was lever-pressing more often than not at a particular target duration, and 3) a final duration during which the animal was again disengaged from lever pressing at a particular target duration more often than pressing (see appendix for details concerning the algorithm).

The trial-by-trial start and stop times were used to calculate the durations, dwell times, of a run, which was simply the stop time minus the start time. The center of a run was (start time plus + time)/2 for the respective target durations on each PI trial. These start, stop, dwell, and center times derived from algorithm 1 were determined for individual subjects for each of the last 250 PI trials and their mean, standard deviation, and coefficient of variation were derived, again for each individual subject ***(9)***. These measures were then averaged across subjects of each exposure group for final inspection and model-comparison analyses, described next.

2.1.4 PI Data Analysis: Model Comparison

The effects of MeHg and ISR exposure on PI timing, as reflected in the parameters of the PLM (Eqs. 1 & 2) were analyzed using an information-theoretic, model comparison approach ***(102)***. By identifying the model that is most likely to represent the data, this approach can also provide support for hypothesized mechanisms by which exposure disrupts PI timing. The general approach entailed examining the effects of MeHg and ISR on responding during PI trials of individual subjects in each group as determined by the relative contribution(s) of start-and-stop criteria (μ), Weber (ω), Poisson (ρ), and constant criterial (c) error from the PLM in predicting the accuracy and precision of PI responding. This approach is ideally suited to testing complex models such as the ones examined here. One reason is that it determines the probability of the model given the data, the reverse of what null hypothesis statistical testing does. A second is that this approach is more likely to identify the best model when a large number of candidate models are being examined ***(102)***.

As described below, because analyses of the raw data (see also appendix) revealed several effects of MeHg and ISR on the accuracy and precision of timing, model-fitting and comparisons were carried out independently for each exposure to determine the best-fitting PLM for each exposure group during Phase 1. Specifically, five different PLMs were compared for each exposure group and these allowed all possible, theoretically consistent, combinations of μ, ω, ρ, and c that could remain constant or vary across target duration (see appendix for details). The five different instantiations of the PLM were fitted to each individual subject's cumulative 8-s and 32-s start and stop distributions for a total of 5 models tested for each exposure group. Specifically, the five different PLMs were estimated for individual subjects of each group by minimizing the sum of squared deviations between PLM-predicted and observed cumulative 8-s and 32-s start and stop distributions using Solver in Microsoft Excel. The results were compared with obtained start/stop distributions, start/center/stop times, start/center/stop standard deviations and CVs, as well as the resulting peak curves for individual subjects of each group.

As mentioned briefly in the introduction, rather than treat c as a free parameter in this analysis, it was assumed, in accordance with previous applications of the PLM ***(101),*** that c is composed primarily of error in estimating the location of start/stop criteria, and subject to the same dispersion function as the estimation of real time. That is, criterial error was modeled as growing as the magnitude of the start/stop criteria increases. Although there are reasons for which this may estimate the true value of c erroneously, in various applications of the PLM ***(101)*** this assumption has proven to account for the data more parsimoniously than when c is treated as a free parameter.

All five models originally allowed 4 different values of μ to be estimated for each subject: 1 for the 8-s start criterion, 1 for the 8-s stop criterion, 1 for the 32-s start criterion, and 1 for the 32-s stop criterion. Thus, the 5 PLMs differed only in the theoretically consistent combinations of ω and ρ that could remain constant or vary across target duration for each individual subject. Specifically, the 5 PLMs compared for each subject were 1) the *Pure Weber PLM*, where only ω (Weber fraction) was allowed to vary, but remained constant across target duration, $\rho = 0$, and $c = \omega\mu$, for a total of 5 free parameters for each subject; 2) the *Pure Poisson PLM,* where only ρ (Poisson fraction) was allowed to vary, but remained constant across target duration, $\omega = 0$, and $c = \sqrt{(\rho\mu)}$, for a total of 5 free parameters for each subject; 3) the *Mixed Poisson PLM,* where only ρ was allowed to vary, but the value of ρ was also allowed to vary across target duration, $\omega = 0$, and $c = \sqrt{(\rho\mu)}$, for a total of 6 free parameters for each subject; 4) the *Weber/Pure Poisson PLM,* where both ω and ρ were allowed to vary, but each remained constant across target duration, and $c = [\omega\mu + \sqrt{(\rho\mu)}]$, for a total of 6 free parameters for each subject; and 5) the *Weber/Mixed Poisson PLM*, where both ω and ρ were

allowed to vary, ω remained constant across target duration, but ρ was also allowed to vary across target duration, and $c = [\omega\mu + \sqrt{(\rho\mu)}]$.

2.2 RESULTS: PHASE 1

2.2.1 PLM Comparison and Parameter Estimates

Table 1 shows the results of the model comparison for each exposure group during Phase 1. The *Mixed Poisson PLM*, which allowed only ρ to vary and the value of ρ could vary across target duration, clearly provided a better fit than the other four models tested for the 0 MeHg, 0 ISR, 0 MeHg, 2 ISR, and 5 MeHg, 2 ISR groups, respectively, as revealed by the much lower AICcs. Because the Akaike weights of all other models tested were 0.00 and the Akaike weights for the *Mixed Poisson PLMs* were 1.00 for each of these three groups, the *Mixed Poisson PLM* was selected as the 'best' model for each of these three groups during Phase 1. Conversely, for the 5 MeHg, 0 ISR group, the *Pure Poisson PLM*, which allowed only ρ to vary, but the value of ρ remained constant across target duration, clearly provided a better fit than the other four models tested, as revealed by the much lower AICcs. Again, because the Akaike weights of all other models tested were 0.00 and the Akaike weight for the *Pure Poisson PLM* was 1.00 for this group, the *Pure Poisson PLM* was selected as the 'best' model for the 5 MeHg, 0 ISR group during Phase 1.

Table 2 shows the parameter estimates obtained from the *Mixed Poisson* or *Pure Poisson PLMs* for the respective exposure groups during Phase 1. The values of *p* estimated under the *Mixed Poisson* PLMs for the 0 MeHg, 0 ISR, 0 MeHg, 2 ISR, and 5 MeHg, 2 ISR groups increased from the 8-s to the 32-s target duration, respectively. For all groups, the distributions of the estimated values of *p* showed heavy positive skew so the harmonic mean of individual subject values of *p* was used as the measure of central tendency as recommended ***(101)***. This transformation reduced the impact of heteroscedasticy, mitigated the impact of large, outlying values of *p*, and enhanced the impact of small, more accurate and precise values. The harmonic mean estimated values of pacemaker period, *p,* are shown in Table 2. As permitted by revised versions of BeT ***(11, 12)***, the increase in the value of *p* from the 8-s to the 32-s target duration for each of these three groups was consistent with a increase in pacemaker period and variability or a decrease in pacemaker rate induced by the decrease in the local rate of reinforcement as a function of elapsing PI trial time and lengthening target duration. Next, the global or overall value of *p* across the two target durations (i.e., *p Global*) was determined for individual subjects and is shown in Table 2. For the three groups with the *Mixed Poisson* PLM as the best-fitting model, *p Global* was calculated by taking the harmonic mean estimated value of *p* at the *short* and estimated value of *p* at the *long* target duration for individual subjects. Finally, for the groups with the *Mixed Poisson* PLM as the best-fitting model, the ratio of the value of *p* at the

long to the value of *p* at the *short* target duration (i.e., *p Ratio*) was determined for individual subjects of each group, also shown in Table 2.

The *Pure Poisson* PLM was the best-fitting PLM for the 5 MeHg, 0 ISR group during Phase 1, so a single value of *p* served across both target durations for individual subjects of this group. According to both original and revised versions of BeT, a constant value of *p* across target durations means that the pacemaker period and, by definition, its variability, was controlled exclusively the overall reinforcement rate in the context and was insensitive to changes in the local rate of reinforcement determined by the target duration. Because the *Pure Poisson PLM* was the best-fitting model for the 5 MeHg, 0 ISR group, the value of *p Global* for individual subjects was identical to the constant value of *p* that served across the two target durations for said subjects. The *p Ratio* value was also calculated for individual subjects in the 5 MeHg, 0 ISR group, but because the *Pure Poisson* PLM was the best-model for this group (i.e., value of *p* constant), the *p Ratio* value for all subjects was set to 0.00 because there was not an increase/change in pacemaker period/variability as a function of target duration (Table 2).

2.2.2 Systematic Error: Peak Curve Accuracy

If all of the factors determining whether a mouse was lever-pressing at a given point in a trial scaled with target duration, that is, if they occurred at the same relative point during the PI trial regardless of absolute target duration, then normalized 8-s and 32-s peak curves for each exposure group would lie on top of each other, or superpose ***(9)***. Normalized peak curves (Figure 1) plot the probability that a run is occurring on the *short* and *long* levers as a function of normalized trial time. Figure 1 shows that the obtained, normalized peak distributions (symbols) from the two target durations did not superpose, indicating violations of the scalar property for each exposure group. In fact, the obtained, normalized peak curves for each group showed substantial deviation from the target durations (1.00 on x-axis), indicative of systematic error in peak curve accuracy. The lines drawn through the data points in Figure 1 show the mean, normalized 8-s and 32-s peak curve predictions from the best-fitting *PLMs* for each exposure group (Tables 1 & 2). These *PLM* predicted, normalized peak curves accounted for about 99% of the variability in the obtained data for each exposure group.

Figure 2 shows the same obtained, normalized peak curves organized by target duration in order to emphasize the distinctiveness of MeHg's effect in the absence of isradipine. Both figures show that for all groups except the 5 MeHg, 0 ISR, 8-s peak curves were shifted leftward relative to the target duration (underestimated), while 32-s peak curves were shifted rightward (overestimated). Figure 2 shows that the 8-s

peak curve for the 5 MeHg, 0 ISR group was, however, shifted rightward relative to the target duration and all other groups, while the 32-s peak curve was shifted leftward, evidence of migration in this exposure group.

If the temporal locations of the rising (starts) and falling limbs (stops) and summits of these peak curves scaled with target duration, then the plots of their normalized values would be flat. As seen in Figure 2, however, these functions were not flat for any exposure group, again indicative of non-scalar systematic error in start, stop, and center proportions. This means that start and stop criteria were asymmetrically located around the target duration and that the direction of asymmetry depended on both the target duration and exposure group. Table 3 summarizes these results by showing the mean 8-s and 32-s start, stop, and center proportions for each exposure group. In accord, Figures 1 – 3 and Table 3 demonstrate that 8-s center proportions were greater than 1.0 (overestimation) and 32-s center proportions less than 1.0 (underestimation) for the 5 MeHg, 0 ISR group only, while the opposite obtained for all other groups.

2.2.3 Trial-to-Trial Variability: Peak Curve Precision

Even if the means of start and stop distributions do not superpose or are asymmetric, the standard deviation, indicative of the degree of peak timing precision, could still be scalar and consistent with Weber's law ***(9)***. If so, then the standard deviations of start and stop distributions will increase proportionally with mean time points and the start, center, and stop CVs will be constant across target duration.

Figure 4 plots the standard deviations of starts and stops at the two target durations as a function of the mean time of those starts and stops. Each point represents an individual subject and the four panels correspond to the different exposure groups. The solid line drawn through the data points in each of the four panels represents predicted standard deviations of start and stop distributions if the growth in error proceeded with strict adherence to Weber's law and scalar timing. As shown in Figure 4, the standard deviations of start and stop distributions increases with mean start and stop time for all groups. In all cases, however, the growth in error grossly deviates from that predicted by Weber's law and scalar timing; the solid lines in Figure 4 grossly overpredict the growth in standard deviations for all groups and the degree of overprediction becomes more extreme as mean start and stop times and, thus, target duration, increase. For all groups, the increase in variability of start to stop points ***within*** a target duration proceeds more slowly than the increase in variability from the *short* to the *long* target duration.

Figure 5 shows the mean obtained, standard deviations of the distributions of start and stop times as in Figure 4 (symbols) as a function of the mean obtained time of those starts and stops for each exposure group, which are delineated by the four panels. The solid lines are the predicted standard deviations of the distributions of start and stop times derived from the best *PLM*s for each exposure group. For all groups,

these *PLM* predicted standard deviations accounted for >96% of the variance in individual subject data for each exposure group.

Figure 6 graphs mean start, center, and stop CVs as a function of the mean time of those starts, centers, and stops for each exposure group (see Table 4 for values). Consistent with Figures 4 and 5, CVs are not constant for any exposure group, confirming large violations of Weber's law and the scalar property. Instead, in accord with previous reports ***(7, 9, 100)***, start CVs are universally higher than stop CVs, with the single exception being slightly lower 32-s start than 8-s stop CVs for the 5 MeHg, 0 ISR group. Consistent with BeT ***(8, 10, 11, 101)***, for all groups, start, stop, and center CVs decrease as their mean times increase, but the rate and extent of this decrease in CVs is greater in the context of the *short*, 8-s target than the *long*, 32-s target duration. Further, across target durations, start CVs decrease at a greater rate and to a greater extent than center CVs, which decrease at a greater rate and to a greater extent than stop CVs. Thus, CVs decrease as the mean response time of the distributions increase, but the rate and extent of the decrease in CVs also decreases as the mean response time of the distribution increases. Importantly, note that 8-s and 32-s CVs are all generally higher for the 5 MeHg, 0 ISR group compared to all other groups, indicating that the relative variability in these response distributions is greater for the 5 MeHg, 0 ISR group than all other groups. The relative variability in these response distributions is generally lower for the 0 MeHg, 2 ISR group compared to all other groups. Finally, notice the 'step-functions' for the 0 MeHg, 0 ISR, 0 MeHg, 2 ISR, and 5 MeHg, 2 ISR, in Figure 5; CVs at the 8-s and 32-s target durations decrease from start to center to stop times, but there is an increase or step-up in 32-s start CVs (fourth data point from the left in each panel) relative to 8-s stop CVs (third data point from the left in each panel) for these three groups. In contrast, for the 5 MeHg, 0 ISR group, 32-s start CVs are lower than 8-s stop CVs.

The lines drawn though the data points in Figure 6 represent the predicted CVs for the distributions of start, center, and stop times derived from the best *PLM* for each exposure group during Phase 1. For the 0 MeHg, 0 ISR, 0 MeHg, 2 ISR, and 5 MeHg, 2 ISR groups, the best-fitting *Mixed Poisson* PLM accurately predicts the obtained start, center, and stop CVs in each phase and, importantly, predicts the higher 32-s start CVs than 8-s stop CVs during Phase 1 (i.e., CV step functions). The *Mixed Poisson* PLM predicts these step-functions because the overall height of the predicted lines is determined by the local rate of reinforcement, which is lower for the 32-s than the 8-s target duration. The slopes are set by a Poisson counting system whose pacemaker period increases significantly with decreased reinforcer rate or increased target duration. For the 5 MeHg, 0 ISR group, the best-fitting *Pure Poisson* PLM during Phase 1 also accurately predicts the obtained start, center, and stop CVs and, importantly, predicts the lower 32-s start

CVs than 8-s stop CVs. For all groups, these *PLM* predicted CVs accounted for >97% of the variance in individual subject data for each exposure group.

2.2.4 Peak Curve Accuracy and Precision: PLM Comparisons

Inspection and analyses concerning peak curve accuracy and systematic error in peak response distributions indicated that 8-s and 32-s peak curves, and underlying start/stop and center distributions, migrated towards one another for the 5 MeHg, 0 ISR group, causing overestimation of the *short*, 8-s target duration and underestimation of the *long,* 32-s target duration. These results are in accord with Vierordt's law and indicative of migration. In contrast, all other groups underestimated the *short*, 8-s target duration and overestimated the *long,* 32-s target duration. As best shown in the peak curves (Figures 1 & 2) and plots of normalized start, stop, and center proportions (Figure 3) for the 5 MeHg, 2 ISR group, ISR eliminated the MeHg-induced overestimation of the 8-s and underestimation of the 32-s target durations. Similarly, inspection and analysis of peak curve precision and trial-to-trial variability in peak response distributions revealed that, while 8-s start and 32-s stop CVs were indistinguishable across exposure groups, 8-s center, 8-s stop, 32-s start, and 32-s center CVs were higher for the 5 MeHg, 0 ISR group than all other groups, which were indistinguishable from one another with the exception of 8-s stop CVs being lower for the 0 MeHg, 0 ISR group compared to the other two groups. These discrepancies were best illustrated by exposure-related distinctions in the difference between 32-s center CVs and 8-s center CVs. Thus, not only were 8-s and 32-s center CVs higher for the 5 MeHg, 0 ISR group compared to all other groups, these elevated 8-s and 32-s center CVs were more disparate (i.e., greater violation of the scalar property) or the difference between 8-s and 32-s center CVs greater, and, thus, so too were the rate and extent of the decrease from 8-s center to 32-s center CVs (Table 4; see appendix for details).

The results for the raw PI data and above discussions of BeT and the PLM suggest that the period of the pacemaker period and the variability in its regulation (*p-Global*) should be higher for the 5 MeHg, 0 ISR group compared to all other groups. This is because the degree and direction of systematic error conformed to Vierordt's law for this group only, and because the relative variability in response distributions (CVs) was generally greater for this group compared to all other groups. In addition, *p-Global* should be lowest for the 0 MeHg, 2 ISR group because response distribution CVs were generally lower for this group compared to all other groups. In accordance, as shown in Table 2, the *p-Global* was highest for the 5 MeHg, 0 ISR group relative to all other groups (~1.95 times higher on average) and lowest for the 0 MeHg, 2 ISR group compared to all other groups (~2.15 times lower on average).

2.3 DISCUSSION: PHASE 1

Chronic, adult-onset exposure to MeHg disrupted both the accuracy and precision of timing early into exposure. In accord with the BeT-PLM-comparison, MeHg's distortions of timing occurred by greatly slowing pacemaker speed and increasing the variability in its regulation. This is the precise pattern observed in PD patients OFF drug ***(40, 41)***. Moreover, the 5 MeHg, 0 ISR group was the only group during Phase 1 to demonstrate a migration effect reminiscent of Vierordt's law. This pattern was also seen, but to a greater quantitative extent, in PD patients OFF the drug L-Dopa. Further, the relative variability in the degree of deviation from Weber's law and scalar timing was greater for this group than all other groups. The 8-s target duration was relatively more variable than the 32-s target duration, both overall and relative to the other three groups, a strong violation of Weber's law and scalar timing. Although the degree of migration was much lower for the 5 MeHg, 0 ISR group compared to PD patients OFF drug, the MeHg-induced elevation in variability and gross violation of the scalar property were strikingly similar to that reported in PD patients OFF drug ***(40, 41)***.

The migration effect observed for this group appears to be a result of MeHg-induced dysfunction during the performance of previously reinforced response classes during PI trials, as opposed to a dysfunction in original learning of these response classes during standard FI trials. For this group, the uncertainty in the estimation of target duration was elevated, an observation that implies and was confirmed to be a result of a slower pacemaker with greater variability in its regulation. In the context of BeT, this means that there were fewer and more variable transitions between different behavioral states and observable responses classes across the two target durations for the 5 MeHg, 0 ISR group. As a result, PI responding was more heavily governed by a single mixture distribution comprising previously, less precisely reinforced response classes and times at both target durations, rather than PI responding at each target duration being governed independently by separate distributions established at each target duration. Thus, due to the disruption of learning processes caused by the slower pacemaker with increased variability in its regulation, which elevated the temporal uncertainty in the subjective estimation of elapsing trial time and current target duration, PI responding at each target duration was more heavily governed by the single, mixture distribution of previously, less precisely reinforced response classes than the estimation of PI trial time or target duration.

Through the above process, the relative variability in PI response distributions in the mice exposed to MeHg alone was reduced, but at the cost of a migration effect, which more heavily affected the *long* target duration, as predicted and described in previous studies ***(38)***. This means that the *long* was underestimated by a relatively greater proportion than the *short* was overestimated. Consequently, the much higher 8-s than 32-s CVs for this group is best understood as a by-product of incorporating the single mixture distribution of

previously reinforced response classes into the uncertain estimation of current PI trial time and target duration.

The hypothesis that the effects of MeHg on PIC timing are the result of MeHg-induced DA depletion in the basal ganglia due to disrupted Ca^{2+} homeostasis, perhaps mediated by CaV 1.3 channels in the SNpc, was tested by the co-administration of ISR. Importantly and consistent with this hypothesis, ISR eliminated the MeHg-induced slowing of the global pacemaker-counter, the increase in its variability, the resulting mixture distribution and migration, and increased the pacemaker's sensitivity to changes in local reinforcement rate. Indeed, the 0 MeHg, 2 ISR group demonstrated the fastest pacemaker-counter or clock system with the lowest variability, and greatest sensitivity to changes in local reinforcement rate, resulting in generally lower response time CVs, but greater "step-up" in the CV function (Figure 6).

CHAPTER 3: EXPERIMENT 2

3.1 PHASE 2

To determine further the effects of MeHg and ISR on bipeak interval timing, Phase 2 assessed PIC timing *later* in exposure (weeks 22 – 32) and when the target durations were changed to 12-s (*short*) and 24-s (*long*), that is, spaced relatively closer to one another such that the ratio of intervals was 1:2.

3.1.1 Materials and Methods

3.1.1.1 Subjects. Subjects were the same as those used in Experiment/Phase 1. One subject died from each of the 0 MeHg groups (both *n*s = 13) and two subjects died from each of the 5 MeHg groups (both *n*s = 13) during Phase 2; their data were excluded from analysis.

3.1.1.2 MeHg and ISR Exposure. MeHg and ISR exposure was identical to Experiment/Phase 1.

3.1.1.3 Apparatus. The apparatus was identical to Experiment/Phase 1.

3.1.1.4 Criteria for Euthanasia. The criteria for euthanasia were identical Experiment/Phase1 1.

3.1.2 General Procedure

The general procedure was identical to that employed in Experiment/Phase 1 with the exception that the target durations for the *short* and *long* target durations were changed to FI/PI 12-s and FI/PI 24-s, respectively (1:2 relative difference; 12-s absolute difference).

3.1.2.1 Standard Trials. In Phase 2, subjects were again initially trained on standard trials that always arranged reinforcement for responding under the 12-s and 24-s target durations. Training under standard trials occurred during the first 3 of the 10 weeks of exposure in Phase 2 (weeks 22 – 25). All other aspects of the procedure were identical to experiment 1.

3.1.2.2 Peak Interval (PI) Trials. Following training under standard trials during the first 3 weeks of

exposure in Phase 2, reliable responding was again established at the 12-s and 24-s target durations, respectively. During the final 7 of the 10 weeks of exposure in Phase 2 (weeks 25-32) peak interval (PI) trials were interspersed within each session. In Phase 2, when the target durations were 12-s and 24-s, PI trials lasted on average 60 s (2.5 times the *long* FI). All other aspects of the procedure were identical to Phase 1.

3.1.3 PI Data Analysis: Raw Data

Raw PI Data analyses were identical to Phase 1.

3.1.4 PI Data Analysis: Model Comparison

The effects of MeHg and/or ISR on the parameters of the PLM during Phase 2 were determined using the same information-theoretic, model comparison approach used in Phase 1 (see appendix for details).

3.2 RESULTS: PHASE 2

3.2.1 PLM Comparison and Parameter Estimates

Table 5 shows the results of the model comparison for each exposure group during Phase 2. As in Phase 1, the *Mixed Poisson PLM* clearly provided a better fit than the other 4 models tested, for all groups except the 5 MeHg, 0 ISR group. Because the Akaike weights of all other models tested were = 0.00 and the Akaike weights for the *Mixed Poisson PLMs* were = 1.00 for each of these three groups, the *Mixed Poisson PLM* was selected as the 'best' model for each of these three groups during Phase 2. Also as in Phase 1, for the 5 MeHg, 0 ISR group, the *Pure Poisson* model clearly provided a better fit than the other 4 models tested during Phase 2, as revealed by the much lower AICcs. Because the Akaike weights of all other models tested were = 0.00 and the Akaike weights for the *Pure Poisson PLM* was = 1.00 for this group, the *Pure Poisson PLM* was selected as the 'best' model for the 5 MeHg, 0 ISR group during Phase 2.

Table 6 shows the parameter estimates obtained from the *Mixed Poisson* or *Pure Poisson PLMs* for each respective exposure groups during Phase 2. The calculations and measures of central tendencies for the values of *p, p Global*, and *p Ratio* were carried out in the same manner as in Phase 1. Similar to Phase 1 and also predicted by BeT, during Phase 2 the value of *p* increased from the 12-s to the 24-s target duration for the three groups with the *Mixed Poisson PLM* as the best-fitting model (*p-Ratios* > 1). As permitted by revised versions of BeT ***(11, 12)***, the increase in the value of *p* from the 12-s to the 24-s target duration for each of these three groups was consistent with a increase in pacemaker period and variability or a decrease in pacemaker rate induced by the decrease in the local rate of reinforcement as a function of elapsing PI trial time and lengthening target duration.

Conversely, because the *Pure Poisson* PLM was again the best-model for the 5 MeHg, 0 ISR group during Phase 2, the value of *p* remained constant across the 12-s and 24-s target duration (*p-Global*).

According to both original and revised versions of BeT, a constant value of *p* across target durations means that the pacemaker period and, by definition, its variability, was controlled exclusively the overall reinforcement rate in the context and was insensitive to changes in the local rate of reinforcement determined by the target duration. Therefore, the value of *p Global* for individual subjects was identical to the constant value of *p* that served across the two target durations and, thus, *p-Ratio* = 0.00 for all subjects (Table 6).

3.2.2 Systematic Error: Peak Curve Accuracy

Figure 7 shows that the obtained, normalized peak distributions (symbols) from the two target durations did not superpose for any exposure group and there was substantial deviation in the summits of these curves from the to-be-timed target durations, indicative of non-scalar systematic error. The lines drawn through the data points in Figure 7 show the mean, normalized 12-s and 24-s peak curve predictions from the best-fitting *PLMs* for each exposure group (Tables 5 & 6). These *PLM* predicted, normalized peak curves accounted for about 99% of the variability in the obtained data for each exposure group.

Figure 8 shows the same obtained normalized peak curves organized by target duration in order to emphasize that the degree and direction of systematic error at each target duration again differed among exposure groups. For all groups, 12-s peak curves were shifted leftward relative to the target duration (underestimated), but to a greater extent for the two 5 MeHg groups than the two 0 MeHg groups, which were indistinguishable, respectively. In contrast, for all groups except the 5 MeHg, 0 ISR group, 24-s peak curves were shifted rightward relative to the target duration (overestimated). The 24-s peak curve for the 5 MeHg, 0 ISR group was, however, shifted grossly leftward relative to the target duration and all other groups (underestimated).

Also in accord with Phase 1, the temporal locations of the rising (starts) and falling limbs (stops) and summits of these peak curves did scale with target duration (superpose) and, thus, the plots of mean normalized start, stop, and center times in Figure 9 were not flat for any exposure groups. Again, this is indicative of non-scalar systematic error in start, stop, and center proportions, meaning that start and stop criteria were asymmetrically located around the target durations and that the direction of asymmetry depended on both the target duration and exposure group. Table 7 summarizes these results by showing the mean 12-s and 24-s start, stop, and center proportions for each exposure group. In accord, Figures 7 – 9 and Table 7 demonstrate that 12-s center proportions were less than 1.0 for all groups, but much the degree of underestimation was much greater for the two 5 MeHg groups than the two 0 MeHg groups. In contrast, the 5 MeHg, 0 ISR group was the only group demonstrating 24-s center proportions less than 1.0, while 24-s center proportions overestimated the target duration for all other groups.

3.2.3 Trial-to-Trial Variability: Peak Curve Precision

Figure 10 plots the standard deviations of 12-s and 24-s start and stop distributions as a function of the mean time of those starts and stops for individual subjects; the four panels correspond to the different exposure groups. The solid line in each of the four panels represents predicted standard deviations of start and stop distributions if the growth in error proceeded with strict adherence to Weber's law and scalar timing. For all groups, the standard deviations of start and stop points increased with mean start and stop points, but in all cases the growth in error deviated substantially from that predicted by Weber's law and scalar timing; Weber's law grossly overpredicted the growth in standard deviations. Thus, all results with this measure observed during Phase 1 were essentially replicated during Phase 2.

Figure 11 shows mean obtained, standard deviations of the distributions of start and stop times as in Figure 10 (symbols) as a function of the mean obtained time of those starts and stops for each exposure group, which are delineated by the four panels. The solid lines are the predicted standard deviations of the distributions of start and stop times derived from the best *PLM*s for each exposure group. For all groups, these predicted standard deviations derived from each group's respective, best-fitting PLM accounted for >95% of the variance in individual subject data in each exposure group.

Figure 12 graphs mean start, center, and stop CVs as a function of the mean time of those starts, centers, and stops for each exposure group (see Table 8 for values). Consistent with Figures 10 and 11, and Phase 1, CVs are not constant for any exposure group, confirming large violations of Weber's law and the scalar property. Instead, start CVs are universally higher than stop CVs, with the single exception being the lower 24-s start than 12-s stop CVs for the 5 MeHg, 0 ISR group. Consistent with BeT and Phase 1, for all groups, start, stop, and center CVs decrease as their mean times increase, but the rate and extent of this decrease in CVs is greater in the context of the *short*, 12-s target than the *long*, 24-s target duration. Further, CVs decrease as the mean response time of the distributions increase, but the rate and extent of the decrease in CVs also decreases as the mean response time of the distribution increases. Importantly, note that 12-s and 24-s CVs are all generally higher for the 5 MeHg, 0 ISR group compared to all other groups, while the relative variability in these response distributions is generally lower for the 0 MeHg, 2 ISR group compared to all other groups. Finally, notice the 'step-functions' for the 0 MeHg, 0 ISR, 0 MeHg, 2 ISR, and 5 MeHg, 2 ISR, in Figure 12; CVs at the 12-s and 24-s target durations decrease from start to center to stop times, but there is an increase or step-up in 24-s start CVs (fourth data point from the left in each panel) relative to 12-s stop CVs (third data point from the left in each panel) for these three groups. In contrast, for the 5 MeHg, 0 ISR group, 24-s start CVs are lower than 12-s stop CVs.

The lines drawn though the data points in Figure 12 represent the predicted CVs for the distributions of start, center, and stop times derived from the best *PLM* for each exposure group during Phase 2. For the 0 MeHg, 0 ISR, 0 MeHg, 2 ISR, and 5 MeHg, 2 ISR groups, the best-fitting *Mixed Poisson* PLM accurately predicts the obtained start, center, and stop CVs in each phase and, importantly, predicts the higher 24-s start CVs than 12-s stop CVs during Phase 2 (i.e., CV step functions). For the 5 MeHg, 0 ISR group, the best-fitting *Pure Poisson* PLM during Phase 1 also accurately predicts the obtained start, center, and stop CVs and, importantly, predicts the lower 24-s start CVs than 12-s stop CVs. For all groups, these *PLM* predicted CVs accounted for >96% of the variance in individual subject data for each exposure group during Phase 2.

3.2.4 Peak Curve Accuracy and Precision: PLM Comparisons

Inspection and analyses concerning peak curve accuracy and systematic error in peak response distributions during Phase 2 indicated that the *short,* 12-s peak curves and accompanying start/stop and center distributions were shifted leftward for all groups, but to a greater extent for the two 5 MeHg than the two 0 MeHg groups. In contrast, the 5 MeHg, 0 ISR group was the only group to underestimate the *long,* 24-s target duration, while all other groups demonstrated overestimation. This means that although ISR did not protect against the MeHg-induced underestimation of the 12-s target duration, ISR eliminated the MeHg-induced underestimation of the 24-s target duration. Thus, in a similar fashion to Phase 1, peak curves at the *long,* 24-s target duration migrated towards the *short*, 12-s target duration for the 5 MeHg, 0 ISR group, while 24-s peak curves separated or moved away from the 12-s target duration for all other groups. Although this result for the 5 MeHg, 0 ISR group is indicative of migration of the *long* target duration, because the 12-s target duration did not demonstrate rightward migration, but instead, also showed a leftward shift, Vierordt's law and true migration were not observed.

Similarly, inspection and analysis of peak curve precision and trial-to-trial variability in peak response distributions revealed that the relative variability in all response distributions was greater for the two 5 MeHg than the two 0 MeHg groups. However, CVs were generally highest for the 5 MeHg, 0 ISR group, and lowest for the 0 MeHg, 2 ISR group. Importantly, ISR eliminated the MeHg-induced elevation in all CVs except for 12-s start CVs. As in Phase 1, note that although 12-s and 24-s CVs were generally higher for the 5 MeHg, 0 ISR group compared to all other groups, the degree of elevation (i.e., group differences) was much greater at the *short* than the *long* target duration (see Table 8 for details), indicating larger violations of the scalar property for the former compared to the latter three groups.

As in Phase 1, the results for the raw PI data and above discussions of BeT, the PLM, and more recent Bayesian models of timing suggest that the period of the pacemaker period and the variability in its

regulation (*p-Global*) should be higher for the 5 MeHg, 0 ISR group compared to all other groups. This prediction should hold because the degree and direction of systematic error conformed most closely to Vierordt's law for the 5 MeHg, 0 ISR group only, and because the relative variability in response distributions (CVs) was generally greater for this group compared to all other groups. Also as in Phase 1, *p-Global* should be lowest for the 0 MeHg, 2 ISR group during Phase 2 because response distribution CVs were generally lower for this group compared to all other groups. In accord, as shown in Table 6, *p-Global* was highest for the 5 MeHg, 0 ISR group, around 1.80-fold higher, on average, compared to all other groups, while *p-Global* was lowest for the 0 MeHg, 2 ISR group, around 2.00-fold lower, on average, compared to all other groups.

3.3 DISCUSSION: PHASE 2

Similar to Phase 1, chronic, adult-onset MeHg exposure distorted both the accuracy and precision of PI timing at the *short* and *long* target durations, despite the fact that this was later into exposure, there was greater experience with the PIC procedure, and the target durations were more closely spaced than in Phase 1. In contrast to Phase 1, chronic, co-exposure to ISR eliminated only the MeHg-induced leftward migration and underestimation of the *long,* 24-s target duration, but not the relatively greater underestimation of the *short,* 12-s target duration. In accord with Phase 1, ISR attenuated or eliminated all MeHg-induced elevations in the relative variability of peak response distributions. These results add to those revealed during Phase 1 and suggest that continued, chronic, adult-onset MeHg exposure disrupts interval timing and time perception and continued ISR exposure eliminates many of these disruptions.

In accord with the BeT-PLM-comparison, recent hypotheses provided by Bayesian models of PI timing, and, to some extent, Phase 1, continued MeHg exposure during Phase 2 disrupted both the accuracy and precision of timing by, in part, slowing mean pacemaker speed and increasing the variability in its regulation, again consistent with effects observed in PD patients OFF drug. During Phase 2, however, an additional MeHg-induced disruption in the accuracy of PI timing was revealed, one that was immune to protection by ISR: Both 5 MeHg groups underestimated the *short,* 12-s target duration to a greater degree relative to the two 0 MeHg groups. The results of Malapani et al. ***(53, 54)***, above discussions, and hypotheses all suggest that this MeHg-induced alteration was due to disruption in the processes governing the reinforcement of accurate response classes at the 12-s target duration during standard FI trials, not an additional disruption in the processes governing subsequent PI trial performance. In relation to BeT, it is as if the increased period of the pacemaker and elevated variability in its regulation caused behavioral states or counts early than those veridical and more highly correlated with responding at the 12-s target duration to be reinforced during standard FI trials. As a result, peak responding at the 12-s target duration was governed by

a highly variable, grossly underestimated and inaccurate distribution of previously response classes and times.

The massive leftward shift and underestimation of the 24-s target duration for the 5 MeHg, 0 ISR group, however, suggests that the MeHg-induced disruption of the processes governing subsequent PI trial performance persisted and resulted in a sort of asymmetrical (leftward) migration. Thus, as in Phase 1, such a migration effect, primarily affecting the *long*, 24-s target duration, is hypothesized to be a result of MeHg-induced dysfunction during performance of previously reinforced response classes during PI trials, while the underestimation of the *short,* 12-s target duration is hypothesized to result from dysfunction in the learning processes during standard FI trials at that target duration only. For the 5 MeHg, 0 ISR group, the uncertainty in the estimation of current target duration was again elevated, due to an increase in pacemaker period and elevated variability in its regulation. This could be the result of continued, MeHg-induced DA depletion in the basal ganglia due to disrupted Ca^{2+} homeostasis, perhaps mediated by Ca^{2+} Ca V1.3 channels in the SNpc. If so, then, as a result, PI responding would be more heavily governed by a mixture distribution comprising previously reinforced times at the two target durations instead of separate PI responding at each target duration being governed by independent distributions established at each target duration. Because of the additional MeHg-induced disruption in the learning processes at the 12-s target duration during FI trial training, however, the mixture distribution would comprise a large proportion of much shorter, previously reinforced behavioral states and classes. Thus, the MeHg-induced disruption in the original learning process at the 12-s target duration during Phase 2 effectively counteracted or masked the rightward migration of the 12-s peak curves, but enhanced the leftward migration of the 24-s peak curves, causing a gross underestimation relative to all other groups and in the absolute sense. Through this process, the relative variability in PI response distributions was reduced at the cost of the migration effect, which more heavily affected the *long* target duration, as predicted by recent theories ***(38)***, which also resulted in the much higher 12-s than 24-s CVs for this group, indicating greater violations of scalar property and adherence to Poisson timing.

To summarize, ISR did not protect against the MeHg-induced disruption in the learning processes at the 12-s target duration but did eliminate the MeHg-induced slowing of the global pacemaker-counter or clock system, the increase in its variability, the resulting migration or mixture distributions, and also increased the sensitivity of the clock system to changes in local reinforcement rate to levels similar to that seen in the two 0 MeHg groups. Indeed, as in Phase 1, the 0 MeHg, 2 ISR group demonstrated the fastest pacemaker-counter or clock system with the lowest variability, and greatest sensitivity to changes in local reinforcement rate,

resulting in generally lower response time CVs, but greater "step-ups" in the CV functions(Figure 12), respectively.

GENERAL DISCUSSION

The goals of the present experiments were to 1) examine the effects of chronic, adult-onset exposure to a relatively low-level of methylmercury (MeHg) on bi-peak interval timing and time perception in aged, adult BALB/c mice; 2) examine the role of Ca^{2+} in MeHg's neurotoxicity and potential protection by chronically co-administering the CaV 1.3 L-type Ca^{2+}blocker, isradipine (ISR). These goals were achieved by examining PIC performance relatively *early* into exposure/life (Phase 1; Exposure weeks 17-20) using target durations spaced relatively far apart (FI/PI 8-s & 32-s; 1:4 relative difference and *later* into exposure/life (Phase 2; Weeks 29-32) using target durations that were spaced closer.

Chronic, adult-onset MeHg exposure distorted both the accuracy and precision of PI timing at the *short* and *long* target durations arranged in each phase, results that are remarkably consistent with those of a study by Laties and Evans, which showed that chronic MeHg exposure lowered response rates, shortened run lengths, and increased run distribution variability in pigeons responding under a Fixed Consecutive Number schedule ***(112)***. This is pertinent because that procedure required the animals to respond a fixed number of times on one response before executing a second one. Thus, both in that procedure and in BeT, effective responding requires a sort of counting process and MeHg apparently disrupted this process in similar ways, even though the specific procedure as well as the species were quite different. Co-exposure to ISR alleviated or protected against the rightward migration of the *short* peak curves in Phase 1, the leftward migrations of the *long* peak curves in both phases, and all MeHg-induced distortions in the precision of PI timing. With the exception of the leftward shift in the *short* peak curves during Phase 2, the degree and direction of distortions by MeHg and protection by were qualitatively similar across the two phases despite differences in the temporal context and the duration of exposure. These results are the first to our knowledge to show that chronic, adult-onset MeHg exposure disrupts interval timing and time perception, thus adding to the literature concerning the compound's neurobehavioral toxicity. These results also add further evidence MeHg exerts its neurobehavioral toxicity, at least in part, by disrupting Ca^{2+} functioning. Isradipine's specific activity at CaV1.3 calcium channels suggests that this toxicity is mediated by DA neurons in the SNpc.

The *PLM* comparison helped identify which theoretical models were potentially applicable and which parameters MeHg and/or ISR influenced. First, the inconstancy of the start, stop, and center CVs for all exposure groups across both phases indicated that the *Pure Weber PLM* could not be the best model for any exposure group during either phase. In accord with predictions of BeT and previous applications of the PLM,

because the overall rate of reinforcement was held constant during each phase and subjects were required to time two target durations simultaneously, the best-*PLM* for all groups in each phase contained at least 1 value of *p*. The original formulation of BeT theorized that the pacemaker's rate and error, *p*, changed only as a function of changes in the overall rate of reinforcement in the experimental context ***(8).*** This prediction held true only for the 5 MeHg, 0 ISR group, as demonstrated by the single estimated value of *p* that remained constant across target duration under the best-fitting *Pure Poisson PLMs* during Phase 1 and 2. More recent, revised formulations of BeT posit that the value of *p* may also change as a function of changes in the local rate of reinforcement ***(10, 11, 101)***, such as elapsed PI trial time or lengthening of target duration. Indeed, this revised prediction held true for all other groups, with two values of *p* estimated during each phase, one for each target duration, respectively, under the best-fitting *Mixed Poisson PLMs* for the 0 MeHg, 0 ISR, 0 MeHg, 2 ISR, and 5 MeHg, 2 ISR groups. Also in accordance with the revised version of BeT, the value of *p* in the *Mixed Poisson PLM* for each of these three groups increased from the *short* to the *long* target durations in each phase. As illustrated in numerous studies ***(8, 11, 12, 101)***, this increase in pacemaker period as a function of increases in target duration was less than proportional for these three groups in both phases (*p-Ratio;* Tables 2 & 6).

The application of recent Bayesian theories and models of interval timing may, in combination with the BeT-PLM model, be well-suited to predict both distortions in the precision and accuracy of PIC performance, such as that seen in PD patients OFF drug or as in the current study with chronic MeHg exposure ***(38, 40, 41)***. Note that these Bayesian models posit that the PD- or MeHg-induced distortions in PIC timing may be related to and/or different degrees of manifestation of Vierordt's law ***(23, 40, 41)***. In relation to BeT and the PLM, the Bayesian models hypothesize that the observations of Vierordt's law in non-PD patients and the elevated variability, violation of the scalar property, and migration effects in PD patients OFF drug and the 5 MeHg, 0 ISR group in the present experiments are, first, the consequence of a DA-dependent slowing in temporal perception during the learning process (FI training). That is, both the BeT-PLM model and the Bayesian models assume that the slowed perception of currently elapsing trial time or, said differently, the increase of temporal uncertainty in the subjective estimation of elapsing time, are due to decreases in pacemaker speed and increased variability in its regulation. This is represented by elevations or increases in *p* and *c* in Eq. 1 and results in greater variability in the peak response distributions derived from the PLM. The Bayesian models then, however, take a further step, positing that as *p* and *c* in Eq. 1 and disruption of learning processes increases, so does the probability that subsequent PI trial responding and testing performance will be governed by a single, mixture distribution comprising previously reinforced sequences of

behavior at all arranged target durations in the context. This then results in an increased probability that peak response distributions will conform to Vierordt's law or more extreme migration, as peak trial performance is biased towards the mean of the mixture distribution, instead of peak responding at each target duration being governed independently by distributions established at the different target durations during FI training, which was exactly what was observed in the 5 MeHg, 0 ISR group during Phase 1 and, to a lesser extent, Phase 2.

Thus, Bayesian models coupled with BeT and the PLM hypothesize a trade-off between the accuracy and precision of responding and performance during PI trial testing. The extent to which the mixture distribution controls the performance processes governing peak responding and, thus, the extent of migration during PI trial testing, then depends on the level of temporal uncertainty in learning processes governing the subjective estimation of currently elapsing trial time. In relation to the BeT-PLM model, this means that the start and stop criteria for different target durations, μ in Eq. 2, will migrate towards one another as *p* and *c* in Eq. 1 increase. Therefore, any intervention that produces bradyphrenia should disrupt the learning processes governing the subjective estimation of elapsing trial time by increasing the period of the pacemaker and the variability in its regulation. This disruption of the learning processes then causes alterations in the performance processes governing the execution of previously reinforced sequences of behavior during PI trial testing, resulting in overall increased variability in start and stop distributions and peak curves and migration of peak response distributions towards the mean of the mixture distribution. Although an intervention producing bradyphrenia should result in overall elevated variability in all peak response distributions, variability will grow according to Poisson, not scalar timing. Although many of these predictions were confirmed in the present experiments, future research may seek to readily apply such a model to PI timing data.

In accord with the previous discussion, during both phases the best-fitting PLM for the 5 MeHg, 0 ISR group indicated that MeHg's effects were due to an elevation in the temporal uncertainty in the estimation of currently elapsing trial time, caused by large increases in the period of the pacemaker and concurrent elevated variability in its regulation. In relation to BeT, this means that the transitions between behavioral states and response classes were slower, fewer, and more variable across the two target durations arranged in each phase. As a result, and in accordance with recent Bayesian models, this impairment in learning processes caused subsequent peak responding and performance during PI trials to be more heavily governed by a single, mixed distribution of previously, but less precisely reinforced response classes across both target durations within each phase, rather than by the subjective estimation of currently elapsing trial time ***(38)***. With peak responding and performance more heavily governed by a single mixture distribution,

rather than independent distributions for each target duration, it essentially compensates for MeHg-induced disruption of the learning processes

Across phases, MeHg disrupted the processes governing the accurate learning of veridical reinforcement times, which, according to BeT represent impairment in the transitioning between behavioral states and reinforcement of behavioral states or count other than those that are veridical to the target duration and the associated response class. Interestingly, MeHg also impaired performance during the subsequent recital of those previously reinforced response classes during PI trial testing, which, according to BeT represents a disruption of performance processes, such as failing to transition to a behavioral state, skipping transitions to subsequent behavioral states, or the mixing of behavioral states from two different sources of reinforcement. This means that exposure to MeHg produced opposite effects on the direction of systematic error (accuracy) in peak curves at the *short* target durations across Phase 1 and 2. Interestingly, exposure to ISR only protected against the MeHg-induced rightward migration and overestimation of the *short* target duration during Phase 1, but had no effect on the MeHg-induced leftward shift and underestimation of the *short* target duration during Phase 2. Together, these results may suggest that: 1) the neurobehavioral mechanisms underlying the MeHg-induced distortions and selective ISR-induced protection at *shorter* target durations were altered in different manners, or different mechanisms/systems were altered altogether, depending on the duration of exposure; 2) the absolute lengths of the *short* and *long* target durations or the differences between the phases altered the way in which MeHg disrupted and ISR selectively preserved the accuracy of PI responding at *shorter* target durations; or 3) both 1) and 2) acted or interacted in some manner.

In contrast, the observation that MeHg produced similar effects on the direction of systematic error, underestimation, in peak curves at the *long* target durations across each phase and produced similar elevations in the relative variability of PI response distributions across each phase, suggests that the neurobehavioral mechanisms underlying these MeHg-induced distortions and protective effects of ISR were altered in similar manners, or similar mechanisms were altered. Further, this also suggests that these effects did not generally depend on the duration of exposure and/or differences in the absolute lengths of the target durations and/or their absolute and relative differences within and across each phase. The necessity of inhibiting previously reinforced times from the *short* upon timing the *long* target duration may require the involvement of an additional inhibitory, striato-pallidal circuit during PI trials only ***(40, 41)***. If so, the results here would suggest that the functioning of these circuits, while potentially disrupted by MeHg, seem not to depend on duration of exposure or context, and may then may also be more readily combated by ISR

exposure. Whether the separable patterns of MeHg-induced dysfunction and ISR-induced protection rely on distinct neural networks or cellular processes within the basal ganglia or their efferent targets remains to be answered by future research.

In conclusion, chronic exposure to 5 ppm MeHg, a relatively low dose, disrupted the accuracy of interval timing under a bi-PIC procedure across two phases of an experiment in a manner that conformed to Vierordt's law, building on previous findings ***(23)*.** Moreover, MeHg also greatly disrupted the precision of PI timing. Interestingly, the respective migration effects observed across Phase 1 and Phase 2 were qualitatively similar to those reported in PD patients tested under PI trials OFF drug, albeit not to the same extent, quantitatively. The large, overall MeHg-induced elevations in PI timing variability and greater deviations from the scalar property induced by MeHg, however, were both qualitatively and quantitatively similar to those reported in PD patients OFF drug. The evidence suggesting that DAergic neurons in the SNpc succumb in PD because of the autonomous pacemaking activities of these neurons driven by the unique L-type, voltage gated Ca^{2+}, CaV 1.3 channels ***(45 – 71)***, together with the observation that ISR protected against most of the MeHg-induced disruptions of interval timing across the present experiments, adds evidence that one mechanism by which MeHg exerts its neurobehavioral toxicity is through these disruption of Ca^{2+} regulation or homeostasis in SNpc DAergic neurons ***(72 – 97)***. Future research should attempt to more fully test this hypothesis and determine if PD and MeHg affect similar neurobiological systems and similar neurobehavioral manifestations.

REFERENCES

[1] Droit-Volet S, Meck WH (2007) How emotions colour our perception of time. Trends in Cog Sci 11: 504–13.

[2] Eagleman DM. (2008) Human time perception and its illusions. Current Opinion in Neurobiology 18: 131–136.

[3] Grondin S (2010) Timing and time perception: A review of recent behavioral and Neuroscience findings and theoretical directions. Attention Perception and Psychophysics 72: 561–82.

[4] Matthews WJ, Meck WH (2014) Time perception: The bad news and the good. Wiley Interdisciplinary Reviews: Cog Sci 5: 429–46.

[5] Merchant H, Harrington DL, Meck WH (2013a) Neural basis of the perception and estimation of time. Ann Rev of Neuro 26: 313 – 36.

[6] Catania AC (1970) Reinforcement schedules and psychophysical judgments: A study of some temporal properties of behavior. In WN Schoenfeld (Ed.), *The theory of reinforcement schedules* (pp. 1 – 42). New York: Appleton-Century-Crofts.

[7] Church RM, Meck WH, Gibbon J (1994) Application of scalar timing theory to individual trials. J Exp Psychol Anim Behav Process. 20(2):135-55.

[8] Killeen PR, Fetterman JG (1988) A behavioral theory of timing. Psych. Rev. 95:274-95.

[9] Gallistel CR, King A, McDonald R (2004) Sources of variability and systematic error in mouse timing behavior. J Exp Psychol Anim Behav Process. 30(1):3-16.

[10] Fetterman JG, Killeen PR (1995) Categorical Scaling of Time: Implications for Clock-Counter Models. J Exp Psych: Ani Beh Proc, 21(1): 43 – 63.

[11] Killeen PR, Fetterman JG (1993) The behavioral theory of timing: Transition Analyses. J Exp Anal Of Behav, 59, 411 – 422.

[12] Gibbon J (1977) Scalar Expectancy Theory and Weber's law in animal timing. Psych Review. 84:279-325.

[13] Gibbon J (1991) Origins of Scalar Timing. Learning and Motivation. 22:3- 38.

[14] Gibbon J (1992) Ubiquity of scalar timing with a Poisson clock. J of Math Psych. 36:283- 293.

[15] Killeen PR, Weiss N (1987) Optimal Timing and the Weber Function. Psych Review, 94, 455 – 468.

[16] Gibbon J, Church RM (1984) Sources of variance in an information processing theory of timing. In HL Roitblatt, TG Bever, & HS Terract (Eds.), *Animal Cognition* (pp. 465 – 488). Hillsdale, NJ: Erlbaum.

[17] Gibbon J, Church RM (1990) Representation of time. Cognition, 32, 23 – 54.

[**18]** Buhusi, CV, Meck WH (2002) Differential effects of methamphetamine and haloperidol on the control of

an internal clock. Behav Neuro 116:291-7.

[19] Buhusi, CV, Meck WH (2005) What makes us tick? Functional and neural mechanisms of timing. Nature Rev Neuro 6:755-65.

[20] Buhusi, CV, Meck WH (2009a) Relative time sharing: New findings and an extension of the resource allocation model of temporal processing. Phil Trans of the Royal Soc – Londong B 364:1875-85.

[21] Buhusi, CV, Meck WH (2009b) Relatively theory and time perception: Single of multiple clocks? PLoS ONE 4(7):e6268.

[22] Grondin S (2005) Overloading temporal memory. J of Exp Psych: Human Perc and Perf 31:869-79.

[23] Gu BM, et al. (2015) Bayesian models of interval timing and distortions in temporal memory as a function of Parkinson's disease and dopamine-related error processing. In A Vatakis & MJ Allman (Eds.), *Time Distortions in Mind: Temporal Processing in Clinical Populations* (pp. 281 – 327). Boston, MA: Leiden & Koninklijke Brill NV.

[24] Jazayeri M, Shadlen MN (2010) Temporal context calibrates interval timing. Nat Neuro 13:1020-6.

[25] Merchant H, et al. (2008b) The context of temporal processing is represented in the multidimensional relationships between timing tasks. PLoS ONE 3(9):e3169.

[26] Gu BM, Meck WH (2011) New perspectives on Vierordt's law: Memory-mixing in ordinal temporal comparison tasks. Lecture Notes in Computer Science 8789 LNAI:67-78.

[27] Lejune H, Wearden JH (2009) Vierordt's *The Experimental Study of the Time Sense* (1868) and its legacy. Euro J of Cog Psych 21:941-60.

[28] Mamassian P, Landy MS (2010). It's that time again. Nat Neuro 13:914-6.

[29] Allman MJ, et al. (2014a) Properties of the internal clock: First- and second-order principles of subjective time. Ann Rev of Psych 65: 743–71.

[30] Allman MJ, Yin B, Meck WH (2014b) Time in the psychopathological mind. In V Arstila & D Lloyd (Eds.), *Subjective Time: The Philosophy, Psychology, and Neuroscience of Temporality* (pp. 637–54). Cambridge, MA: MIT Press.

[31] Coull JT, et al. (2012) Dopamine precursor depletion impairs timing in healthy volunteers by attenuating activity in putamen and supplementary motor area. J of Neuro 32: 16704–15.

[32] Coull JT, et al. (2013) Dopaminergic modulation of motor timing in healthy volunteers differs as a function of baseline DA precursor availability. Timing and Time Perception 1: 77–98.

[33] Meck WH (2006a) Frontal cortex Lesions Eliminate the Clock Speed Effect of Dopaminergic Drugs on Interval Timing. Brain Res 1108: 157–67.

[34] Meck WH (2006b) Neuroanatomical localization of an internal clock: A functional link between mesolimbic, nigrostriatal, and mesocortical dopaminergic systems. Brain Res 1109: 93–107.

[35] Meck WH (2006c) Temporal memory in mature and aged rats is sensitive to choline acetyltransferase inhibition. Brain Res 1108: 168–75.

[36] Allman MJ, Meck WH (2012) Pathological distortions in time perception and time performance. Brain 135:656-77.

[37] Harrington DL, et al. (2014) Dissociation of neural mechanisms for intersensory timing deficits in Parkinson's disease. Timing and Time Perception 2:17-43.

[38] Jahanshani M, et al. (2006) The substantia nigra pars compacta and temporal processing. J of Neuro 26:1266-73.

[39] Jones CRG, et al. (2008) Basal ganglia, dopamine and temporal processing: Performance on three timing tasks on and off medication in Parkinson's disease. Brain and Cog 68:30-41.

[40] Malpani C, Rakitin B, Meck WH, Deweer B, Dubois B, and Gibbon J (1998b) Coupled temporal memories in Parkinson's disease: A dopamine-related dysfunction. J Cognit. Neurosci.10:316-331.

[41] Malapani C, Deweer B, Gibbon J (2002) Separating storage from retrieval dysfunction of temporal memory in Parkinson's disease. J of Cog Neuro 12:311-22.

[42] Guzman JN, Sánchez-Padilla J, Chan CS, Surmeier DJ (2009) Robust pacemaking in substantia nigra dopaminergic neurons. J Neurosci 29:11011–11019.

[43] Khaliq ZM, Bean BP (2010) Pacemaking in dopaminergic ventral tegmental area neurons: depolarizing drive from background and voltage-dependent sodium conductances. J Neurosci 30: 7401–7413.

[44] Puopolo M, Raviola E, Bean BP (2007) Roles of subthreshold calcium current and sodium current in spontaneous firing of mouse midbrain dopamine neurons. J Neurosci 27:645–656.

[45] Surmeier DJ, Guzman JN, Sanchez-Padilla J (2010) Calcium, cellular aging, and selective neuronal vulnerability in Parkinson's disease. Cell Calcium 13:323-30.

[46] Surmeier DJ, Guzman JN, Sanchez-Padilla J, Schumacker PT (2011) The role of calcium and mitochondrial oxidant stress in the loss of substantia nigra pars compacta dopaminergic neurons in Parkinson's disease. Neuroscience 198:221-31.

[47] Bonci A, Grillner P, Mercuri NB, Bernardi G (1998) L-type calcium channels mediate a slow excitatory synaptic transmission in rat midbrain dopaminergic neurons. J Neurosci 18:6693–6703.

[48] Chan CS, Guzman JN, Ilijic E, Mercer JN, Rick C, Tkatch T, Meredith GE, Surmeier DJ (2007) "Rejuvenation" protects neurons in mouse models of Parkinson's disease. Nature 447:1081–1086.

[49] Grace AA, Bunney BS (1983) Intracellular and extracellular electrophysiology of nigral dopaminergic neurons—2, action potential generating mechanisms and morphological correlates. Neuroscience 10:317-331.

[50] Ping HX, Shepard PD (1996) Apamin-sensitive Ca(2+)-activated K channels regulate pacemaker activity in nigral dopamine neurons. Neuroreport 7:809–814.

[51] Romo R, Schultz W (1990) Dopamine neurons of the monkey mid- brain: contingencies of responses to active touch during self-initiated arm movements. J Neurophysiol 63:592–606.

[52] Sinnegger-Brauns MJ, Huber IG, Koschak A, Wild C, Obermair GJ, Einzinger U, Hoda JC, Sartori SB, Striessnig J (2009) Expression and 1,4-dihydropyridine-binding properties of brain L-type calcium channel isoforms. Mol Pharmacol 75:407–414.

[53] Striessnig J, Koschak A, Sinnegger-Brauns MJ, Hetzenauer A, Nguyen NK, Busquet P, Pelster G, Singewald N (2006) Role of voltage-gated L-type Ca2 channel isoforms for brain function. Biochem Soc Trans 34:903–909.

[54] Berridge MJ, Lipp P, Bootman MD (2000) The versatility and univer- sality of calcium signalling. Nat Rev Mol Cell Biol 1:11–21.

[55] Guzman JN, Sanchez-Padilla J, Wokosin D, Kondapalli J, Ilijic E, Schumacker PT, Surmeier DJ (2010) Oxidant stress evoked by pacemaking in dopaminergic neurons is attenuated by DJ-1. Nature 468:696–700.

[56] Hanson GT, Aggeler R, Oglesbee D, Cannon M, Capaldi RA, Tsien RY, Remington SJ (2004) Investigating mitochondrial redox potential with redox-sensitive green fluorescent protein indicators. J Biol Chem 279:13044–13053.

[57] Orrenius S, Zhivotovsky B, Nicotera P (2003) Regulation of cell death: the calcium-apoptosis link. Nat Rev Mol Cell Biol 4:552–565.

[58] Wilson CJ, Callaway JC (2000) Coupled oscillator model of the dopaminergic neuron of the substantia nigra. J Neurophysiol 83:3084–3100.

[59] Becker C, Jick SS, Meier CR (2008) Use of antihypertensives and the risk of Parkinson disease. Neurology 70:1438–1444.

[60] German DC, Manaye KF, Sonsalla PK, Brooks BA (1992a) Midbrain dopaminergic cell loss in Parkinson's disease and MPTP-induced parkinsonism: sparing of calbindin-D28k-containing cells. Ann N Y Acad Sci 648:42–62.

[61] Koschak A, Reimer D, Huber I, Grabner M, Glossmann H, Engel J, Striessnig J (2001) Alpha 1D (Cav1.3) subunits can form l-type Ca2 channels activating at negative voltages. J Biol Chem 276:22100 –22106.

[62] Ritz B, Rhodes SL, Qian L, Schernhammer E, Olsen JH, Friis S (2010) L-type calcium channel blockers and Parkinson disease in Denmark. Ann Neurol 67:600–606.

[63] Scholze A, Plant TD, Dolphin AC, Nürnberg B (2001) Functional expression and characterization of a voltage-gated CaV1. 3 (alpha1D) calcium channel subunit from an insulin-secreting cell line. Mol Endocrinol 15:1211–1221.

[64] Yamada T, McGeer PL, Baimbridge KG, McGeer EG (1990) Relative sparing in Parkinson's disease of substantia nigra dopamine neurons containing calbindin-D28K. Brain Res 526:303–307.

[65] Hirsch EC, Hunot S (2009) Neuroinflammation in Parkinson's disease: a target for neuroprotection?

Lancet Neurol 8:382–397.

[66] Abou-Sleiman PM, Muqit MM, Wood NW (2006) Expanding insights of mitochondrial dysfunction in Parkinson's disease. Nat Rev Neurosci 7:207–219.

[67] Calne DB, Langston JW (1983) Aetiology of Parkinson's disease. Lancet 2:1457–1459.

[68] Moore DJ, West AB, Dawson VL, Dawson TM (2005a) Molecular pathophysiology of Parkinson's disease. Annu Rev Neurosci 28: 57– 87.

[69] Schapira AH (2008a) Mitochondria in the etiology and pathogenesis of Parkinson's disease. Lancet Neurol 7:97–109.

[70] Sulzer D (2007) Multiple hit hypotheses for dopamine neuron loss in Parkinson's disease. Trends Neurosci 30:244–250.

[71] Schapira AH (2008b) Progress in neuroprotection in Parkinson's disease. Eur J Neurol 15 (Suppl 1):5–13.

[72] Chin-Chan M, Navarro-Yepes J, Quintanilla-Vega B (2015) Environmental pollutants as risk factors for neurodegenerative disorders: Alzheimer's and Parkinson diseases. Front Cell Neuro 9:124.

[73] Cory-Slechta DA, Weiss B, Cranmer J (2008) The environmental etiologies of neurobehavioral deficits and disorders: Weaving complex outcomes and risk modifiers into the equation. Neurotox 29(5):759-760.

[74] Weiss B (2010) Lead, manganese, and methylmercury as risk factors for neurobehavioral impairment in advanced age. Inter J of Alzheimer's Disease 2011:1-11.

[75] Weiss B, Clarkson TW, Simon W (2002) Silent latency periods in methylmercury poisoning and in neurodegenerative disease. Environ Health Persp 110(5):851-4.

[76] Weiss B, Simon W (1975) Quantitative perspectives on the long-term toxicity of methylmercury and similar poisons. In B Weiss & VG Laties (Eds.), *Behavioral Toxicology* (pp. 429 – 35). New York, NY, Plenum.

[77] Basu N, Klenavic K, Gamberg M, O'Brien M, Evans D, Scheuhammer AM, and Chan HM (2005a) Effects of mercury on neurochemical receptor-binding characteristics in wild mink. Environ. Tox. Chem. 24:1444- 50.

[78] Basu N, Scheuhammer A, Grochowina N, Klenavic K, Evans D, O'Brien M, and Chan HM (2005b) Effects of mercury on neurochemical receptors in wild river otters (lontra canadensis). Environmental Sci. Tech. 39:3585-91.

[79] Faro LR, Duran R, do Nascimento JL, Perez-Vences D, and Alfonso M (2003) Effects of successive intrastriatal methylmercury administrations on dopaminergic system. Ecotoxicol Environ Saf. 55(2):173- 177.

[80] Faro LR, Rodrigues KJ, Santana MB, Vidal L, Alfonso M, Duran R (2007) Comparative effects of organic and inorganic mercury on in vivo dopamine release in freely moving rats. Braz J Med Biol Res.

40(10):1361- 5.

[81] Møller-Madsen B (1991) Localization of mercury in CNS of the rat. Iii. Oral administration of methylmercuric chloride (ch3hgcl). Fund. App. Toxicol. 16:172-87.

[82] Shao Y, Chan H (2015) Effects of methylmercury on dopamine release in MN9D neuronal cells. Toxicol Mechs and Meths 25(8):637-44.

[83] Atchinson WD (2003) Effects of toxic environmental contaminants on voltage-gated calcium channel function: From past to present. J Bioenerg Biomembr 35:507-32.

[84] Atchison WD, Hare MF (1994) Mechanisms of methylmercury-induced neurotoxicity. FASEB J 8:622-9.

[85] Bearss JJ, Limke TL, Atchison WD (2001) Methylmercury (MeHg) causes calcium release from smooth endoplasmic reticulum (SER) inositol- 1, 4, 5-triphosphate receptors in rate cerebellar granule neurons. Toxicologist 60:184.

[86] Limke TL, Bearss JJ, Atchison WD (2004) Acute exposure to methylmercury causes Ca^{2+} dysregulation and neuronal death in rat cerebellar granule cells through an M_3 muscarinic receptor. Toxicol Sci 80(1):60-8.

[87] Limke TL, Otero-Montanez JKL, Atchison WD (2003) Evidence for interaction between intracellular calcium stores during methylmercury-induced intracellular dysregulation in rat cerebellar granule neurons. J Pharmacol Exp Ther 305:949-58.

[88] Marty MS, Atchison WD (1997) Pathways mediating Ca^{2+} entry in rat cerebellar granule cells following in vitro exposure to methylmercury. Toxicol Appl Pharmacol 147:319-30.

[89] Marty MS, Atchison WD (1998) Elevations in intracellular Ca^{2+} as a probable contributor to decrease viability in cerebellar granule cells following acute exposure to methylmercury. Toxicol Appl Pharmacol 150:98-105.

[90] Minnema DJ, Cooper GP, and Greenland RD (1989) Effects of methylmercury on neurotransmitter release from rat brain synaptosomes. Toxicol. App. Pharmacol. 99:510-21.

[91] Yuan Y, Atchison WD (1994) Comparative effects of inorganic divalent mercury, methylmercury and phenylmercury on membrane excitability and synaptic transmission of CA1 neurons in hippocampal slices of the rat. Neurotoxicology 15(2):403-411.

[92] Yuan Y. Atchison WD (1999) Comparative effects of methylmercury on parallel-fiber and climbing-fiber responses of rat cerebellar slices. J Pharmacol Exp Ther 288(3):1015-1025

[93] Yuan Y, Atchison WD (2005) Methylmercury induces a spontaneous, transient slow inward chloride current in Purkinje cells of rat cerebellar slices. J Pharmacol Exp Ther 313(2):751-64.

[94] Yuan Y, Atchison WD (2003) Methylmercury differentially affects GABA(A) receptor-mediated spontaneous IPSCs in Purkinje and granule cells of rat cerebellar slices. J Physiol 550(Pt 1):191-204.

[95] Yuan Y, Atchison WD (2007) Methylmercury-induced increase of intracellular Ca^{2+} increases

spontaneous synaptic current frequency in rat cerebellar slices. Mol Pharmacol 71(4):1109-21.

[96] Bailey JM, Hutsell BA, Newland MC (2013) Dietary nimodipine delays the onset of methylmercury neurotoxicity in mice. NeuroTox 37:108-17.

[97] Sakamoto M, Ikegami N, Nakano A (1996) Protective effects of Ca^{2+} channel blockers against methyl mercury toxicity. Basic Clin Pharmacol Toxicol 78:193-9.

[98] Treisman M (1963) Temporal discrimination and the indifference interval: Implications for a model of the "internal clock." Psych Monographs, 77 (Whole No. 576).

[99] Killeen PR, Pellón R (2013) Adjunctive behaviors are operants. Learn Behav 41:1-24.

[100] Sanabria F, Killeen PR (2007) Temporal generalization accounts for response resurgence in the peak procedure. Behav Proc 74: 126 – 141.

[101] Killeen PR, Fetterman JG, Bizo LA (1997) Time's Causes. In CM Bradshaw & E Szabadi (Eds.), *Time and Behavior: Psychological and Neurobehavioural analyses* (pp. 79 – 131). Amsterdam: Elsevier Science.

[102] Burnham KP, Anderson DR (2002) *Model selection and multimodal inference: A practical information-theoretic approach*. New York, NY: Springer-Verlag.

[103] Guilford JP (1954) *Psychometric methods*. New York, NY: McGraw-Hill.

[104] Thurstone LL (1927a) Psychophysical analysis. American J of Psych 38:361-89.

[105] Thurstone LL (1927b) The phi gamma hypothesis. J of Exp Psych 11:293-305.

[106] Thurstone LL (1955) *The measurement of values*. Chicago, IL: Univ of Chicago Press.

[107] Stevens SS (1957) On the psychophysical law. Psych Rev 64:153-181.

[108] Luce RD (1963a) Detection and recognition. In RD Luce, R Bush, & E Galanter (Eds.), *Handbook of Mathematical Psychology*, (Vol. 1, pp., 103 – 189). New York, NY: Wiley.

[109] Luce RD (1963b) A threshold theory for simple detection experiments. Psych Rev 70:61-79.

[110] Luce RD (1977) Thurstone's discriminal processes fifty years later. Psychometrika 42:461-489.

[111] Fetterman JG, Killeen PR (1992). Time discrimination in Columa livia and Homo sapiens. J Exp Psych: Ani Beh Proc, 18:80-94.

[112] Laties VG, Evans HL. Methylmercury-induced changes in operant discrimination by the pigeon. J Pharmacol Exp Ther. 1980;214:620-8.

TABLES: EXPERIMENT/PHASE 1

Table 1. PLM Model Comparison: Phase 1

0 ppm MeHg, 0 ppm ISR

Model	***ω***	***ρ***	***μ***	RSS	*k*	*n*	AICc	Akaike Weight
Pure Weber	1	0	4	2.79	70	952	-5400.8	0.00
Pure Poisson	0	1	4	1.12	70	952	-6267.1	0.00
Mixed Poisson	**0**	**2**	**4**	**0.30**	**84**	**952**	**-7493.6**	**1.00**
Weber/Pure Poisson	1	1	4	0.37	84	952	-7288.6	0.00
Weber/Mixed Poisson	1	2	4	0.29	98	952	-7484.2	0.00

0 ppm MeHg, 2 ppm ISR

Model	***ω***	***ρ***	***μ***	RSS	*k*	*n*	AICc	Akaike Weight
Pure Weber	1	0	4	1.94	70	952	-5745.8	0.00
Pure Poisson	0	1	4	1.65	70	952	-5902.9	0.00
Mixed Poisson	**0**	**2**	**4**	**0.21**	**84**	**952**	**-7844.9**	**1.00**
Weber/Pure Poisson	1	1	4	0.41	84	952	-7177.3	0.00
Weber/Mixed Poisson	1	2	4	0.20	98	952	-7837.7	0.00

5 ppm MeHg, 0 ppm ISR

Model	***ω***	***ρ***	***μ***	RSS	*k*	*n*	AICc	Akaike Weight
Pure Weber	1	0	4	3.15	75	1020	-5733.8	0.00
Pure Poisson	**0**	**1**	**4**	**0.38**	**75**	**1020**	**-7895.6**	**1.00**
Mixed Poisson	0	2	4	0.38	90	1020	-7849.4	0.00
Weber/Pure Poisson	1	1	4	0.37	90	1020	-7884.2	0.00
Weber/Mixed Poisson	1	2	4	0.35	105	1020	-7888.8	0.00

5 ppm MeHg, 2 ppm ISR

Model	***ω***	***ρ***	***μ***	RSS	*k*	*n*	AICc	Akaike Weight
Pure Weber	1	0	4	2.95	75	1020	-5802.0	0.00
Pure Poisson	0	1	4	1.02	75	1020	-6884.2	0.00
Mixed Poisson	**0**	**2**	**4**	**0.33**	**90**	**1020**	**-8010.3**	**1.00**
Weber/Pure Poisson	1	1	4	0.34	90	1020	-7971.4	0.00
Weber/Mixed Poisson	1	2	4	0.32	105	1020	-7995.6	0.00

[3]For each exposure group, the model typed in **BOLD** was selected as the best PLM.

Table 2. Parameter estimates from the best-fitting PLM model for each exposure group during Phase 1.

	8-s Target Duration			32-s Target Duration				
EXPOSURE GROUP	*ρ*	*μ Start*	*μ Stop*	*ρ*	*μ Start*	*μ Stop*	***ρ Ratio***	***ρ Global***
0 MeHg, 0 ISR	0.49	0.35	1.29	0.98	0.66	1.78	2.50	0.75
0 MeHg, 2 ISR	0.20	0.30	1.25	0.67	0.62	1.75	^3.44	^0.42
5 MeHg, 0 ISR	1.16	*0.58	*1.53	1.16	*0.47	*1.39	*0.00	*1.16
5 MeHg, 2 ISR	0.47	0.39	1.32	1.03	0.64	1.74	2.30	0.78

Table 3. Mean 8-s and 32-s start, center, & stop proportions for each exposure group during Phase 1.

	8-s Target Duration			32-s Target Duration		
EXPOSURE GROUP	*Start*	*Center*	*Stop*	*Start*	*Center*	*Stop*
0 MeHg, 0 ISR	0.36	0.82	1.29	0.66	1.22	1.78
0 MeHg, 2 ISR	0.30	0.77	1.25	0.62	1.18	1.74
5 MeHg, 0 ISR	*0.58	*1.05	*1.53	*0.47	*0.93	*1.39
5 MeHg, 2 ISR	0.39	0.85	1.32	0.64	1.19	1.74

[1]Asterisks (*) represent that mean start, center, and/or stop proportions at a particular target duration were significantly different for the 5 ppm MeHg, 0 ppm ISR group compared to all other groups. See appendix for details.

Table 4. Mean 8-s and 32-s start, center, and stop CVs and the difference between 8-s and 32-s center CVs for each exposure group during Phase 1.

	8-s Target Duration			32-s Target Duration			
Group	*Start CV*	*Center CV*	*Stop CV*	*Start CV*	*Center CV*	*Stop CV*	*Center CV Diff.*
0 MeHg, 0 ISR	0.57	0.36	0.29	0.31	0.23	0.20	0.13
0 MeHg, 2 ISR	0.50	0.30	^0.23	0.26	0.19	0.18	0.12
5 MeHg, 0 ISR	0.66	*0.51	*0.41	*0.38	*0.30	0.23	*0.22
5 MeHg, 2 ISR	0.58	0.38	0.31	0.32	0.24	0.20	0.14

[2]Asterisks (*) represent that mean start, center, and/or stop CVs at a particular target duration and/or the difference between 8-s and 32-s center CVs were significantly different for the 5 ppm MeHg, 0 ppm ISR group compared to all other groups. Carrots (^) represent that mean start, center, and/or stop CVs at a particular target duration and/or the difference between 8-s and 32-s center CVs were significantly different for the 0 ppm MeHg, 2 ppm ISR group compared to all other groups.

TABLES: EXPERIMENT/PHASE 2

Table 5. PLM Model Comparison: Phase 2

0 ppm MeHg, 0 ppm ISR

Model	***ω***	***ρ***	***μ***	RSS	*k*	*n*	AICc	Akaike Weight
Pure Weber	1	0	4	1.73	65	884	-5371.0	0.00
Pure Poisson	0	1	4	0.30	65	884	-6928.4	0.00
Mixed Poisson	**0**	**2**	**4**	**0.19**	**78**	**884**	**-7299.1**	**1.00**
Weber/Pure Poisson	1	1	4	0.29	78	884	-6908.6	0.00
Weber/Mixed Poisson	1	2	4	0.19	91	884	-7267.3	0.00

0 ppm MeHg, 2 ppm ISR

Model	***ω***	***ρ***	***μ***	RSS	*k*	*n*	AICc	Akaike Weight
Pure Weber	1	0	4	1.13	65	884	-5750.7	0.00
Pure Poisson	0	1	4	0.39	65	884	-6684.8	0.00
Mixed Poisson	**0**	**2**	**4**	**0.17**	**78**	**884**	**-7418.7**	**1.00**
Weber/Pure Poisson	1	1	4	0.18	78	884	-7324.7	0.00
Weber/Mixed Poisson	1	2	4	0.16	91	884	-7409.3	0.00

5 ppm MeHg, 0 ppm ISR

Model	***ω***	***ρ***	***μ***	RSS	*k*	*n*	AICc	Akaike Weight
Pure Weber	1	0	4	2.19	65	884	-4966.8	0.00
Pure Poisson	**0**	**2**	**4**	**0.27**	**65**	**884**	**-6815.8**	**1.00**
Mixed Poisson	0	2	4	0.27	78	952	-6982.2	0.00
Weber/Pure Poisson	1	1	4	0.28	78	884	-6953.9	0.00
Weber/Mixed Poisson	1	2	4	0.26	91	884	-6978.3	0.00

5 ppm MeHg, 2 ppm ISR

Model	***ω***	***ρ***	***μ***	RSS	*k*	*n*	AICc	Akaike Weight
Pure Weber	1	0	4	2.00	65	884	-5245.7	0.00
Pure Poisson	0	1	4	0.34	65	884	-6815.8	0.00
Mixed Poisson	**0**	**2**	**4**	**0.28**	**78**	**884**	**-6953.8**	**1.00**
Weber/Pure Poisson	1	1	4	0.29	78	884	-6928.6	0.00
Weber/Mixed Poisson	1	2	4	0.27	91	884	-6940.3	0.00

Table 6. Parameter estimates from the best-fitting PLM model for each exposure group during Phase 2.

	12-s Target Duration			24-s Target Duration				
GROUP	*ρ*	*μ Start*	*μ Stop*	*ρ*	*μ Start*	*μ Stop*	***ρ-Ratio***	***ρ-Global***
0 MeHg, 0 ISR	0.55	0.36	1.26	0.71	0.67	1.74	1.37	0.63
0 MeHg, 2 ISR	0.24	0.32	1.23	0.40	0.63	1.73	^1.83	^0.37
5 MeHg, 0 ISR	0.96	0.38	#1.04	0.96	*0.54	#*1.24	*0.00	*0.96
5 MeHg, 2 ISR	0.58	0.32	#1.07	0.73	0.61	#1.65	1.25	0.68

Table 7. 12-s and 24-s start, center, & stop proportions for each exposure group during Phase 2.

	12-s Target Duration			24-s Target Duration		
GROUP	*Start*	*Center*	*Stop*	*Start*	*Center*	*Stop*
0 MeHg, 0 ISR	0.37	0.82	1.26	0.68	1.21	1.74
0 MeHg, 2 ISR	0.32	0.77	1.23	0.64	1.18	1.73
5 MeHg, 0 ISR	0.38	#0.71	#1.04	*0.54	*0.89	#*1.24
5 MeHg, 2 ISR	0.32	#0.69	#1.07	0.61	1.13	#1.65

[1]Pound symbols (#) represent that start, center, and/or stop proportions at a particular target duration were significantly different between 5 ppm and 0 ppm MeHg groups. Asterisks (*) again represent that the 5 ppm MeHg, 0 ppm ISR group had significantly different start, center, or stop proportions compared to all other groups at a particular target duration.

Table 8. Mean 12-s and 24-s start, center, and stop CVs and the difference between 12-s and 24-s center CVs for each exposure group during Phase 2.

	12-s Target Duration			24-s Target Duration			
GROUP	*Start CV*	*Center CV*	*Stop CV*	*Start CV*	*Center CV*	*Stop CV*	*Center CV Diff.*
0 MeHg, 0 ISR	0.47	0.30	0.26	0.29	0.20	0.18	0.10
0 MeHg, 2 ISR	0.41	^0.23	^0.20	^0.23	0.17	^0.15	^0.05
5 MeHg, 0 ISR	#0.62	*0.48	*0.39	*0.38	*0.30	*0.25	*0.20
5 MeHg, 2 ISR	#0.55	0.35	0.29	0.31	0.21	0.19	0.13

FIGURE CAPTIONS: EXPERIMENT/PHASE 1

Figure 1. Mean, obtained 8-s (open symbols) and 32-s (filled symbols) normalized peak curves for each exposure group (four panels) during Phase 1; the vertical grey line in each panel represents the normalized 8-s and 32-s target duration times. Normalized peak curves plot the normalized probability a run is in progress as a function of normalized PI trial time (i.e., time into trial divided by target duration), averaged across subjects of each exposure group. For each exposure group, the mean 8-s and 32-s peak curves are the cumulative distributions of starts (the rising phase or ascending limb) minus the cumulative distributions of stops (the falling phase or descending limb) averaged across subjects of each exposure group. Equivalently, these peak curves are the mean, probability a run is in progress (that is has started and not stopped) at the 8-s and 32-s target durations for each exposure group. The solid and dashed lines in each panel represent the mean predictions derived from the best-fitting PLM (Eqs. 1 & 2) for each exposure group. See text for additional details.

Figure 2. The left and right panels compare mean, obtained (symbols) and PLM predicted (lines) normalized peak curves for each exposure group at the 8-s and 32-s target durations, respectively. Compared to all other groups, 8-s peak curves for the 5 MeHg, 0 ISR group are shifted rightward (overestimation), while 32-s peak curves for this group are shifted leftward (underestimation). Additionally, compared to all other groups, the rising and falling phase/limbs of both the 8-s and 32-s peak curves for the 5 MeHg, 0 ISR group are more gradual (less steep), because CVs for the 8-s and 32-s response distributions are higher for the this group compared to the other three groups. See text for additional details.

Figure 3. The left four panels show mean 8-s and 32-s start (open symbols; below horizontal grey line) and stop (closed symbols; above horizontal grey line) times as a proportion of target duration for each exposure group (i.e., normalized start/stop times). The right panel compares the resulting mean 8-s and 32-s center times as a proportion of target duration (i.e., normalized center times) for each exposure group. Compared to all other groups, mean 8-s center proportions for the 5 ppm MeHg, 0 ppm ISR group are higher and located later than target duration (overestimation), while 32-s center proportions for this group are lower and located earlier than the target duration (underestimation). Vertical error bars represent +/- 1 SEM. See text for additional details.

Figure 4. Standard deviations of the distributions for starts and stops at the 8-s (open circles) and 32-s (closed circles) target durations for individual subjects of each exposure group (four panels) as a function of the mean time of those 8-s and 32-s starts and stops for individual subjects of each exposure group. The solid, straight lines in each panel represent the predicted standard deviations of 8-s and 32-s starts and stops if error grew strictly in accordance with Weber's law and scalar timing. For subjects in all groups, Weber's law and scalar timing grossly overpredict the growth in error (standard deviations) of 8-s and 32-s starts and stops; the standard deviations of 8-s and 32-s starts/stops increase much less than proportionally with increases in the time at which those starts/stops occur. See text for additional details.

Figure 5. Mean, obtained standard deviations of the distributions for starts and stops at the 8-s (open circles) and 32-s (closed circles) target durations as a function of the mean time of those starts and stops for each exposure group (four panels). In each panel, the solid line represents the mean predictions derived from the best-fitting PLM (Eq. 1) for each exposure group. As illustrated in each panel, the mean, PLM-predicted standard deviations for 8-s and 32-s starts and stops provide an excellent account of the mean, obtained standard deviations for 8-s and 32-s starts and stops for each exposure group. See text for additional details.

Figure 6. Mean, obtained CVs of the distributions of starts, centers, and stops at the 8-s (open circles) and 32-s (closed circles) target durations as a function of the mean time of those starts, centers, and stops for each exposure group (four panels). In each panel, the solid line represents the mean predictions derived from the best-fitting PLM (Eq. 1) for each exposure group. Vertical error bars represent +/- 1 SEM. See text for additional details.

FIGURE CAPTIONS: EXPERIMENT/PHASE 2

Figure 7. Mean, obtained normalized 12-s (open symbols) and 24-s (closed symbols) peak curves for each of the four exposure groups (four panels) during Phase 2. The solid and dashed lines in each panel represent the mean predictions derived from the best-fitting PLM (Eqs. 1 & 2) for each exposure group. See text for additional details.

Figure 8. The left and right panels compare mean, obtained (symbols) and PLM predicted (lines) normalized peak curves for each exposure group at the 12-s and 24-s target durations, respectively. Compared to the two 0 MeHg groups, 12-s peak curves for the two 5 MeHg groups are shifted leftward (underestimation). Conversely, compared to all other groups, 24-s peak curves for the 5 MeHg, 0 ISR group are also shifted leftward (underestimation). Additionally, compared to all other groups, the rising and falling phase/limbs of both the 12-s and 24-s peak curves for the 5 MeHg, 0 ISR group are more gradual (less steep), because CVs for the 12-s and 24-s response distributions are higher for the this group compared to the other three groups. See text for additional details.

Figure 9. The left four panels show mean 12-s and 24-s start (open symbols; below horizontal grey line) and stop (closed symbols; above horizontal grey line) times as a proportion of target duration for each exposure group (i.e., normalized start/stop times). The right panel compares the resulting mean 12-s and 24-s center times as a proportion of target duration (i.e., normalized center times) for each exposure group. Compared to the two 0 ppm MeHg groups, mean 12-s center proportions for the two 5 ppm MeHg groups are higher and located later than target duration (overestimation). In contrast, compared to all other groups, 24-s center proportions for the 5 ppm MeHg, 0 ppm ISR group are lower and located earlier than the target duration (underestimation). Vertical error bars represent +/- 1 SEM. See text for additional details.

Figure 10. Standard deviations of the distributions for starts and stops at the 12-s (open circles) and 24-s (closed circles) target durations for individual subjects of each exposure group (four panels) as a function of the mean time of those 12-s and 24-s starts and stops for individual subjects of each exposure group. The solid, straight lines in each panel represent the predicted standard deviations of 12-s and 24-s starts and stops if error grew strictly in accordance with Weber's law and scalar timing. For subjects in all groups, Weber's law and scalar timing grossly overpredict the growth in error (standard deviations) of 12-s and 24-s starts and stops; the standard deviations of 12-s and 24-s starts/stops increase much less than proportionally with increases in the time at which those starts/stops occur. See text for additional details.

Figure 11. Mean, obtained standard deviations of the distributions for starts and stops at the 12-s (open circles) and 24-s (closed circles) target durations as a function of the mean time of those starts and stops for each exposure group (four panels). In each panel, the solid line represents the mean predictions derived from the best-fitting PLM (Eq. 1) for each exposure group. As illustrated in each panel, the mean, PLM-predicted standard deviations provide an excellent account of the mean, obtained standard deviations for 12-s and 24-s starts and stops for each exposure group. See text for additional details.

Figure 12. Mean, obtained CVs of the distributions of starts, centers, and stops at the 12-s (open circles) and 24-s (closed circles) target durations as a function of the mean time of those starts, centers, and stops for each exposure group (four panels). In each panel, the solid line represents the mean predictions derived from the best-fitting PLM (Eq. 1) for each exposure group. See text for additional details.

FIGURES: EXPERIMENT/PHASE 1

Figure 1.

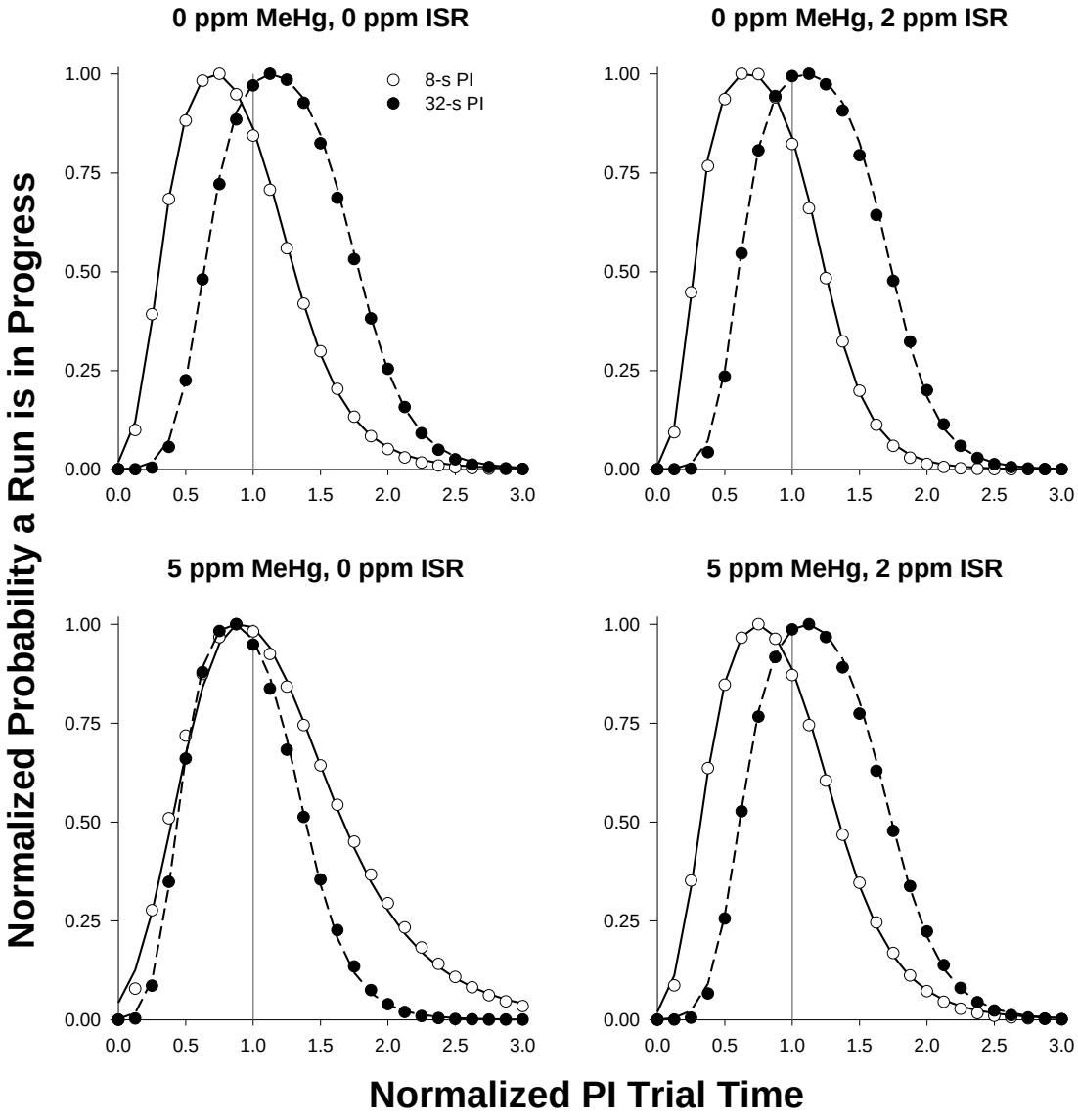

Figure 2.

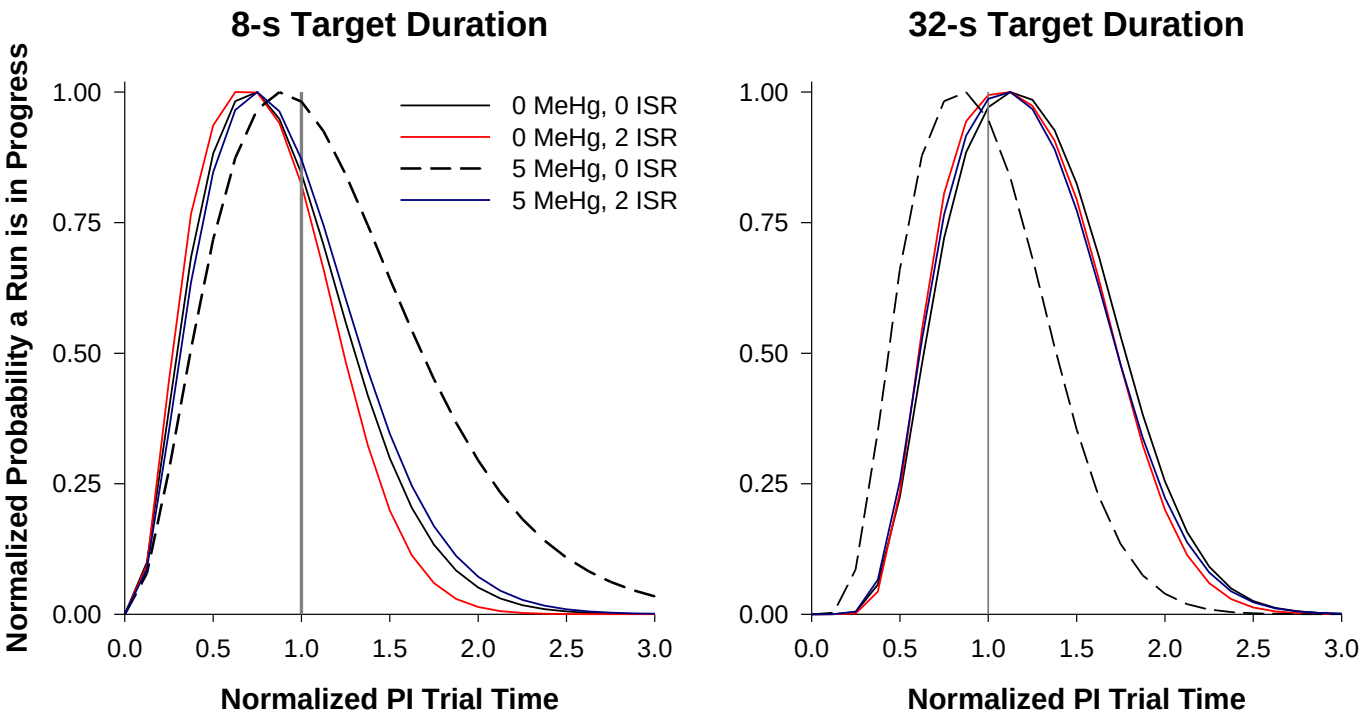
8-s Target Duration
32-s Target Duration
Normalized Probability a Run is in Progress
1.00
0.75
0.50
0.25
0.00
0.0
0.5
1.0
1.5
2.0
2.5
3.0
Normalized PI Trial Time
0 MeHg, 0 ISR
0 MeHg, 2 ISR
5 MeHg, 0 ISR
5 MeHg, 2 ISR

Figure 3.

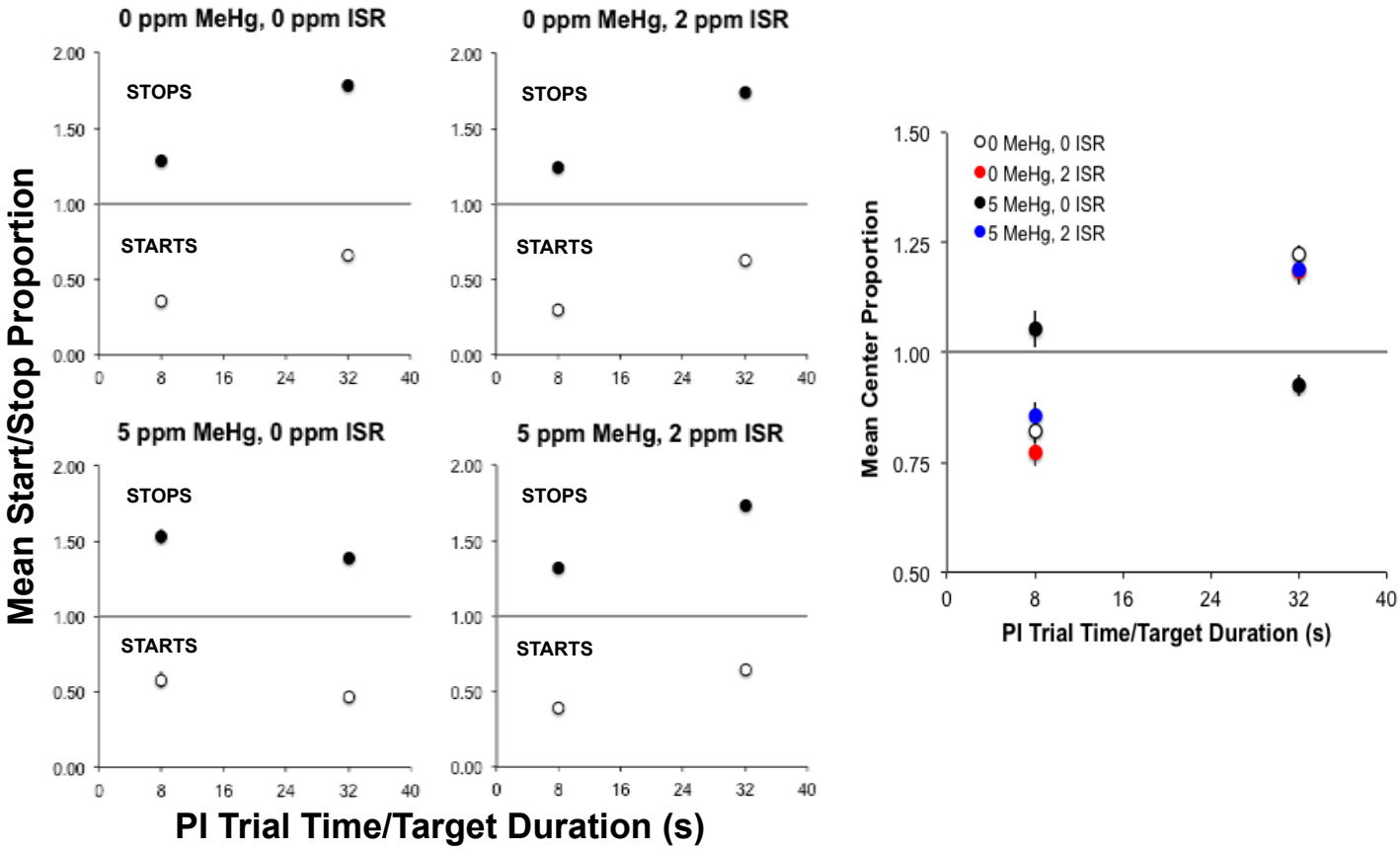
0 ppm MeHg, 0 ppm ISR
0 ppm MeHg, 2 ppm ISR
5 ppm MeHg, 0 ppm ISR
5 ppm MeHg, 2 ppm ISR
STOPS
STARTS
Mean Start/Stop Proportion
PI Trial Time/Target Duration (s)
0 MeHg, 0 ISR
0 MeHg, 2 ISR
5 MeHg, 0 ISR
5 MeHg, 2 ISR
Mean Center Proportion
PI Trial Time/Target Duration (s)

Figure 4.

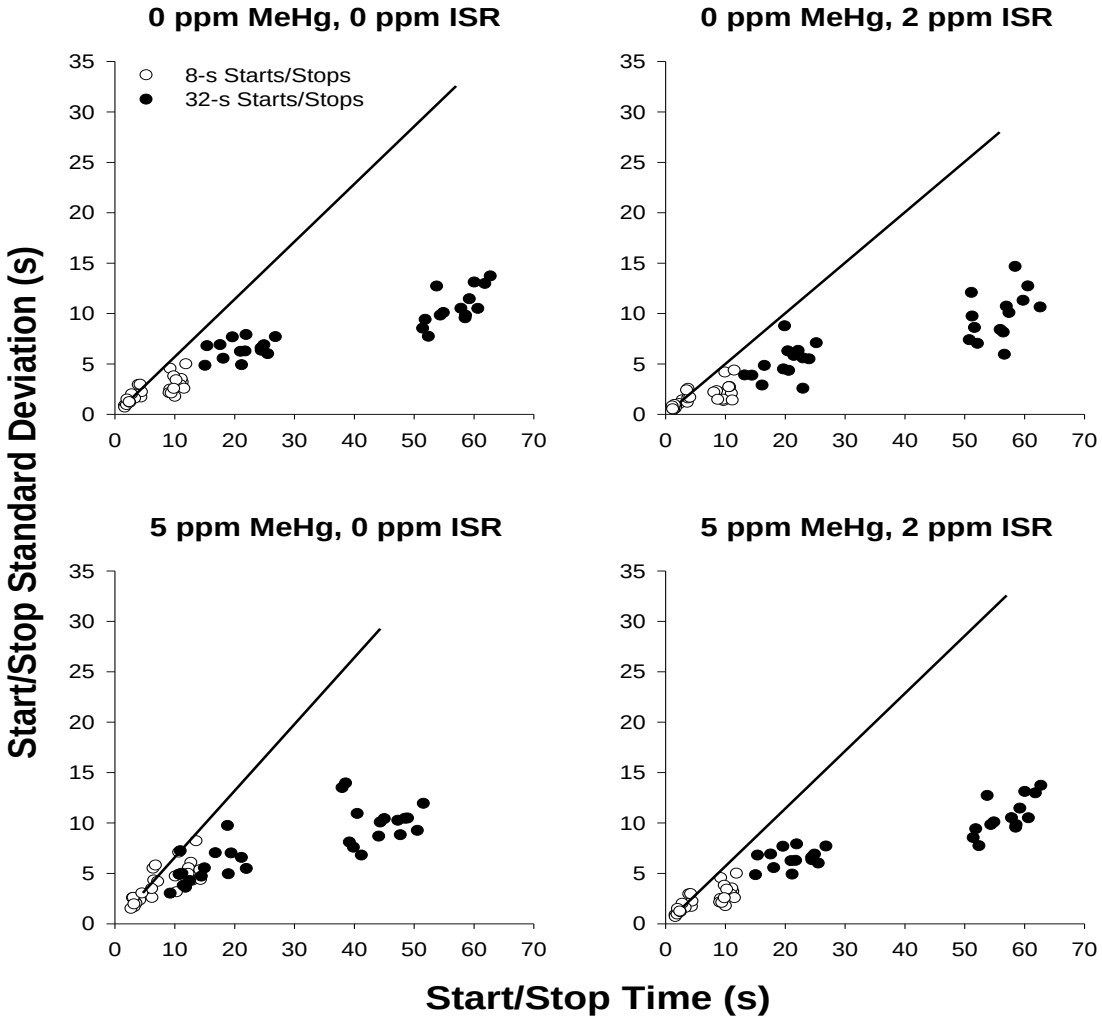
0 ppm MeHg, 0 ppm ISR
0 ppm MeHg, 2 ppm ISR
5 ppm MeHg, 0 ppm ISR
5 ppm MeHg, 2 ppm ISR
8-s Starts/Stops
32-s Starts/Stops
Start/Stop Standard Deviation (s)
Start/Stop Time (s)
0
5
10
15
20
25
30
35
40
50
60
70

Figure 5.

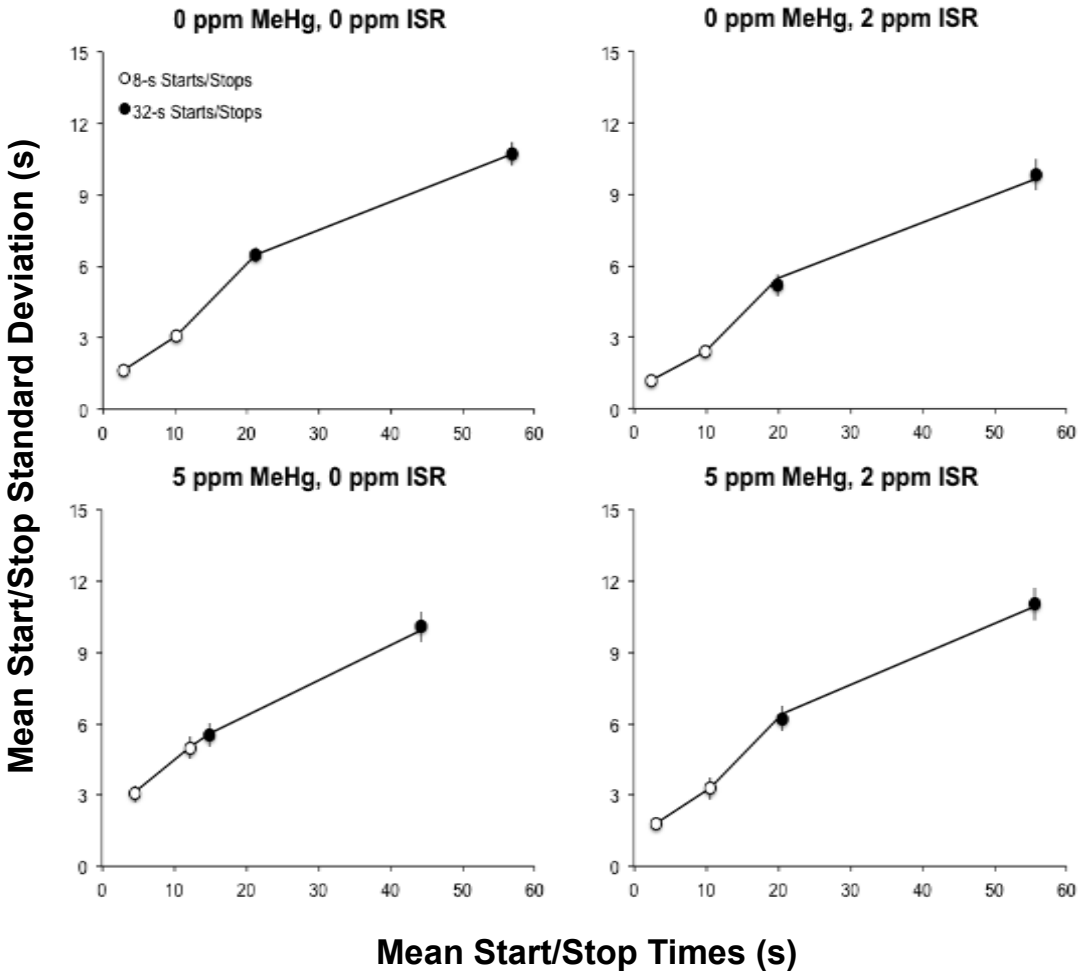

Figure 6.

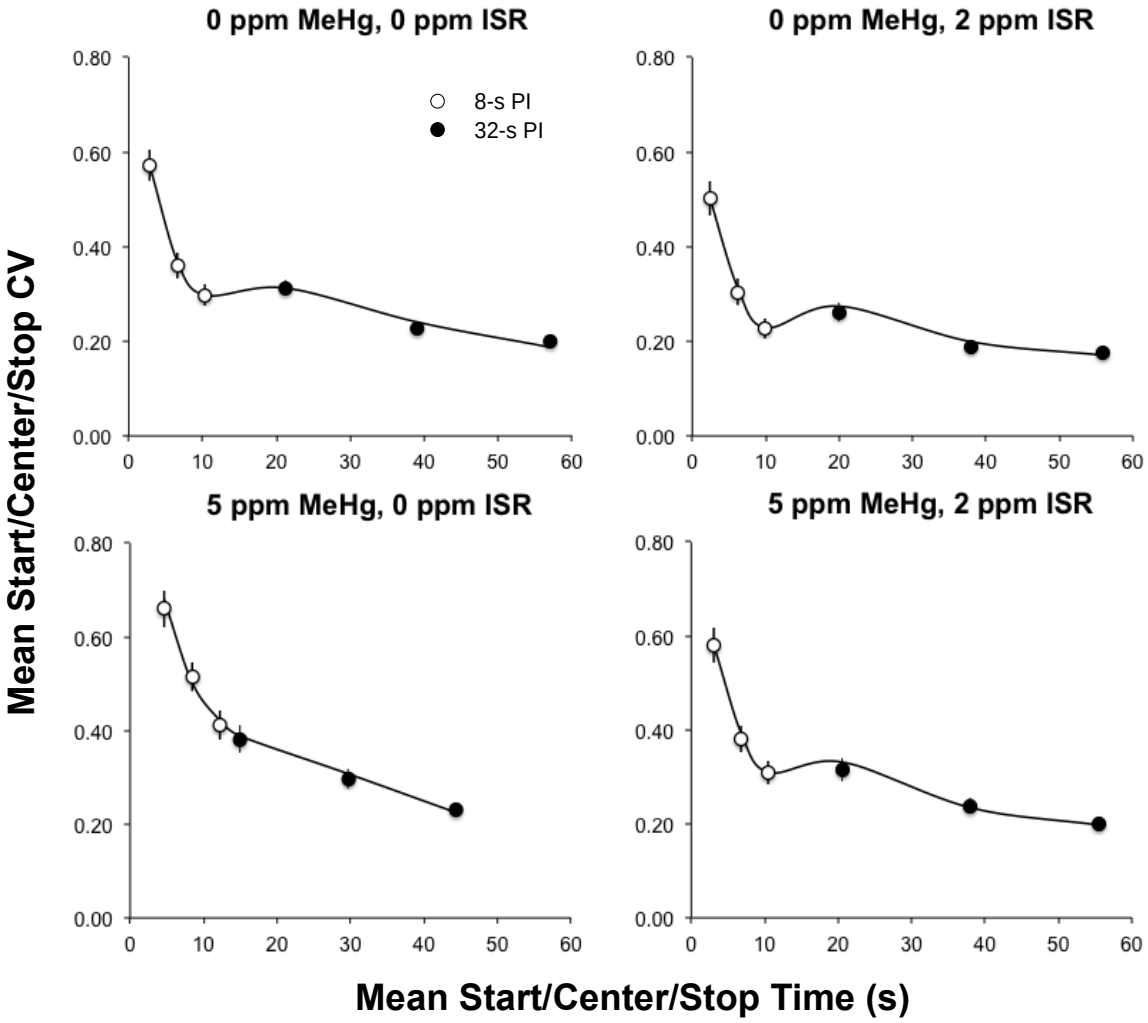
0 ppm MeHg, 0 ppm ISR
0 ppm MeHg, 2 ppm ISR
5 ppm MeHg, 0 ppm ISR
5 ppm MeHg, 2 ppm ISR
8-s PI
32-s PI
Mean Start/Center/Stop CV
Mean Start/Center/Stop Time (s)
0.00
0.20
0.40
0.60
0.80
0
10
20
30
40
50
60

FIGURES: EXPERIMENT/PHASE 2

Figure 7.

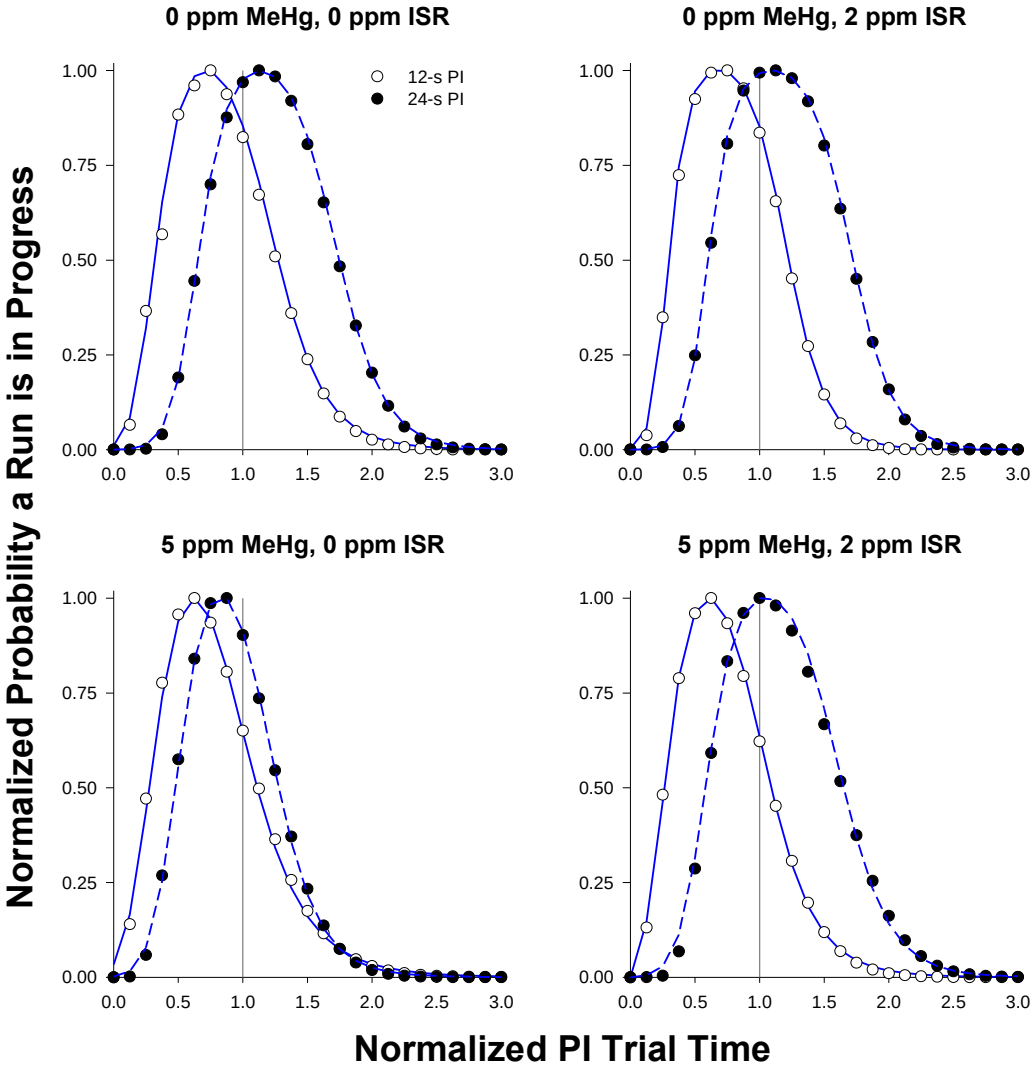

Figure 8.

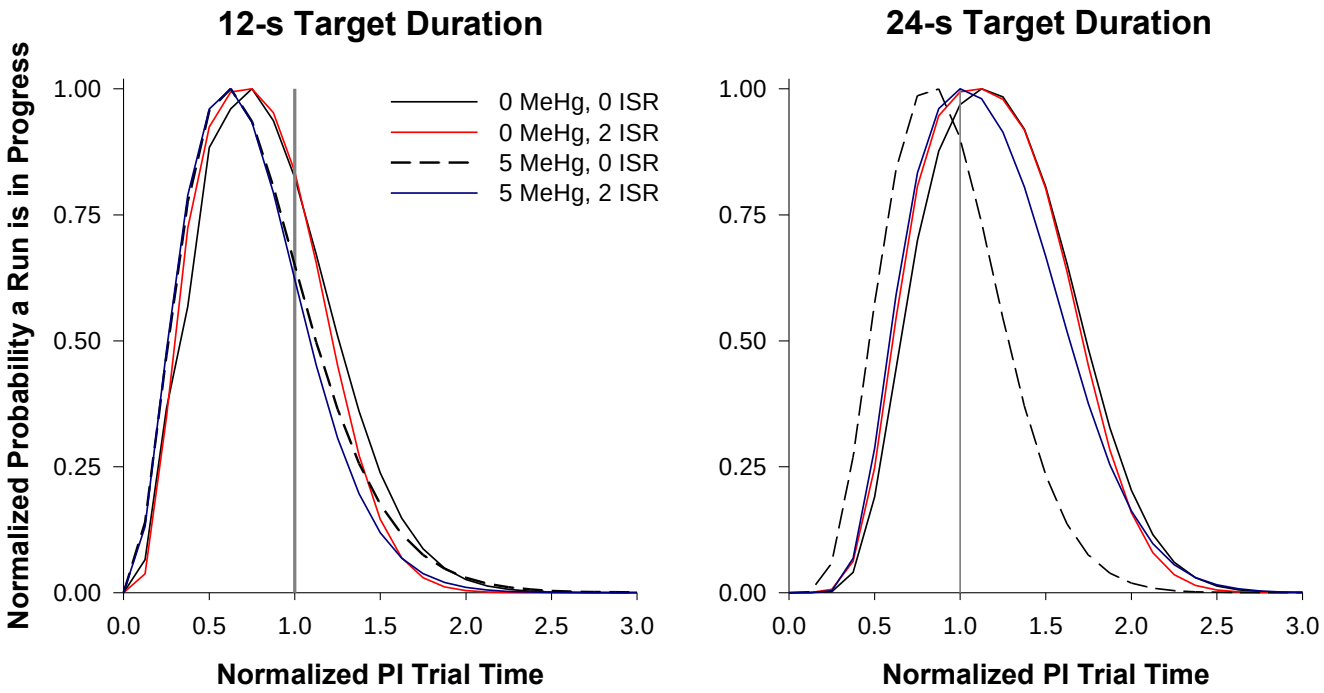
12-s Target Duration
24-s Target Duration
Normalized Probability a Run is in Progress
1.00
0.75
0.50
0.25
0.00
0.0
0.5
1.0
1.5
2.0
2.5
3.0
Normalized PI Trial Time
0 MeHg, 0 ISR
0 MeHg, 2 ISR
5 MeHg, 0 ISR
5 MeHg, 2 ISR

Figure 9.

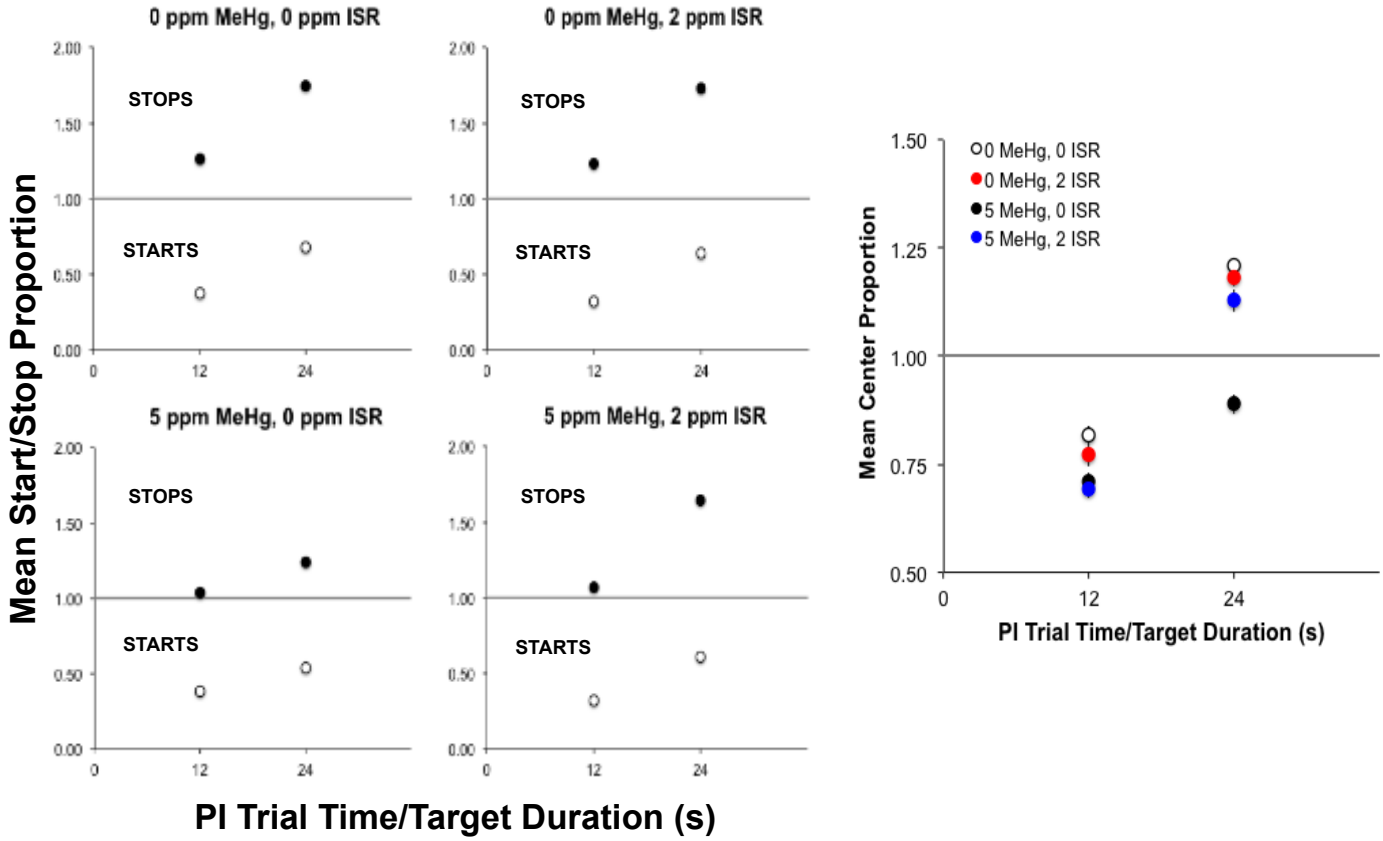
0 ppm MeHg, 0 ppm ISR
0 ppm MeHg, 2 ppm ISR
5 ppm MeHg, 0 ppm ISR
5 ppm MeHg, 2 ppm ISR
STOPS
STARTS
Mean Start/Stop Proportion
PI Trial Time/Target Duration (s)
0 MeHg, 0 ISR
0 MeHg, 2 ISR
5 MeHg, 0 ISR
5 MeHg, 2 ISR
Mean Center Proportion
PI Trial Time/Target Duration (s)

Figure 10.

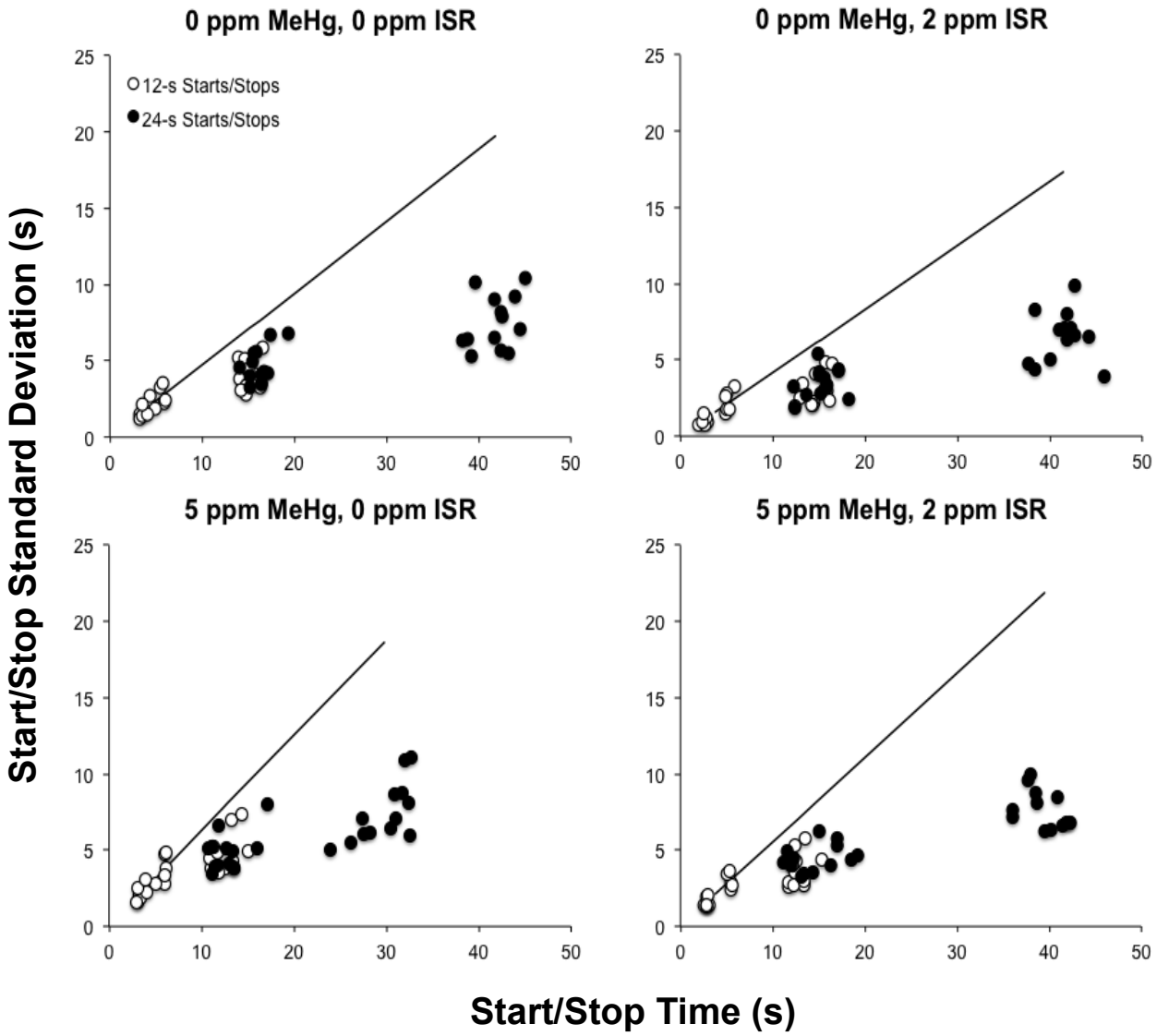
0 ppm MeHg, 0 ppm ISR
0 ppm MeHg, 2 ppm ISR
5 ppm MeHg, 0 ppm ISR
5 ppm MeHg, 2 ppm ISR
12-s Starts/Stops
24-s Starts/Stops
Start/Stop Standard Deviation (s)
Start/Stop Time (s)
0
5
10
15
20
25
30
40
50

Figure 11.

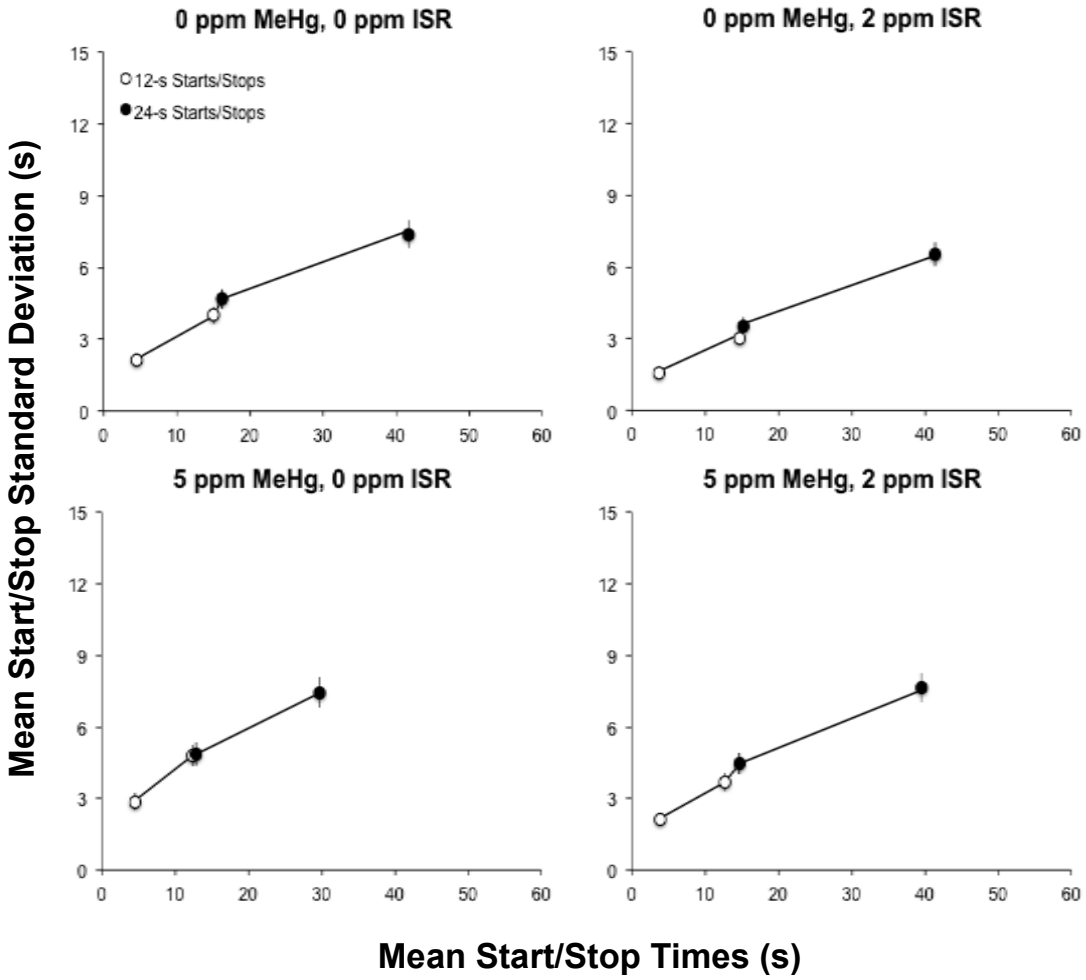
0 ppm MeHg, 0 ppm ISR
0 ppm MeHg, 2 ppm ISR
5 ppm MeHg, 0 ppm ISR
5 ppm MeHg, 2 ppm ISR
12-s Starts/Stops
24-s Starts/Stops
Mean Start/Stop Standard Deviation (s)
Mean Start/Stop Times (s)

Figure 12.

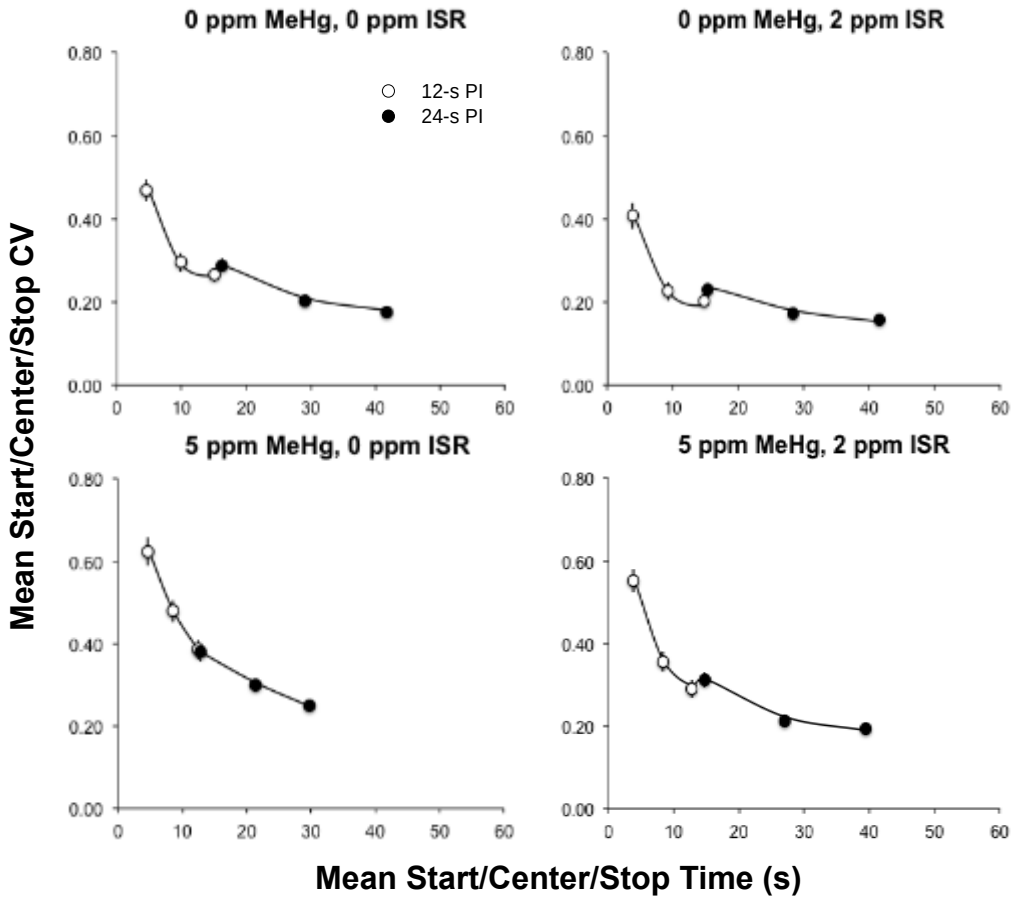
0 ppm MeHg, 0 ppm ISR
0 ppm MeHg, 2 ppm ISR
5 ppm MeHg, 0 ppm ISR
5 ppm MeHg, 2 ppm ISR
12-s PI
24-s PI
Mean Start/Center/Stop CV
Mean Start/Center/Stop Time (s)

APPENDIX: METHODS

PI Data Analysis: Raw Data, an Algorithm for Finding Start and Stop Times

In each phase, the trial times that maximized the following quantity for responding at the *short* (Phase 1 = 8-s; Phase 2 = 12-s) and, independently, *long* (Phase 1 = 32-s; Phase 2 = 24-s) target durations was obtained on every PI trial for individual subjects of each exposure group:

$$x = t_1(r-r_1)+t_2(r_2-r)+t_3(r-r_3)$$ (Algorithm 1; Church et al., 1984),

where, for peak responding at a target duration (short or long), t_1 is the duration from the beginning of the trial, t_0, until responding begins in the run or high-state; that is, the time the run state at a particular target duration begins (start), $t_1 - t_0$ is the duration in which the animal is disengaged from lever-pressing at a target duration more often than engaged (i.e., low-rate), and r_1 represents the rate of responding from t_0 (trial onset) to t_1 (i.e., first "break").The variable t_2 represents the time at which the run state ends (stop) at a particular target duration, t_2-t_1 gives the duration of the run state (i.e., dwell time or spread), r_2 represents the rate of responding from t_1 (start) to t_2 (stop), that is, the response rate during the run or high-state for a particular target duration, and after responding stops at a target duration, t_3 represents the time at which the lever correlated with a particular target duration retracts. Thus, after the run state stops at the shorter target duration, t_3 represents the time at which the first press at the longer target duration occurs, which retracts the shorter lever and disallows further presses at the shorter target duration, while after the run state stops at the longer target duration, t_3 represents the time at which the longer lever retracts, which is always the time a trial for a given target duration terminates. For each target duration, $t_3 - t_2$ is the duration of the second "break" during which lever-pressing again occurs at a low-rate, r_3 represents the rate of responding from t_2 to t_3 (i.e., rate during second "break"). Lastly, r represents the overall rate of responding at a particular target duration during the time the lever correlated with that target duration was available for responding. That is, for shorter or longer target durations, r would be equal to the total number of responses at a target duration divided by the time available for responding at that target duration.

Model Comparison

As mentioned in-text, during each phase, the effects of MeHg and ISR on the parameters of the PLM were determined using an information-theoretic, model comparison approach (Burnham & Anderson, 2002). The model-comparison approach may be foreign to most interval researchers, as the majority of PI data are analyzed using null hypothesis statistical testing (NHST), specifically, multi-way analyses of variance (ANOVA), but has at least three advantages upon initial consideration. First, is the model is fitted to the data by using Eqs. 1 and 2 (PLM) to calculate the probability of the observed data given the model, which is the true goal of data analysis. The second is that this approach encourages the evaluation of a large number of different models, all based on the PLM, but with different numbers of free parameters, without penalizing the number of different models tested, decreasing the probability of both Type I and Type II errors. Finally, the model-comparison allows for the determination of the best model evaluated given the data, relative to all other models evaluated, by generating a value called the Akaike Weight, which is equivalent to the Bayesian posterior probability under savvy prior probabilities and easily interpretable (Anderson, 2008).

Criterion for Model Selection. Because the traditional measures of goodness-of-fit, such as residual sums of squares (RSS) or percentage of variance accounted for (VAC), do not take into account the number of free parameters in a model, the model with the greatest number of free parameters will always provide the lowest RSS or highest VAC (i.e., best fits). The Akaike Information Criterion (AIC) (Burnham & Anderson, 2002) corrects the model's residual sum of squares for the number of free parameters in the model to provide an unbiased estimate of the information-theoretic distance between model and data. Here, the criterion for model selection for each strain was determined using the corrected Akaike Information Criterion (AICc) (Burnham & Anderson, 2002), which penalizes small sample sizes,

$$AIC_c = 2k + n\,ln\left(\frac{RSS}{n}\right) + \left[\frac{2k(k+1)}{(n-k-1)}\right] \qquad (A1)$$

where RSS is the residual sum of squares over all mice in a particular exposure group, k is the number of free parameters in the model (across all mice in each group), and n is the total number of observations (data points) for mice in each group. AICc covaries positively with residual sum of squares (RSS) and number of

free parameters, therefore a lower AICc (i.e., less positive or a more negative value) indicates a better account of the data given the degrees of freedom in the model.

In each phase, in all models described and tested, exactly 4 start/stop criteria (μ; Eq. 2) were estimated. Thus, during Phase 1, all models described below estimated an 8-s start, 8-s stop, 32-s start, and 32-s stop criterion for individual subjects of each exposure group, respectively. In Phase 2, all models described below estimated a 12-s start, 24-s stop, 24-s start, and 24-s stop criterion for individual subjects of each exposure group, respectively. In both Phase 1 and 2, the four estimated start/stop criteria (μ) derived from the PLMs for subjects of each exposure group accounted for over 99% of the variance in the obtained, individual subject 8-s and 32-s start, stop, and center times for each group in Phase 1 and individual subject 12-s and 24-s start, stop, and center times, respectively. This means that analyses of group differences (or lack thereof) in the locations of estimated start/stop/center criteria were identical to the analyses discussed above and presented in Tables 3 and 4 (Phase 1) and Tables 7 & 8 (Phase 2) (see also below) for the obtained start/stop/center criteria. Thus, for sake of parsimony and to spare the reader redundancies, the obtained start/stop criteria for individual subjects were used in all subsequent model-fitting for Phase 1 and 2, respectively.

Next, in each phase, the following models (Eq. 1) were evaluated:

1) Pure Weber Model. Only $\omega > 0$, but ω remained constant across target durations (1 value of w for each target duration; 5 total parameters), $c_{start} = w\mu_{start}$,and $c_{stop} = w\mu_{stop}$, and $\rho = 0$);

2) *Pure Poisson Model*. Only $\rho > 0$, ρ remained constant across target durations (1 value of ρ for each target duration; 5 total parameters), $c_{start} = \text{SQRT}[pu_{start}]$, and $c_{stop} = \text{SQRT}[pu_{stop}]$, and $\omega = 0$

3) *Mixed Poisson Model*. Only $\rho > 0$, but ρ was allowed to vary across target durations (2 values of ρ, one for each target duration; 6 total parameters), $c_{start}(short/long) = \text{SQRT}[pu_{start}(short/long)]$, and $c_{stop}(short/long) = \text{SQRT}[pu_{stop}(short/long)]$, and], and $\omega = 0$

4) *Weber/Poisson Model*. ω and $\rho > 0$, but both ω and ρ remained constant across target durations (1 value of ω & 1 value of ρ for each target duration; 6 total parameters), $c_{start} = (w\mu_{start} + \text{SQRT}[pu_{start}])$, and $c_{stop} = (w\mu_{stop} + \text{SQRT}[pu_{stop}])$ (and, finally,

5) *Weber/Mixed Poisson Model*: ω and $\rho > 0$, ω remained constant across target durations, but ρ was allowed to vary across target durations (1 value of ω for each target duration; 2 values of ρ, one for each target duration; 7 total parameters), $c_{start}(short/long) = (w\mu_{start} + \text{SQRT}[pu_{start}(short/long)]$, and $c_{stop}(short/long) = (w\mu_{stop} + \text{SQRT}[pu_{stop}(short/long)]$ (

After AICcs for each model were computed for subjects of each exposure group in each phase, the model with the lowest AICc was first identified as the 'best' model. Relative AICc scores were then computed to identify the best PLM given the data for each exposure group. After all possible PLMs were analyzed for each group, we first identified the PLM for each group with the lowest AICc (i.e., the best PLM). The comparison between the best PLM and all other PLMs was made by subtracting each of the other PLMs' AICcs from the best PLM's AICc, and this was done for each exposure group, respectively. This gave the best PLM for each group a relative AICc of 0 and all other PLMs a positive value, indicating how much worse (in probability units) the alternative PLMs were relative to the best-PLM for each group, respectively. The smaller the relative AICc the better the adjusted fit to the data, and although the best PLM for each group has value of 0, the question was whether the next-best PLM(s) were significantly different from the best PLM for each group. For instance, if the next-best PLM for an exposure group had a relative AICc = 4, it means that the peak data for that particular group were e^4 , ~55 times, more probable under the best PLM for that group than under the next-best PLM tested for that group after taking into account the difference in number of free parameters across these different PLMs.

In order to normalize relative AICc values, Akaike weights were then determined for all PLMs tested for each exposure group. Akaike weights are used in model averaging to evaluate the likelihood that a model was the best model given the data, relative to all models tested. To calculate Akaike weights for the different PLMs for each group, we first calculated the relative likelihood of each PLM for each group, which is $= e^{(-0.5 * \text{Relative AICc for that model})}$. The Akaike weight for a given PLM for each group is then just the relative likelihood of that PLM, as calculated above, divided by the sum of these values across all PLMs tested for each group, respectively. An Akaike weight of ~1.0 indicates a ~100% likelihood a particular PLM was the best PLM tested, given the data for each group. An Akaike weight greater than 0.50 (a very conservative value) was our criterion for claiming strong support for one PLM over another, and this was carried out independently for data from each exposure group.

APPENDIX: RESULTS

EXPERIMENT 1

2.1 PHASE 1

2.2 RESULTS AND DISCUSSION: PI RAW DATA

2.2.1 Systematic Error: Peak Curve Accuracy

A two-way ANOVA on 8-s start proportions with MeHg and ISR dose as between-subject factors confirmed significant main effects of MeHg [F (1, 54) = 14.39, $p < 0.01$] and ISR [F (1, 54) = 9.28, $p < 0.01$]. Post-hoc tests showed that 8-s start proportions were significantly higher (later) for the 5 ppm than the 0 ppm MeHg groups ($p = 0.01$). Further, post-hoc tests showed that 8-s start proportions were significantly higher (later) for the 5 ppm MeHg, 0 ppm ISR group compared to all other groups (all $ps < 0.01$), which were undifferentiated (all $ps > 0.12$). Two-way ANOVAs on 8-s stop and 8-s center proportions also confirmed significant MeHg X ISR interactions [both Fs (1, 54) > 5.17, both $ps < 0.03$], respectively. Post-hoc tests showed that 8-s stop and center proportions were higher (later) for the 5 ppm MeHg, 0 ppm ISR group compared to all other groups (all $ps < 0.001$), which were undifferentiated; that is, all other post-hoc tests did not reach significance (all $ps > 0.08$).

Two-way ANOVAs on 32-s start, stop, and center proportions all revealed significant MeHg X ISR interactions [all $Fs > 10.93$, all $ps < 0.01$]. Post-hoc tests showed that 32-s start, stop, and center proportions were all lower (earlier) for the 5 ppm MeHg, 0 ppm ISR group compared to all other groups (all $ps < 0.01$), which were all undifferentiated (all $ps > 0.29$).

2.2.2 Trial-to-Trial Variability: Peak Curve Precision

A two-way ANOVA on 8-s start CVs with MeHg and ISR as between-subjects factors revealed significant main effects of MeHg [F (1, 54) = 5.63, $p = 0.02$] and ISR [F (1, 54) = 4.51, $p < 0.04$]. Post-hoc tests, however, showed that there were no differences in start CVs within or across any exposure group (all $ps > 0.08$). A two-way ANOVA on 8-s stop CVs did, however, reveal significant main effects of MeHg [F (1, 54) = 15.89, $p < 0.01$] and ISR [F (1, 54) = 12.40, $p < 0.01$]. Post-hoc tests illustrated that 8-s stop CVs were higher for the 5 ppm MeHg, 0 ppm ISR group relative to all other groups (all $ps < 0.027$) and that 8-s stop CVs were lower for the 0 ppm MeHg, 2 ppm ISR group relative to all other groups (all $ps < 0.05$). A two-way ANOVA on 32-s start CVs also revealed significant main effects of MeHg [[F (1, 54) = 7.74, $p = 0.01$] and ISR [F (1, 54) = 6.87, $p = 0.01$]. Post-hoc tests illustrated that 32-s start CVs were higher for the 5 ppm MeHg, 0 ppm ISR group relative to all other groups (all $ps < 0.01$), which were undifferentiated (all $ps > 0.08$). Next, a two-way ANOVA on 32-s stop CVs revealed main effects of MeHg [F (1, 54) = 5.85, $p = 0.02$] and ISR [F (1, 54) = 5.34, $p < 0.03$]. Post-hoc tests, however, showed that there were no differences in 32-s stop CVs within or across any exposure group (all $ps > 0.06$).

A two-way ANOVAs on 8-s center CVs revealed significant main effects of MeHg [F (1, 54) = 16.53 $p < 0.01$] and ISR [F (1, 54) = 11.54, $p < 0.01$] and a two-way ANOVA on 32-s center CVs revealed a significant main effects of MeHg [F (1, 54) = 13.67, $p < 0.01$] and ISR [F (1, 54) = 9.54, $p < 0.01$]. Post-hoc tests revealed that both 8-s and 32-s center CVs were higher for 5 ppm than 0 ppm MeHg groups, and each highest, for the 5 ppm MeHg, 0 ppm ISR group relative to all other groups (all $ps < 0.012$), which were undifferentiated (all $ps > 0.06$). Because visual inspection of Figure 4 revealed that the degree of elevation in 8-s center CVs for the 5 ppm MeHg, 0 ppm ISR group was larger than the elevation in 32-s center CVs for the 5 ppm MeHg, 0 ppm ISR group compared to all other groups, the difference between 8-s center CVs and 32-s center CVs was calculated for individual subjects of each group and are shown in Table 2. A two-way ANOVA on the center CV difference scores revealed a significant main effect of MeHg [F (1, 54) = 11.53, $p < 0.01$] and ISR [F (1, 54) = 8.56, $p < 0.01$]. Post-hoc tests revealed that the difference between 8-s and 32-s center CVs was significantly higher for the 5 ppm MeHg, 0 ppm ISR group compared to all other groups (all $ps > 0.28$). This means that although both 8-s and 32-s center CVs were higher for the 5 ppm MeHg, 0 ppm ISR group compared to all other groups, 8-s center CVs were much greater for the former group than 8-s center CVs for the latter groups compared to the higher 32-s center CVs for the former than the latter groups, respectively. That is, the disparity in 8-s center CVs for the 5 ppm MeHg, 0 ppm ISR group compared to all other groups was significantly higher than the disparity in 32-s center CVs for the 5 ppm MeHg, 0 ppm ISR group compared to all other groups. Thus, 32-s center CVs were more similar between groups than 8-s center CVs, albeit still significantly higher for the former group compared to the latter three groups.

2.4.1 PLM PARAMETER ESTIMATES AND GROUP COMPARISONS

A two-way ANOVA on the harmonic mean value of *p* across the 8-s and 32-s target durations (i.e., *p Global*) revealed significant main effects of MeHg [F (1, 54) = 13.11, $p < 0.01$] and ISR [F (1, 54) = 11.39, $p < 0.01$]. Post-hoc tests revealed that the global value of *p* was higher and highest for the 5 MeHg, 0 ISR group relative to all other groups (all *ps* < 0.02; ~1.95 times higher on average) and lower and lowest for the 0 MeHg, 2 ISR group compared to all other groups (all *ps* < 0.04; ~2.15 times lower on average).

A two-way ANOVA on the ratio of *p* at the 32-s to *p* at the 8-s target duration (i.e., *p Ratio*) for all exposure groups (note this value was set to 0.00 for all subject in the 5 MeHg, 0 ISR group) revealed a significant MeHg X ISR interaction [F (1, 54) = 5.05, $p < 0.03$]. Post-hoc tests revealed that the ratio of *p* at the 32-s to *p* at the 8-s target duration was, obviously, lower and lowest for the 5 MeHg, 0 ISR group relative to all other groups (all *ps* < 0.001; mean ratio = 0.00) and higher and highest for the 0 MeHg, 2 ISR group (mean ratio = 3.44) compared to both the 0 MeHg, 0 ISR (mean ratio = 2.50) and the 5 MeHg, 2 ISR (mean ratio = 2.30) groups (both *ps* < 0.001), which were undifferentiated ($p > 0.40$).

EXPERIMENT 2

3.1 PHASE 1

3.2 RESULTS AND DISCUSSION: PI RAW DATA

3.2.1 Systematic Error: Peak Curve Accuracy

A two-way ANOVAs on 12-s start proportions revealed no significant main effects or interactions [all *Fs* (1, 48) < 4.00, all *ps* > 0.05]. However, two-way ANOVAs on 12-s stop and center proportions each revealed a significant main effect of MeHg [both *Fs* (1, 48) > 16.00, both *ps* < 0.01]. Post-hoc tests showed that 12-s stop and center proportions were significantly lower (earlier) for the 5 ppm than the 0 ppm MeHg groups (all *ps* < 0.01), but there were no differences between the two 5 ppm MeHg or the two 0 ppm MeHg groups, respectively (all *ps* > 0.19).

Two-way ANOVAs on 24-s start, stop, and center proportions with MeHg and ISR dose as between-subject factors all revealed significant MeHg X ISR interactions [all *Fs* > 6.00, all *ps* < 0.02]. Post-hoc tests showed that 24-s start, stop, and center proportions were all significantly lower (earlier) for the 5 ppm than the 0 ppm MeHg groups ($p < 0.01$). Additionally, post-hoc tests showed that 24-s start, stop, and center proportions were significantly lower (earlier) for the 5 ppm MeHg, 0 ppm ISR group compared to all other groups, (all *ps* < 0.024). Post-hoc tests also showed, however, that although 24-s start and center proportions were undifferentiated between the 0 ppm MeHg, 0 ppm ISR, 0 ppm MeHg, 2 ppm ISR, and 5 ppm MeHg, 2 ppm ISR groups (all *ps* > 0.08), 24-s stop proportions were significantly lower for the 5 ppm MeHg, 2 ppm ISR group than the two 0 ppm MeHg groups (both *ps* < 0.04), which were, again, undifferentiated ($p = 0.72$).

3.2.2 Trial-to-Trial Variability: Peak Curve Precision

A two-way ANOVA on 12-s start CVs with MeHg and ISR as between-subjects factors revealed significant main effect of MeHg [F (1, 48) = 23.77, $p < 0.01$] and ISR [F (1, 48) = 4.78, $p < 0.035$], such that 12-s start CVs were higher for the 5 ppm than 0 ppm MeHg groups, but within each group, 12-s start CVs were undifferentiated (all *ps* > 0.15). A two-way ANOVA on 12-s stop CVs did, however, reveal significant main effects of MeHg [F (1, 48) = 27.51, $p < 0.01$] and ISR [F (1, 48) = 15.30, $p < 0.01$]. Post-hoc tests illustrated that 12-s stop CVs were higher for the 5 ppm MeHg, 0 ppm ISR group relative to all other groups (all *ps* < 0.01) and that 12-s stop CVs were lower for the 0 ppm MeHg, 2 ppm ISR group relative to all other groups (all *ps* < 0.03). A two-way ANOVA on 24-s start CVs also revealed significant main effects of MeHg [MeHg [F (1, 48) = 19.84, $p < 0.01$] and ISR [F (1, 48) = 10.27, $p < 0.01$], such that 24-s start CVs were higher for 5 ppm than 0 ppm MeHg groups. Post-hoc tests also showed that 24-s start CVs were higher for the 5 ppm MeHg, 0 ppm ISR group relative to all other groups (all *ps* < 0.02) and that 24-s start CVs were lower for the 0 ppm MeHg, 2 ppm ISR group relative to all other groups (all *ps* < 0.045). A two-way ANOVA on 24-s stop CVs revealed a significant also revealed significant main effects of MeHg [MeHg [F (1, 48) = 20.50, $p < 0.01$] and ISR [F (1, 48) = 11.03, $p < 0.01$]. Post-hoc tests showed that 24-s stop CVs were higher for both 5 ppm MeHg groups compared to the 0 ppm MeHg, 2 ppm ISR group (both *ps* < 0.02), but 24-s stop CVs were not different between the 5 ppm MeHg, 2 ppm ISR and 0 ppm MeHg, 2 ppm ISR group with the 0 ppm MeHg, 0 ppm ISR group, respectively (both *ps* > 0.10). Importantly, post-hoc tests also revealed that 24-s stop CVs were lower for the 5 ppm MeHg, 0 ppm ISR group than the 5 ppm MeHg, 2 ppm ISR group ($p = 0.01$), and, thus, lower relative to all other groups (all *ps* < 0.02).

A two-way ANOVAs on 12-s center CVs revealed significant main effects of MeHg [F (1, 48) = 41.58, $p < 0.01$] and ISR [F (1, 48) = 15.92, $p < 0.01$]. Post-hoc tests showed that 12-s center CVs were higher for the 5 ppm MeHg, 0 ppm ISR group relative to all other groups (all *ps* < 0.01) and that 12-s center CVs were lower for the 0 ppm MeHg, 2 ppm ISR group relative to all other groups (all *ps* < 0.05). A two-way ANOVA on 24-s center CVs revealed a significant MeHg X ISR interaction [F (1, 48) = 4.05, $p < 0.048$]. Post-hoc tests revealed that 24-s center CVs were higher for 5 ppm than 0 ppm MeHg groups, and highest for the 5 ppm MeHg, 0 ppm ISR group relative to all other groups (all *ps* < 0.01), which were undifferentiated (all *ps* > 0.08). A two-way ANOVA on the center CV difference scores revealed significant main effects of MeHg and ISR [both *Fs* (1, 48) > 11.00, both *ps* < 0.01]. Post-hoc tests revealed that the difference between 12-s and 24-s center CVs was significantly higher for the 5 ppm MeHg, 0 ppm ISR group compared to all other groups (all *ps* < 0.03) and significantly lower for the 0 ppm MeHg, 0 ppm ISR group compared to all other groups (all *ps* < 0.05).

3.4 BEST PLM MODELS AND PARAMETERS: PHASE 2

A two-way ANOVA on the harmonic mean value of *p* across the 12-s and 24-s target durations (i.e., *p Global*) revealed significant main effects of MeHg [F (1, 48) = 12.68, $p < 0.01$] and ISR [F (1, 48) = 8.96, $p < 0.01$]. Post-hoc tests revealed that the global value of *p* was higher and highest for the 5 MeHg, 0 ISR group relative to all other groups (all *ps* < 0.02; ~1.84 times higher on average) and lower and lowest for the 0 MeHg, 2 ISR group compared to all other groups (all *ps* < 0.048; ~2.02 times lower on average), which were undifferentiated ($p > 0.56$).

A two-way ANOVA on the ratio of *p* at the 24-s to *p* at the 12-s target duration (i.e., *p Ratio*) for each exposure group (note this value was again set to 0.00 for all subject in the 5 MeHg, 0 ISR group) revealed a significant MeHg X ISR interaction [F (1, 48) = 5.99, $p = 0.01$]. Post-hoc tests revealed that *p Ratio* was, obviously, lower and lowest for the 5 MeHg, 0 ISR group relative to all other groups (all *ps* < 0.001; mean ratio = 0.00) and higher and highest for the 0 MeHg, 2 ISR (mean ratio = 1.83) compared to both the 0 MeHg, 0 ISR (mean ratio = 1.37) and the 5 MeHg, 2 ISR (mean ratio = 1.25) groups (both *ps* < 0.001), which were undifferentiated ($p > 0.20$).

Table A1. High-state (run) response rates for the 8-s and 32-s target durations during Phase 1 for each exposure group.

	Phase 1 Response Rates	
Exposure Group	**8-s Target Duration**	**32-s Target Duration**
0 MeHg, 0 ISR	2.83 s^{-1}	0.85 s^{-1}
0 MeHg, 2 ISR	2.89 s^{-1}	0.79 s^{-1}
5 MeHg, 0 ISR	3.08 s^{-1}	0.97 s^{-1}
5 MeHg, 2 ISR	3.17 s^{-1}	1.02 s^{-1}

[1]Two-way ANOVAs on response rates at the 8-s and 32-s target duration, respectively, with MeHg and ISR exposure as between subjects factors revealed no significant main effects or interactions [*all Fs* (1, 54) < 1.80, all *ps* > 0.45].

Table A2. High-state (run) response rates for the 12-s and 24-s target durations during Phase 2 for each exposure group.

	Phase 2 Response Rates	
Exposure Group	**12-s Target Duration**	**24-s Target Duration**
0 MeHg, 0 ISR	2.12 s^{-1}	1.14 s^{-1}
0 MeHg, 2 ISR	2.18 s^{-1}	1.22 s^{-1}
5 MeHg, 0 ISR	2.37 s^{-1}	1.44 s^{-1}
5 MeHg, 2 ISR	2.26 s^{-1}	1.46 s^{-1}

[2]Two-way ANOVAs on response rates at the 12-s and 24-s target duration, respectively, with MeHg and ISR exposure as between subjects factors revealed no significant main effects or interactions [*all Fs* (1, 48) < 2.20, all *ps* > 0.25].